AD_____

Award Number: W81XWH-05-1-0469

TITLE: Novel Molecular Interactions and Biological Functions of the Neurofibromatosis 2 Tumor Suppressor Protein, Merlin

PRINCIPAL INVESTIGATOR: Olli Carpén, M.D., Ph.D.

CONTRACTING ORGANIZATION: University of Helsinki
Yliopistokatu 4, Helsinki 00014

REPORT DATE: August 2008

TYPE OF REPORT: Final

PREPARED FOR: U.S. Army Medical Research and Materiel Command
Fort Detrick, Maryland 21702-5012

REPORT DOCUMENTATION PAGE

Form Approved
OMB No. 0704-0188

1. REPORT DATE	2. REPORT TYPE	3. DATES COVERED
1 aug 2008	Final	29 Jul 2005 – 28 Jul 2008

4. TITLE AND SUBTITLE

Novel Molecular Interactions and Biological Functions of the Neurofibromatosis 2 Tumor Suppressor Protein, Merlin

5a. CONTRACT NUMBER

5b. GRANT NUMBER
W81XWH-05-1-0469

5c. PROGRAM ELEMENT NUMBER

6. AUTHOR(S)
Olli Carpén, M.D., Ph.D.

E-Mail: olli.carpen@helsinki.fi

5d. PROJECT NUMBER

5e. TASK NUMBER

5f. WORK UNIT NUMBER

7. PERFORMING ORGANIZATION NAME(S) AND ADDRESS(ES)

University of Helsinki
Yliopistokatu 4, Helsinki 00014

8. PERFORMING ORGANIZATION REPORT NUMBER

9. SPONSORING / MONITORING AGENCY NAME(S) AND ADDRESS(ES)
U.S. Army Medical Research and Materiel Command
Fort Detrick, Maryland 21702-5012

10. SPONSOR/MONITOR'S ACRONYM(S)

11. SPONSOR/MONITOR'S REPORT NUMBER(S)

12. DISTRIBUTION / AVAILABILITY STATEMENT
Approved for Public Release; Distribution Unlimited

13. SUPPLEMENTARY NOTES

14. ABSTRACT

The project has studied the functions of the neurofibromatosis 2 tumor suppressor protein merlin and the related ERM protein ezrin. We identified novel binding partners and functions for both proteins. Merlin was shown to regulate both the microtubule and actin cytoskeleton. Two important kinases, protein kinase A (PKA) and AKT, were shown to phosphorylate merlin at S10. This phosphorylation affects actin dynamics, cell morphology and migration of mouse embryonic fibroblasts (MEF) and Schwann cells. Thus, merlin may serve as a regulator of PKA and AKT induced changes in actin cytoskeleton. We identified a link between merlin and cell cycle control by demonstrating a novel functional interaction between merlin and HEI10. In studies of the biological activities of ezrin we discovered that oncogenic tyrosine kinases Src and c-Met phosphorylate ezrin at Y477. Using reconstituted MEF cells from ezrin -/- mice we studied the biological importance of Y477 phosphorylation. Our results show that ezrin is a key regulator of Src induced malignant behavior in three dimensional culture conditions.

15. SUBJECT TERMS
Neurofibromatosis 2, merlin, ezrin, phosphorylation, PKA, Src, microtubule, cytoskeleton

16. SECURITY CLASSIFICATION OF:			17. LIMITATION OF ABSTRACT	18. NUMBER OF PAGES	19a. NAME OF RESPONSIBLE PERSON
a. REPORT	b. ABSTRACT	c. THIS PAGE			19b. TELEPHONE NUMBER *(include area code)*
U	U	U	UU	92	USAMRMC

Table of Contents

Page

Introduction

The neurofibromatosis 2 (NF2) gene product merlin and the ezrin-radixin-moesin (ERM) family protein ezrin are structurally related proteins that demonstrate some functional similarities and interact with each other, but possess opposite effects on cell growth. The experiments of this proposal aim to explore the poorly understood molecular and cell biological basis of the tumor suppressor function of merlin. Specific emphasis has been given to cell cycle stage-dependent targeting of merlin (task 1), analysis of molecular interactions of merlin previously identified by us (tasks 2 and 3), and comparative analysis of phosphorylation-dependent regulation of ezrin and merlin (task 4). All four tasks proposed in the research plan have been pursued and the goals in most tasks have been accomplished. Results from this project and from simultaneous efforts by other groups have opened some new avenues for future work. The project was originally recommended to the list of alternate funding on Sept. 24th, 2004. Funding was granted on May 10th, 2005 and the funding period started July 29th, 2005. Due to the over 1 year period between submission of the grant proposal and the initiation of the funding, some progress in the project (especially tasks 3 and 4) was made prior to initiation of the award. This progress will be shortly described in this report, but these results are not be included in Reportable Outcomes.

Body

The progress of the project is described in accordance with the tasks outlined in the proposal.

Task 1. *To analyze the mechanisms, regulation and functional consequences of the cell cycle dependent nucleocytoplasmic regulation of merlin.*

To identify factors that regulate nucleocytoplasmic shuttling of merlin, two potential nuclear localization signals (NLS) in merlin (aa 15-20 and aa 309-312) were mutated. These regions consist of a stretch of basic amino acids, which often are involved in nuclear targeting. However, mutation of neither potential NLS affected merlin's transfer into the nucleus. As full-length merlin does not enter nucleus efficiently, similar deletions

were introduced into a shorter 4.1-ezrin-radixin-moesin (FERM)-domain construct, merlin 1-339. This construct, when transfected to mammalian cells, can be detected mostly in the nucleus. Again, introduction of the mutations did not prevent nuclear targeting of merlin.

The role of importins in nuclear targeting was tested. We analyzed, whether merlin preferentially binds to certain importin subunits. Recombinant GST-importins were produced, purified and used for pull-down assays (Fig. 1). None of the tested importins were able to bind *in vitro* translated merlin with high affinity. Therefore, this research avenue was not pursued further.

Phosphorylation may be one potential way of regulating the nucleocytoplasmic shuttling of merlin. To study, whether phosphorylation regulates nuclear targeting of merlin, mutants replacing S518 with alanine (A) or aspartate (D) were generated. S518 is a target residue for protein kinase A (PKA) (Alfthan et al. 2004) and p21 activated kinase (PAK) (Kissil et al. 2002). S518A mutant cannot be phoshorylated, whereas S518D is thought to mimic a constitutively phosphorylated protein. Mutant merlin constructs were transfected to cells and compared with wild-type merlin. No differences were detected suggesting that phosphorylation of S518 does not play a role in the regulation of nucleocytoplasmic shuttling. On the other hand, the mutants appear to function in other experiments not related to merlin's nuclear function (see below).

During the study, we noticed that also serine 10 is phosphorylated by PKA (Laulajainen et al. 2008) and by AKT (see Task 4), and have therefore generated mutants replacing S10 with alanine (A) or aspartate (D). The S10A mutant cannot be phoshorylated, whereas S10D is thought to mimic a constitutively phosphorylated protein. We also generated double mutants of both PKA phosphorylation sites. Wild type and mutant merlin constructs were transfected into HEK293, Nf2-/- mouse embryonic fibroblasts (MEFs) and to Nf2 -/- mouse Schwann cells. Analysis of the subcellular localization of merlin S10A and S10D mutants did not show preferential nuclear targeting of either construct (Laulajainen et al. 2008, Fig. 2, 3 and 5, see appendix).

It has previously been shown that oxidative stress can induce the transfer of merlin into the nucleus after cleavage by activated μ-calpain (Kaneko, 2001). We set up the methods to study calpain regulation of merlin and activated μ-calpain mediated cleavage of merlin in transfected COS-7 and 293HEK cells. Calpain was activated in cells expressing wild type merlin, and cells stained with an N- or C-terminal antibody to identify the subcellular localization of the cleavage products. Calpain activation resulted in the relocalization of merlin from the membrane to the perinuclear region, which was not seen in cells treated with a specific calpain inhibitor, Z-Llal. Nuclear localization was not, however, detected. It has previously been shown that PKA regulates calpain function (Shiraha et al., 2002). Therefore, the PKA pathway was also activated or inactivated in merlin wild type expressing cells, or cells transfected with S10A or S10D, but no difference was detected. All experiments resulted in the relocalization of merlin (Fig. 2).

Kressel et al. (2002) showed that a cytoplasmic retention signal is present in exon 2 and a nuclear export signal in exon 15 of merlin, and that merlin constructs with exon2 deleted and the export signal mutated localize to the nucleus. Within the export signal motif, two amino acids are highly conserved in merlin from different species, glutamic acid at positions 545 and 547. We converted the charge of the residues from negative to positive (lysine). We created constructs with the E545K and E547K mutations and/or exon 2 deletions, to study their nuclear localization. COS-7 and 293HEK cells transfected with E545K+E547K still localized to the membrane, most likely because they still contained the cytoplasmic retention signal in exon 2. When exon 2 was deleted in isoform I, the protein relocated to the perinuclear region but no nuclear merlin could be seen. Interestingly, the exon 2 deletion in isoform II still localized to the membrane. When exon 2 was deleted and 545 and 547 mutated, no merlin could be detected at the membrane, instead nuclear and perinuclear staining could be seen (Fig. 3).

In order to find merlin's interaction partners in the nucleus we immunoprecipitated merlin from nuclear extracts or whole cell lysates. Precipitates were run on SDS-PAGE, silver stained, and bands enriched in the nuclear fraction were cut out for mass

spectrometry analysis. The resulting protein sequences obtained did not, however, include specific components and this approach was not pursued further.

Bimolecular fluorescence complementation analysis, BiFC, allows the direct visualization of protein interactions in living cells. This approach is based on complementation between two nonfluorescent fragments of the yellow fluorescent protein (YFP) when they are brought together by interactions between proteins fused to each fragment (Hu et al., 2002). Thus, fluorescence is seen only in regions were tested proteins interact *in vivo*, and these interactions can be directly visualized in cells. This method has been used in many studies for interaction analysis of nuclear proteins. We decided to set up this system, in order to test whether known merlin interactions take place also in the nucleus. We introduced merlin, ezrin and control constructs to the BiFC-vectors, and showed that the system is applicable to merlin-ezrin interaction studies. Merlin wild type and ezrin including the T567D mutation to mimic an open conformation, exhibited fluorescence complementation at the plasma membrane. The mutation of serine 518 to alanine (S518A), previously reported to decrease merlin-ezrin binding *in vitro* (Alfthan et al., 2004), affected dimer interaction showing mainly cytoplasmic localization and reduced fluorescence complementation (Fig. 4). However, this approach could not demonstrate that specific forms of merlin would be targeted to the nucleus.

Task 2. *To characterize the association between merlin and microtubules and its functional relevance.*

A report on the biochemical and functional aspects of the interplay between merlin and microtubules was published (Muranen et al. 2007, see appendix). As a summary, our study demonstrated that:

- Merlin and microtubules colocalize at certain cell cycle stages, especially at G2 and during mitosis (Muranen et al. 2007, Fig. 1). The colocalization is more evident in U251 glioma cells than in primary mouse Schwann cells.
- Merlin binds polymerized tubulin in vitro via two different sites, one localized at the FERM domain and one in the C-terminus (Muranen et al. 2007, Fig. 2).
- The binding between merlin and microtubules is regulated by merlin's intramolecular association and by phosphorylation of serine 518 (Muranen et al. 2007, Fig. 3).
- Full length merlin but not a merlin construct lacking the C-terminus (merlin 1-547) enhances tubulin polymerization in vitro (Muranen et al. 2007, Fig. 4).
- Schwann cells lacking merlin demonstrate abnormal microtubule organization, which can be reorganized by virally induced expression of wild-type merlin (Muranen et al. 2007, Fig. 5).
- Recovery of depolymerized microtubules is faster in merlin-expressing Schwann cells than in merlin –deficient cells (Muranen et al. 2007, Fig. 6).

In conclusion, these results indicate that merlin plays a key role in the regulation of Schwann cell microtubule cytoskeleton and suggest a mechanism by which loss of merlin leads to cytoskeletal defects observed in human schwannomas.

In additional studies, transfected merlin constructs (wild-type WT and merlin 1-547 patient mutant) were transfected to 293HEK and HeLa cells and their effect on spindle formation was evaluated. The results indicated that expression of merlin 1-547 does not colocalize with microtubules in dividing cells and that expression of merlin 1-547 results in an increased amount of multipolar mitotic spindles (Fig. 5). Tubulin was also studied in human mesothelioma cell lines, either expressing or lacking merlin (Pylkkänen et al. 2002) (Fig. 6 and 7). In these cells, a negative correlation was seen between the presence of acetylated tubulin and expression of merlin, whereas a positive correlation was seen between overall tubulin amount and merlin expression, as verified by immunoblotting.

Task 3. *To study the role of merlin -- HEI10 interaction and its role in regulation of cell growth.*

A report describing the interaction between merlin and Human Enhancer of Invasion 10 (HEI10) has been published (Grönholm et al. 2006, see appendix). Unfortunately, due to a mistake by the authors, this publication fails to cite the current research contract W81XWH05-1-0469. As a summary, our study demonstrated that:

- The interaction is mediated by the α-helical domain in merlin and the coiled-coil domain in HEI10 and requires conformational opening of merlin (Grönholm et al. 2006, Fig. 1-3). The merlin-related protein ezrin does not bind HEI10.
- The association appears to be transient *in vivo*, as the two proteins show only partial subcellular colocalization, which depends on cell cycle stage and cell adhesion (Grönholm et al. 2006, Fig. 4-5).
- To study the interplay of the proteins in a relevant cell model, human primary Schwann cell and schwannoma cultures were utilized. Analysis of these cells demonstrated that the distribution of HEI10 depends on merlin expression (Grönholm et al. 2006, Fig. 6).
- Experiments in a cellular transfection model showed that a constitutively open merlin construct affects HEI10 protein integrity (Grönholm et al. 2006, Fig. 7).

In summary, these results link merlin to the cell cycle control machinery and may thus help understanding of its tumor suppressor function. Further work in these studies has involved generation of HEI10 antibodies. This has proven out to be difficult as recombinant HEI10 is difficult to produce in sufficient quantities and synthetic HEI10 peptides have been poorly immunogenic. Several attempts to generate novel mouse mAb:s or rabbit antisera have failed. Finally, antisera against HEI10 were raised commercially (AgriSera, Vännäs, Sweden) in chicken using recombinant HEI10 produced by us. Although these antisera recognized HEI10 in ELISA and showed some reactivity against recombinant GST-HEI10 fusion protein, they do not react with transfected or endogenous HEI10 in cellular lysates (Fig. 8). Neither do they recognize HEI10 in immunofluorescence staining. Due to several attempts with negative results, we decided not to further pursue HEI10 antibody production.

During the course of the study, very little new information on HEI10 has been published, perhaps reflecting some of the difficulties in obtaining tools for biochemical and cell biological studies on HEI10. However, a recent genetic study showed that in mice, HEI10 mutations can cause sterility by disrupting meiosis and altering the function of the DNA repair system known as mismatch repair (Ward et al. 2007). This finding opens at least two interesting questions: is the meiotic defect associated with microtubule control mediated by merlin, and is the mismatch repair defect related to the mechanism, by which merlin fucbnctions as tumor suppressor.

Task 4. To understand how kinase activity differentially regulates the functional activity of merlin and ezrin.

Our previous studies had indicated that the FERM-domain of merlin contains a PKA phosphorylation site (Alfthan et al. 2004). In further experiments, we identified this site and demonstrated its biological function (Laulajainen et al. 2008, see appendix). As a summary, this study showed that:

- PKA phosphorylates merlin in vivo at an N-terminal site within the first 100 residues of the FERM domain. Mutation of S10 but not T28 or T53 abolishes phosphorylation. An S10/S518 double mutant merlin is not phosphorylated by PKA (Laulajainen et al. 2008, Fig. 1).
- Phosphorylation of S10 does not induce a change in the electrophoretic mobility of merlin (unlike phosphorylation of S10) (Laulajainen et al. 2008, Fig. 2).
- Phosphorylation of S10 does not affect phosphorylation of S518 or ezrin-merlin heterodimerization (Laulajainen et al. 2008, Fig. 2).
- Phosphorylation of S10 regulates the morphological changes induced by merlin (Laulajainen et al. 2008, Fig. 3).
- Cells expressing S10A merlin have less actin filaments than cells expressing wild-type merlin (Laulajainen et al. 2008, Fig. 4).

- Phosphomimetic S10D merlin protects actin filaments from depolymerization in vivo (Laulajainen et al. 2008, Fig. 5).
- Mutation of S10 leads to defects in cell migration and lamellipodia formation (Laulajainen et al. 2008, Fig. 6).

To summarize, these studies for the first time demonstrate a direct role for merlin in actin regulation in vivo.

As described in Task 1, PKA regulates calpain function (Shiraha et al., 2002). We have tested whether mutations of merlin's N-terminal PKA phosphorylation site, serine 10, affect the calpain mediated cleavage of merlin. The PKA phosphorylated N-terminal GST-construct was cleaved to a lesser extent than the unphosphorylated protein *in vitro*. Interestingly, in μ-calpain-activated COS-7 cells expressing merlin the hyperphosphorylated form of merlin was not present while the hypophosphorylated form increases. This indicates and interplay between merlin phosphorylation status and calpain, and that μ-calpain may regulate the phosphorylation of serine 518 (Fig. 9).

The PI3 kinase/AKT pathway is activated in human vestibular schwannoma, suggesting a role for merlin-dependent AKT regulation in the formation of these tumors (Ammoun et al. 2008). To further characterize the modification of merlin by kinases we tested, whether it serves as a substrate for AKT. By using bacterially produced recombinant fragments of merlin, we could show that the N-terminal S10 residue in merlin serves as a substrate for AKT (Fig. 10). We could further demonstrate that all three different human AKT isoforms phosphorylate merlin at S10 (Fig. 11). On the other hand, we could not reproduce the results by Tang et al. (2007), which indicated that T230 and S315 would serve as AKT substrates. As can be seen in Fig. 11 mutation of T230 or S315 or combined mutation of both residues does not alter AKT catalyzed phosphorylation, whereas further mutation of S10 abolishes phosphorylation in all constructs. In additional experiments we tested, whether AKT1 associates with merlin. When we passed cell lysates containing transiently expressed AKT1 over glutathione columns containing

various GST-merlin constructs, we could show that both N- and C-terminal merlin fragment have affinity for AKT1, whereas GST does not bind AKT (Fig. 12). A further indication for a physical link was obtained with immunofluorescence microscopy, in which activated AKT partially colocalized with merlin underneath the cell membrane, whereas inactive AKT was retained in the cytoplasm (Fig. 13). In conclusion, these studies demonstrate a physical and biological interplay between merlin and the serine/threonine kinase AKT.

Most of the goals the Task "Characterization of the Src induced tyrosine phosphorylation of ezrin" were carried out, while the funding was not finalized (alternate funding status) and a report of this work has been published (Heiska and Carpen, 2005). Therefore, the results are only briefly summarized here and not included in Reportable Outcomes. The results were:

- Src phosphorylates ezrin in vitro and in vivo (Heiska and Carpen, 2005, Fig. 1 and 2).
- Residue Y477 is the major substrate of Src, whereas other residues appeared not to serve as significant substrates (Heiska and Carpen, Fig. 3). The result was confirmed *in vivo* by expressing wild type and mutant ezrin in cells, in which Src family kinase activity can be stimulated (Heiska and Carpen, Fig. 4).
- A phosphospecific antibody, which recognizes the phosphorylated ezrin Y477 residue was generated. The antibody works in immunoblotting and further confirms that Y477 is a Src substrate *in vivo* (Heiska and Carpen, Fig. 5).
- Y477 phosphorylation does not affect T566 phosphorylation or ezrin dimerization (Heiska and Carpen, Fig. 6).
- Y477 phosphorylation induces an interaction between ezrin and KTBDB2, a novel member of Kelch-protein family (Heiska and Carpen, Fig. 8).

To further analyze the role of Src induced phosphorylation of ezrin Y477, we have generated stable cell lines with various forms of ezrin with or without Src, using mouse embryonic fibroblasts (MEF) from ezrin knock-out mice (Saotome et al. 2004) as parent

cells. These cell lines were used to study, whether Src and ezrin act in concert in tumorigenesis. The results are summarized in a manuscript (Heiska et al., 2008, see appendix) and only shortly presented here.

- In two-dimensional cultures, Src induced malignant features independent of whether the MEF cells expressed WT or mutant ezrin or were ezrin deficient (Heiska et al. 2008, Figs. 2 and 3). The features included alterations in actin cytoskeleton, increased proliferation rate and changes in cell adhesion.
- However, marked differences were seen in experiments, in which cells were cultured in three dimensional environment or without possibility for matrix attachment. Whereas WT and mutant ezrin expressing cells had identical morphology on culture plates (Heiska et al. 2008, Fig. 2) they showed marked differences in three dimensional matrix, where only wild-type ezrin was targeted to specific regions on the plasma membrane (Heiska et al. 2008, Fig. 4).
- Only cells expressing WT ezrin and active Src grew efficiently in soft agar (Heiska et al. 2008, Fig. 5).
- WT but not Y477F ezrin promoted Src-induced growth in suspension (Heiska et al. 2008, Fig. 6A). Furthermore, expression of ezrin significantly promoted Src-induced growth and invasion in Matrigel, a three-dimensional extracellular matrix from mouse tumor (Heiska et al. 2008, Fig. 6B and C).

The results lead us to conclude that the pathways activated by Src depend on the type of environment and that ezrin is a crucial element of Src-induced malignant features of cells growing in three dimensional matrices. A remaining open question is, which down-stream pathways are mediating ezrin's oncogenic activities. We tested, whether cells WT ezrin/Src/MEFs and Y477F ezrin/Src/MEFs grown in methylcellulose would differ in activation of mTOR, AKT or ERK pathways. However, we could not find any differences in the expression phosphorylated p70s6 (marker of mTOR activation), phosphoAKT or phosphoERK (not shown).

Merlin and ezrin have been suggested to serve opposite functions on cell growth, possibly by controlling each others activity. The MEF cell lines characterized above (Heiska et al.) were further used to evaluate, whether merlin can suppress the oncogenic phenotype induced by active Src and ezrin. By retroviral expression technique, we introduced GFP-merlin (WT or S518A mutant thought to be constitutively tumor suppressive) or GFP into ezrin -/- +Src MEFs or add-back WT ezrin + Src MEF cells and analyzed the effect of merlin on Src/ezrin-induced malignant features in 2-D and 3-D growth conditions. The cell lines expressed merlin as verified by immunofluorescence staining and by western blotting (Fig. 14).

To analyze, whether the transduced merlin is active in MEF cells, we measured the proliferation activity of MEF cells expressing WT ezrin and active Src with or without transduced merlin. As shown in Figure 15, merlin expression reduced proliferation by approximately 30%. This reduction is in line with previous publications and demonstrates that merlin is functionally active in MEF cells.

We then tested, whether merlin can counteract the oncogenic properties induced by ezrin and Src in 3D environment. The cells were grown in Matrigel. In this assay, merlin expression did not inhibit cell growth (Fig. 16). In additional experiments, the MEF cells were seeded on collagen matrix and allowed to scatter. As shown (Heiska et al. submitted), cells expressing wild-type ezrin and active Src demonstrated a scattering phenotype as compared to cells expressing the phosphorylation deficient ezrin mutant Y477. In this assay, expression of merlin did not alter the scattering ability of either cell line. These results demonstrate that merlin is not able to counteract the oncogenic properties induced by active Src and ezrin. However, the experiments do not rule out the possibility that ezrin and merlin would directly oppose each others biological activities in other cellular models.

Previous studies have indicated that in addition to Src, the oncogenic tyrosine kinase c-Met phosphorylates ezrin (Crepaldi et al. 1997). However, the phosphorylation sites have not been identified. The hepatocyte growth factor - c-Met pathway is a major regulator of

cell invasion, which according to our data is controlled by ezrin. To further study the regulation of ezrin by kinases, we tested whether ezrin can serve as a taeget for c-Met. Using recombinant proteins we could show that c-Met phosphorylates ezrin at tyrosine 477 similarly to Src. However, the C-terminus of ezrin contains also another site, tyrosine 482 (Fig. 18). The result indicates that multiple oncogenic kinases can control ezrin's activity.

Key Research Accomplishments

- Identification of two tubulin binding sites in merlin
- Demonstration that the interaction with tubulin is regulated by intramolecular association and phosphorylation of merlin
- Demonstration that merlin regulates microtubule polymerization *in vitro* and *in vivo*
- Demonstration that microtubule cytoskeleton is markedly alterated in Schwann cells lacking merlin
- Detailed molecular characterization of the interaction between merlin and HEI10
- Demonstration that merlin regulates the integrity of HEI10 *in vivo*
- Identification of a second protein kinase A substrate residue in merlin
- mapping of the N-terminal PKA phosphorylation site to serine 10
- demonstration that serine 10 does not affect serine 518 phosphorylation, the electrophoretic mobility of merlin, or ezrin binding
- demonstration that the expression of S10D stabilizes actin filaments
- demonstration that the expression of S10A causes long extensions in cells, reduces the amount of F-actin and affects lamellipodia formation
- demonstration that PKA regulates calpain cleavage of merlin
- demonstration that activation of calpain affects the subcellular localization of merlin
- demonstration that Src induced phosphorylation of ezrin at Y477 regulates cytoskeletal organization in three dimensional environment
- demonstration that Src induced phosphorylation of ezrin at Y477 is required for colony formation of MEF cells in soft agar

- demonstration that Src induced phosphorylation of ezrin at Y477 is required for anchorage independent growth of MEF cells
- demonstration that Src induced phosphorylation of ezrin at Y477 is required for growth of MEF cells in Matrigel
- demonstration that Src induced phosphorylation of ezrin at Y477 is controls invasive capacity of MEF cells in Matrigel
- demonstration that merlin does not counteract oncogenic pathways induced by active Src and ezrin
- demonstration that cMET oncogen phosphorylates ezrin at Y477 and Y482.

Reportable Outcomes

Publications:

Grönholm M., T. Muranen, G. Toby, T. Utermark, CO. Hanemann, EA. Golemis, O. Carpén. A functional association between merlin and HEI10, a cell cycle regulator. *Oncogene* 25:4389-4398, 2006. (Due to the authors' error, this publication does not cite the current research contract W81XWH05-1-0469).

Muranen T, Grönholm M, Lampin A, Lallemand D, Zhao F, Giovannini M, Carpén O. The tumor suppressor merlin interacts with microtubules and modulates Schwann cell microtubule cytoskeleton. *Hum. Mo.l Gen.* , 16:1742-51, 2007.

Laulajainen M. [#], T. Muranen[#], O. Carpén, M Grönholm. Protein kinase A mediated phosphorylation of the NF2 tumor suppressor protein merlin at serine 10 affects actin cytoskeleton. ([#]equal contribution) *Oncogene,* 27:3233-3243, 2008.

Grönholm M. Novel Functions of the Neurofibromatosis 2 Tumour Suppressor Protein Merlin. Ph.D. Thesis, Faculty of Medicine, University of Helsinki, Finland. 2005. (Award for best thesis of the Faculty of Medicine, University of Helsinki, in 2005)

Laulajainen M. Characterization of merlin's cell-extension activity. M. Sc. Thesis. Department of Biological and Environmental Sciences, University of Helsinki, Finland. 2005.

Muranen T. The Neurofibromatosis 2 tumor suppressor merlin in cytoskeleton organization and cell cycle regulation. Ph.D. Thesis, Faculty of Medicine, University of Helsinki, Finland. 2007 (http://urn.fi/URN:ISBN:978-952-10-4253-9).

Presentations:

4-6.6. 2006. Minja Laulajainen, Carboxy-terminus regulates morphogenic activities of merlin. Poster presentation. **2006 Children's Tumor Foundation International Neurofibromatosis Consortium. Aspen, CO**.

4-6.6. 2006. Taru Muranen, Merlin interacts with microtubules in a regulated manner and affects the microtubule cytoskeleton of the mouse primary Schwann cells. Poster presentation. **2006 Children's Tumor Foundation International Neurofibromatosis Consortium. Aspen, CO.**

09-13.12.2006. Leena Heiska, Fang Zhao, Itsiko Saotome, Andrea I. McClatchey, Olli Carpén, Ezrin Promotes Src-dependent Functions Associated with Malignancy. Poster presentation **46th Annual Meeting of the American Society of Cell Biology, San Diego, CA**

10-12.6.2007. Minja Laulajainen and Taru Muranen, Regulation of Merlin by Protein Kinase A. Poster presentation. **Children's Tumor Foundation International Neurofibromatosis Consortium. Park City, Utah**.

27-30.6.2007. Taru Muranen, Regulation of Merlin by Protein Kinase A. Poster presentation. **European Cytoskeletal Forum. Dijon, France**.

11.5.2007. Taru Muranen, The tumor suppressor merlin interacts with microtubules and modulates Schwann cell microtubule cytoskeleton. Scientific talk. **The Cell Biology Club. Lammi, Finland.**

10.6.2008. Olli Carpén. Ezrin Mediates Src-Induced Malignant Phenotype in Three-Dimensional Environment via Pathways that Are Not Inhibited by Merlin. Invited talk. **2008 NF Conference**, Gen**es to Complications to Treatments Bonita Springs, Florida**

Degrees:

Grönholm M. Ph. D. degree, University of Helsinki, Finland 2005.

Muranen T. Ph.D., University of Helsinki, Finland 2007.

Laulajainen M. M. Sc. University of Helsinki, Finland, 2005.

Novel research tools:

retroviral plasmid constructs of wild-type ezrin and ezrin Y477F, ezrin Y145F and ezrin Y353F mutants for expression in mammalian cells

stable MEF cell lines expressing wild-type or mutant (Y145F, Y353F, Y477F) cell lines with or without constitutively active Src.

plasmid constructs with altered merlin S10 and S518 residues

Bimolecular fluorescence complementation, BiFC

Mutation constructs including exon 2 deletions and E545K and E547K mutations

and single and double mutants of S10 and S518

Merlin retroviral constructs

An antibody against the amino-terminus of merlin

Conclusions

The research project has advanced well in all areas related to the four main tasks. The work has resulted in several interesting observations on the biology of the NF2 tumor suppressor protein, merlin, and in three publication and one submitted manuscript. The study has contributed to three academic degrees and further two Ph.D theses (Leena Heiska, Minja Laulajainen) are expected. We have identified novel functions for merlin

as a regulator of both microtubule and actin cytoskeleton. The microtubule regulatory function is a timely finding as independent studies have indicated a role for merlin in growth factor receptor endocytosis, an event controlled by microtubules (Maitra et al. 2006). The actin organizing role is also of interest as Nf2 deficient schwannoma cells exhibit cytoskeletal anormalities manifested by morphological changes and F-actin instability (Pelton et al., 1998). Studies between merlin and HEI10 have provided findings that for the first time link merlin directly to molecules involved in cell cycle regulation.

Posttranslational modification via phosphorylation seems to be an important mechanism in the regulation of both merlin and ezrin. An additional demonstration of this was recent identification of a merlin phosphatase and demonstration that inhibition of the phosphatase prevents merlin's tumor suppressor activity (Jin et al. 2006). Our studies focus on kinase activity, the other side of the coin. The results extend previous findings on the interplay between PKA signaling pathway and merlin by identifying a second PKA phosphorylation site in merlin. PKA activity has been linked to increased proliferative potential of Schwann cells (Kim et al. 1997). In addition, our unpublished findings link another important signaling pathway, the AKT-PI3K (Ammoun et al. 2008) route to the posttranslational control of merlin. As Schwann cells are susceptible to tumor formation in NF2 disease, our findings may provide clues on the molecular pathways involved in this tumorigenetic events.

Finally, the association between Src family kinases and ezrin may prove out to be of importance for understanding of NF2 disease. Our studies on the interplay between ezrin and Src have identified ezrin as a key regulator of Src induced malignant phenotype in three dimensional environment. In fact, ezrin is the first identified molecule that controls the three most important phenotypic characteristics of malignant behavior: anchorage independent growth, proliferation and invasion in three dimensional matrix. The results may have implications in development of novel therapeutic approaches for inhibition of invasive/metastatic growth. Src activity is associated with proliferative activity of

Schwann cells, and thus the findings may have relevance in the biology of schwannomas, the hallmark tumors of NF2.

References

Alfthan K., Heiska L., Grönholm M., Renkema G.H. and Carpen O. (2004) Cyclic AMP-dependent protein kinase phosphorylates merlin at serine 518 independently of P21-activated kinase and promotes merlin-ezrin heterodimerization. *J. Biol. Chem.*, **279**, 18559-18566.

Ammoun S, Flaiz C, Ristic N, Schuldt J, Hanemann CO. (2008) Dissecting and targeting the growth factor-dependent and growth factor-independent extracellular signal-regulated kinase pathway in human schwannoma. *Cancer Res*. **68**, 5236-5245.

Crepaldi T, Gautreau A, Comoglio PM, Louvard D, Arpin M. (1997) Ezrin is an effector of hepatocyte growth factor-mediated migration and morphogenesis in epithelial cells. *J Cell Biol*. **138**, 423-434.

Heiska, L., O. Carpén. Src phosphorylates ezrin at tyrosine 477 and induces a phosphospecific interaction between ezrin and a kelch-repeat protein family member. (2005) *J. Biol. Chem***. 280**, 10244-10252.

Hu CD, Chinenov Y, Kerppola TK. (2002) Visualization of interactions among bZIP and Rel family proteins in living cells using bimolecular fluorescence complementation. *Mol Cell*. **9**, 789-798.

Jin H., Sperka T., Herrlich P. and Morrison H. (2006) Tumorigenic transformation by CPI-17 through inhibition of a merlin phosphatase. *Natur*e, **442**, 576-579.

Kaneko T, Yamashima T, Tohma Y, Nomura M, Imajoh-Ohmi S, Saido TC, Nakao M, Saya H, Yamamoto H, Yamashita J. (2001) Calpain-dependent proteolysis of merlin occurs by oxidative stress in meningiomas: a novel hypothesis of tumorigenesis. *Cancer*. **92**, 2662-2672.

Kissil J.L., Johnson K.C., Eckman M.S. and Jacks T. (2002) Merlin phosphorylation by p21-activated kinase 2 and effects of phosphorylation on merlin localization. *J. Biol. Chem.*, **277**, 10394-10399.

Kressel M, Schmucker B. (2002) Nucleocytoplasmic transfer of the NF2 tumor suppressor protein merlin is regulated by exon 2 and a CRM1-dependent nuclear export signal in exon 15. *Hum Mol Genet*. **11**, 2269-2278.

Maitra S., Kulikauskas R.M., Gavilan H. and Fehon R.G. (2006) The tumor suppressors merlin and expanded function cooperatively to modulate receptor endocytosis and signaling. *Curr. Biol.*, **16**, 702-709.

Pylkkänen L., Sainio M., Ollikainen T., Mattson K., Nordling S., Carpen O., Linnainmaa K., Husgafvel-Pursiainen K. (2002) Concurrent LOH at multiple loci in human malignant mesothelioma with preferential loss of NF2 gene region *Oncol. Rep*., **9,** 955-959.

Saotome I, Curto M, McClatchey AI. (2004) Ezrin is essential for epithelial organization and villus morphogenesis in the developing intestine. *Dev. Cell.* **6**, 855-864.

Shiraha H, Glading A, Chou J, Jia Z, Wells A. (2002) Activation of m-calpain (calpain II) by epidermal growth factor is limited by protein kinase A phosphorylation of m-calpain. *Mol Cell Biol*. **22**, 2716-2727.

Tang X, Jang SW, Wang X, Liu Z, Bahr SM, Sun SY, Brat D, Gutmann DH, Ye K. (2007) Akt phosphorylation regulates the tumour-suppressor merlin through ubiquitination and degradation. *Nat Cell Biol*. **9**, 1199-1207.

Ward JO, Reinholdt LG, Motley WW, Niswander LM, Deacon DC, Griffin LB, Langlais KK, Backus VL, Schimenti KJ, O'Brien MJ, Eppig JJ, Schimenti JC. (2007) Mutation in mouse hei10, an e3 ubiquitin ligase, disrupts meiotic crossing over. PLoS Genet. 2007 3:e139.

Appendices:

Figure legends:

Figure 1. Interaction between merlin and importins. Recombinant GST-importin α and β-subunits were produced in insect cells, purified and bound to glutathione-Sepharose beads. ^{35}S -methionine labeled full-length merlin was produced by *in vitro* translation (IVT) in rabbit reticulocyte lysates. IVT-merlin was pulled down with GST-importins and precipitates were run on SDS-PAGE. IVT produced nucleoprotein was used as a positive control with GST-importin α-5 and plain GST as a negative control. Merlin does not show preferential binding to any of the importin subunits.

Figure 2. Calpain activation results in perinuclear localization of merlin. COS-7 cells were transfected with wild type merlin. Calpain was activated and cells treated with either a calpain inhibitor Z-Llal or PKA activators Forskolin and IBMX. Cells were stained with an N- (A-19) or C-terminal (KF10) antibody to identify merlin. Calpain activation resulted in the relocalization of merlin from the membrane to the perinuclear region except for in cells treated with the calpain inhibitor, Z-Llal.

Figure 3. **Merlin mutant constructs relocalize to the perinuclear and nuclear region.** COS-7 (upper two rows) and 293HEK (lower two rows) cells were transfected with full

length merlin which contained mutations E545K+E547K and/or exon 2 deletions and stained with the merlin antibody A-19. Merlin with the E545K+E547K mutation still localizes to the membrane. Merlin relocalizes to the perinuclear region in cells with the exon 2 deletion in isoform I but not in isoform II. When exon 2 is deleted and 545 and 547 mutated, no merlin can be detected at the membrane, instead nuclear and perinuclear staining can be seen.

Figure 4. Visualization of merlin-ezrin interactions using bimolecular fluorescence complementation (BiFC) analysis. COS-7 cells were transfected with merlin wt and mutant constructs in BiFC vectors. Fluorescence is seen only in regions, where tested proteins interact. Wild-type merlin (WT)-ezrin T567D heterodimer fluorescence was associated preferentially with the plasma membrane. S10D and S518A reduced the efficiency of fluorescence complementation and resulted in unspecific localization mainly in the cytoplasm. However, the double alanine mutant (S10A+S518A) had no effect on fluorescence complementation with ezrin T567D.

Figure 5. Merlin 1-547 does not colocalize with tubulin and alters the morphology of mitotic structures. a, 293 cells stably expressing wild-type (wt) merlin or a carboxy-terminal deletion construct (1-547) were double-stained for merlin and tubulin. Wild-type merlin and tubulin colocalize in mitotic spindles in analogy with endogenous merlin. In contrast, merlin 1-547 accumulates underneath the cortical membrane without any colocalization with tubulin. **b-c,** 293HEK cells transfected with wt merlin or merlin 1-547 were evaluated for the morphology of mitotic figures. The figures were categorized as unipolar, normal or multipolar and their number was counted. Mean percentage +/- SE from four different experiments is shown. Mitotic figures of cells overexpressing wild-type merlin do not differ from control cells, whereas cells expressing merlin 1-547 have a significantly higher number of multipolar spindles. Scale bar 30 μm.

Figure 6. Lack of merlin correlates with the presence of acetylated tubulin in human malignant mesothelioma cell lines. Five patient mesothelioma cell lines were blotted for

merlin and acetylated tubulin. Mesothelioma cell lines M14 and M38 expressed merlin wheras lines M10, M25 and M146 did not. The expression of acetylated tubulin correlated negatively with and the presence of tubulin correlated positively with merlin expression. Ezrin was used as a loading control. Acetylated tubulin marks the presence of older and more rigid microtubular structures.

Figure 7. Immunocytochemical analysis of acetylated tubulin in mesothelioma cell lines. Mesothelioma cells were immunostained for acetylated tubulin. In line with immunoblotting result acetylated tubulin staining was more intensive in cells lacking merlin (cell lines M10K, M25K, M146K) as compared to those expressing merlin (M14K, M38K).

Figure 8. Analysis of HEI10 antibody produced in chicken. Polyclonal IgY antibody was produced by immunizing chicken with recombinant aGST-HEI10 fusion protein. Preliminary screening by ELISA indicated that the antiserum recognizes recombinant GST-HEI10. For further testing 293 HEK cells were transfected HA-tagged HEI10, the cells were lyzed, lysates run on SDS-PAGE and immunoblotted with chicken antiserum or with HA-antibody. The chicken HEI10 antibody (right) does not recognize the transfected HEI10, which is detected by anti-HA antibody (left).

Figure 9. Interplay between merlin phosporylation and calpain

A) GST-merlin N-terminus 1-314 (N) or the same construct phosphorylated by PKA (pN) were incubated with activated μ–calpain. Proteins were run on SDS-PAGE and immunoblotted with merlin A-19 antibody (left) or silver stained (right) for loading control. The PKA phosphorylated N-terminus was cleaved to a lesser extent than the unphosphorylated protein. B) COS-7 cells were transfected with merlin wt or mutation constructs and calpain activated. WT cells were also treated with the PKA activators Forskolin and IBMX. Cells were lysed, run on SDS-PAGE and immunblotted with A-19. Upper panel shows longer exposure time than lower panel, to detect all phosphorylation variants. Calpain activation causes the hyperphosphorylated form to disappear while the hypophosphorylated form increases, except for in cells with activated PKA.

Figure 10. Human merlin contains an Akt phosphorylation site, serine 10 at the N-terminal domain. Bacterially expressed GST-merlin fusion proteins were phosphorylated *in vitro* using γ^{33}P ATP and human recombinant Akt1/PKBα. Proteins were separated on SDS-PAGE, dried and exposed (upper panel). The Coomassie-staining shows loading of proteins (lower panel). Merlin 1-100, 1-314 and 1-547 are phosphorylated by Akt. Mutation of serine 10 to alanine abolishes the phosphorylation in all constructs. Merlin C-terminus (amino acids 492-595) is not phosphorylated by Akt.

Figure 11. Serine 10, but not threonine 230 or serine 315, is phosphorylated *in vitro* by all Akt isoforms. Bacterially expressed GST-merlin fusion proteins were phosphorylated *in vitro* using γ^{33}P ATP and different human recombinant Akt isoforms (Akt1/PKBα, Akt2/PKBβ, Akt3/PKBγ). Proteins were separated on SDS-PAGE, dried and exposed (upper panels). Coomassie-staining shows equal loadings (lower panels). Merlin 1-547 is phosphorylated by all Akt isoforms and S10A mutation abolishes the phosphorylation. Mutation of the previously characterized phosphorylation sites in mouse, threonine 230 or serine 315 does not affect the Akt phosphorylation of human merlin.

Figure 12. Merlin binds Akt1 *in vitro*. GST-merlin constructs were incubated with lysates from Akt1 transfected COS-7 cells. Bound proteins were separated on SDS-PAGE and detected with Akt Ab (upper panel) and GST Ab (lower panel). Merlin N-terminus (amino acids 1-314), merlin C-terminus (amino acids 492-595) and merlin 1-547 bind Akt1. The Akt binding affinity is not abolished by mutations of serine 10, threonine 230 or serine 315 in merlin.

Figure 13. Merlin colocalizes with activated Akt in cells. Mouse embryonic fibroblasts lacking merlin (Nf2-/- MEFs) were transiently transfected with different merlin constructs and Akt1, and either serum starved or EGF+insulin treated to activate Akt. Cells were stained for merlin (green) and Akt (red). Merlin colocalizes with activated Akt

at the cell membrane. Mutation of either serine 10 or serine 315 has no effect on merlin-Akt colocalization.

Figure 14. Characterization of Src-ezrin MEF cells tranduced with merlin constructs. Left panel shows expression of GFP-merlin after retroviral transduction. Right panel shows western blot analysis of MEF cells transduced with four different constructs. Each construct is blotted at expected size.

Figure 15. Merlin reduces the growth of Src-ezrin expressing MEF cells in 2D cultures. The tumor suppressor activity of merlin was tested using an MTT proliferation assay of MEF cells expressing wild-type ezrin+active Src and transduced with GFP-merlin and GFP-merlinS518A. Expression of merlin reduces cell growth approximately 30% in line with published results.

Figure 16. Merlin does not regulate Src-ezrin- dependent malignant features in Matrigel. The growth of Ezrin-Src MEFs with or without merlin was analyzed in Matrigel (right panel). Merlin does not reduce cell growth in 3D environment. The expression of merlin was verified by immunostaining (left panel) and western blot analysis (middle panel). In growth assay, the growth of control cells is normalized to the value of 100.

Figure 17. Merlin does not regulate Src-ezrin- dependent cell scattering phenotype. WT ezrin + active Src and Y477F ezrin + active Src expressing cells were allowed to scatter on collagen matrix. As reported (Heiska et al. submitted), WT ezrin + active Src induce cell scattering and a rounded cell phenotype. Expression of merlin does not alter the phenotype.

Figure 18. cMET phosphorylates ezrin in vitro at Y477 and Y482. The C-terminal half of ezrin (aa309-585) was expressed in *E. coli* as GST-fusion proteins, purified and phosphorylated with recombinant cMET. The kinase reactions were separated in SDS-PAGE followed by Western blotting using the indicated antibodies. Upper half: Anti-

ezrin-pY477 detects wild type ezrin phosphorylated by cMET (lane 3), but not unphosphorylated wild type ezrin (lane 1) nor phosphorylated ezrin in which an Y477F substitution has been made (lane 4). Lower half: An antibody against pTyr detects wild type ezrin, ezrin mutated in Y477 or Y482 (lanes 1-3), but not ezrin doubly mutated in both Y477 and Y482 (lane 4). The anti-GST antibody shows that equal amounts of protein were loaded in each lane.

Figures 1-18.

Articles and manuscript

Grönholm M., T. Muranen, G. Toby, T. Utermark , CO. Hanemann, EA. Golemis, O. Carpén. A functional association between merlin and HEI10, a cell cycle regulator. *Oncogene* **25**:4389-4398, 2006.

Muranen T, Grönholm M, Lampin A, Lallemand D, Zhao F, Giovannini M, Carpén O. The tumor suppressor merlin interacts with microtubules and modulates Schwann cell microtubule cytoskeleton. *Hum. Mo.l Gen.* **16**:1742-51, 2007.

Laulajainen M. [#], T. Muranen[#], O. Carpén, M Grönholm. Protein kinase A mediated phosphorylation of the NF2 tumor suppressor protein merlin at serine 10 affects actin cytoskeleton. ([#]equal contribution) *Oncogene* **27**:3233-3243, 2008.

Heiska L., F. Zhao, S. Saotome, A. McClathley, O. Carpén. Ezrin is key regulator of Src-induced malignant phenotype in three-dimensional environment. Manuscript.

Figure 1.

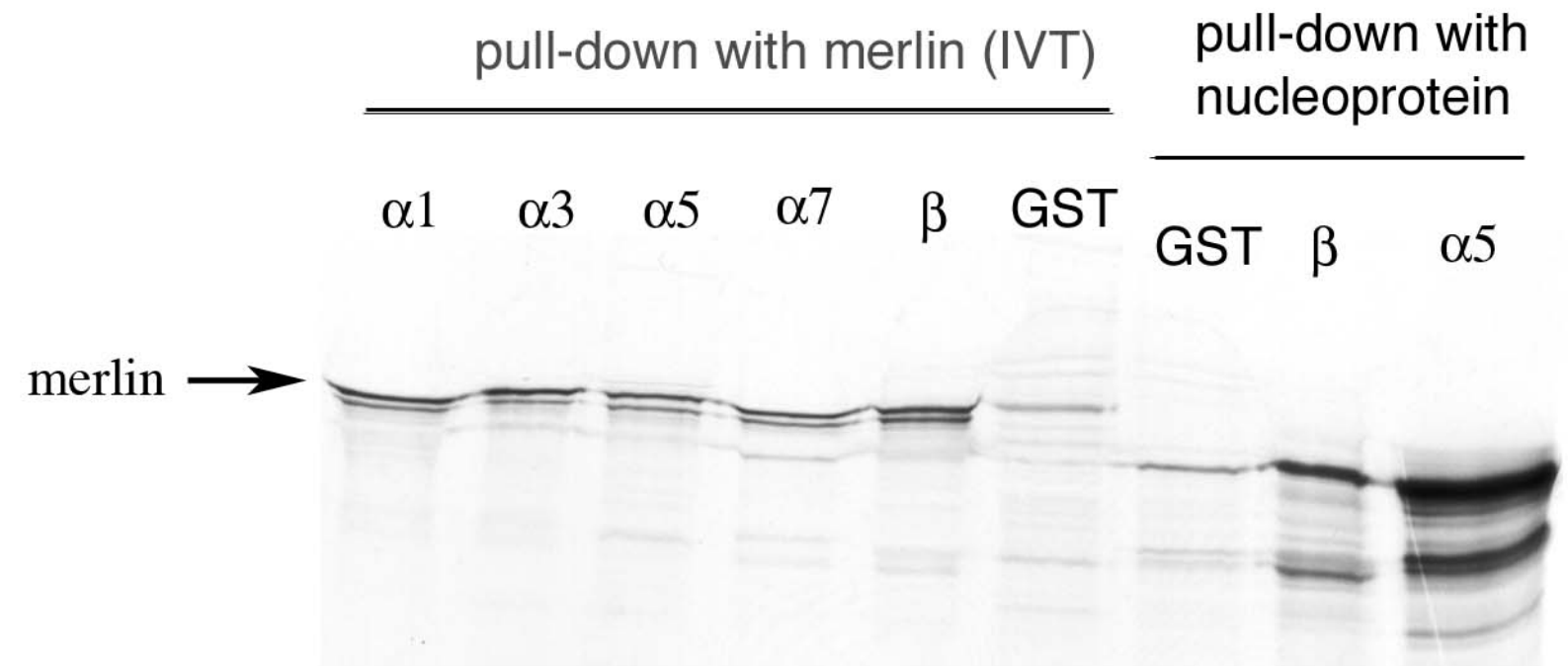
pull-down with merlin (IVT)
pull-down with nucleoprotein
α1
α3
α5
α7
β
GST
GST
β
α5
merlin

Figure 2.

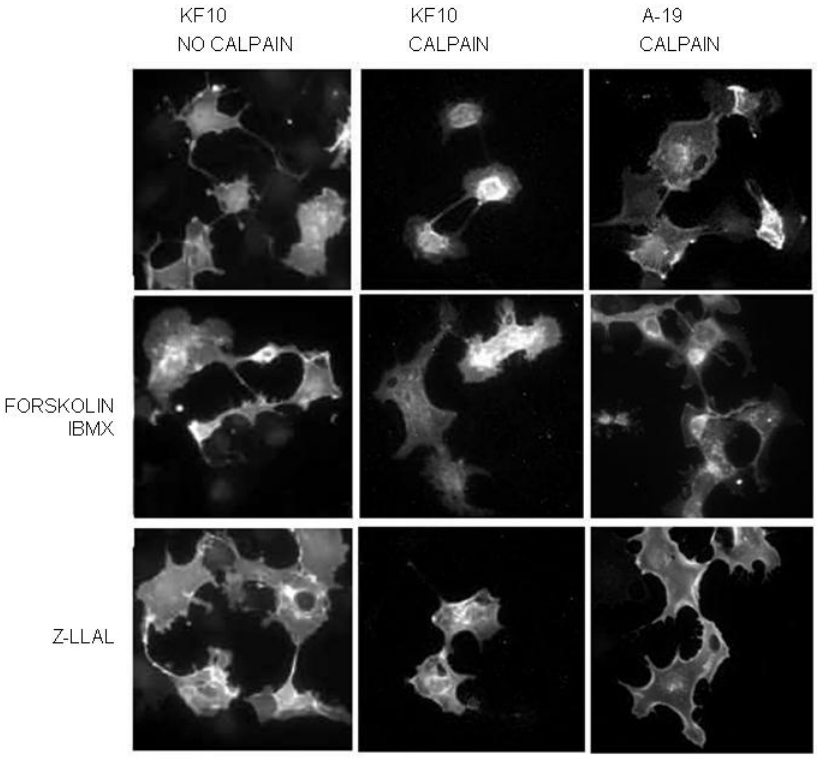
KF10
NO CALPAIN
KF10
CALPAIN
A-19
CALPAIN
FORSKOLIN
IBMX
Z-LLAL

Figure 3.

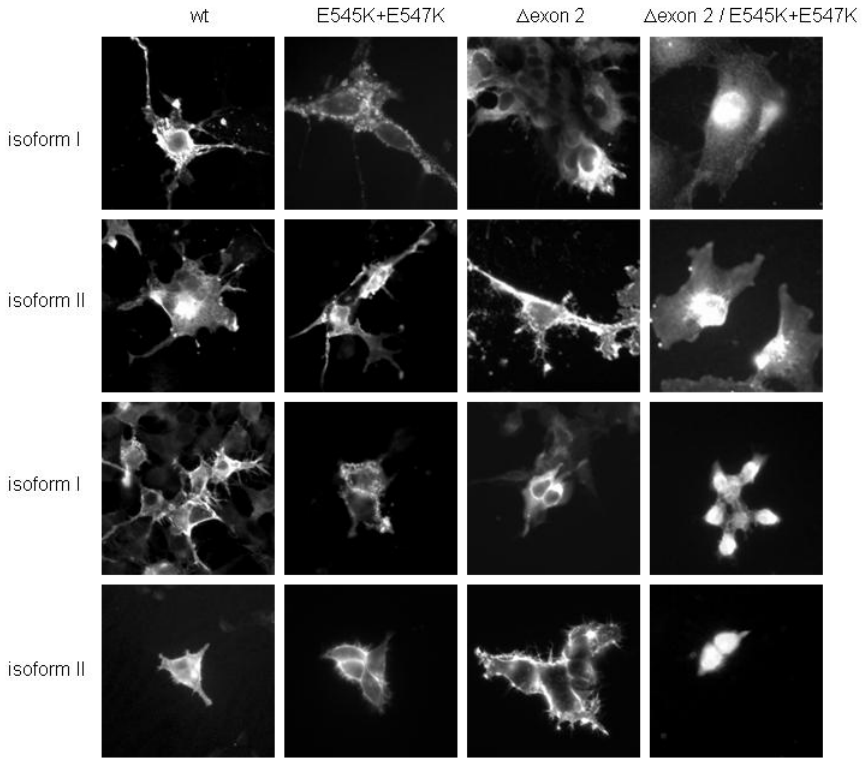
wt
E545K+E547K
Δexon 2
Δexon 2 / E545K+E547K
isoform I
isoform II
isoform I
isoform II

Figure 4.

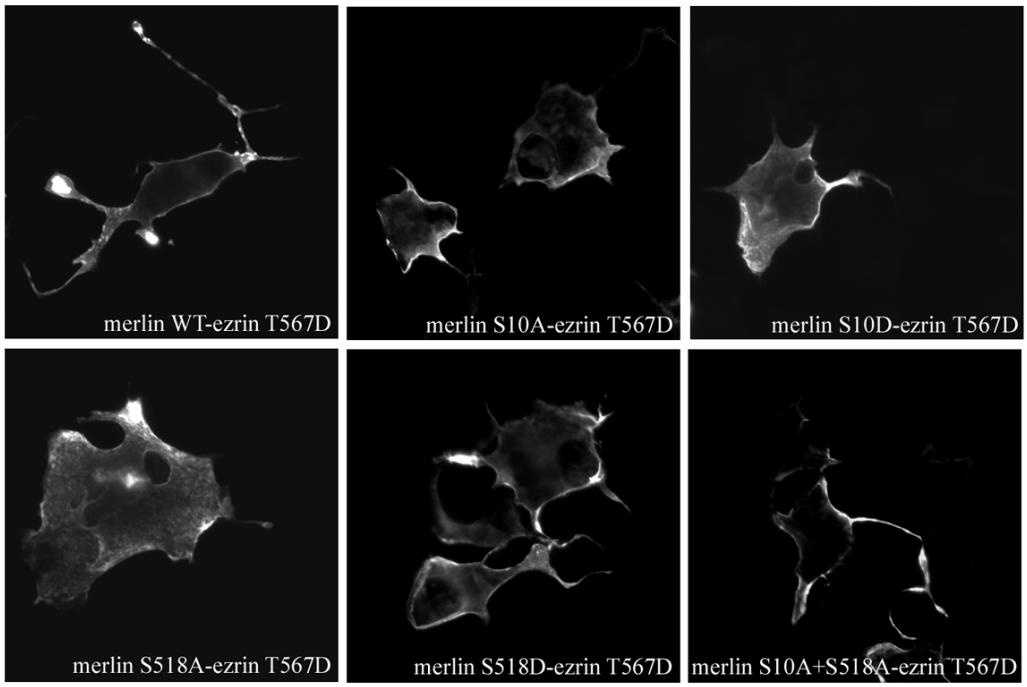
merlin WT-ezrin T567D
merlin S10A-ezrin T567D
merlin S10D-ezrin T567D
merlin S518A-ezrin T567D
merlin S518D-ezrin T567D
merlin S10A+S518A-ezrin T567D

Figure 5.

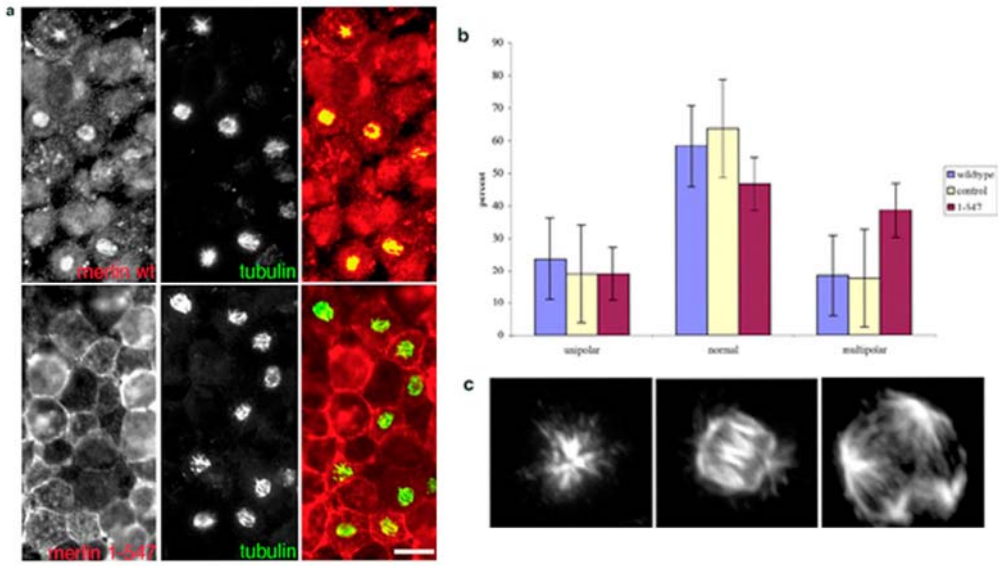
a
merlin wt
tubulin
merlin 1-547
tubulin
b
percent
90
80
70
60
50
40
30
20
10
0
unipolar
normal
multipolar
wildtype
control
1-547
c

Figure 6.

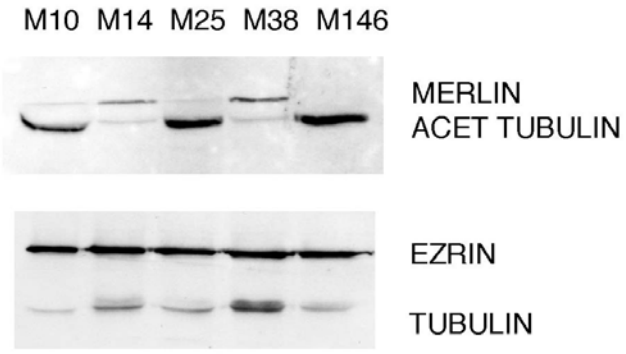

Figure 7.

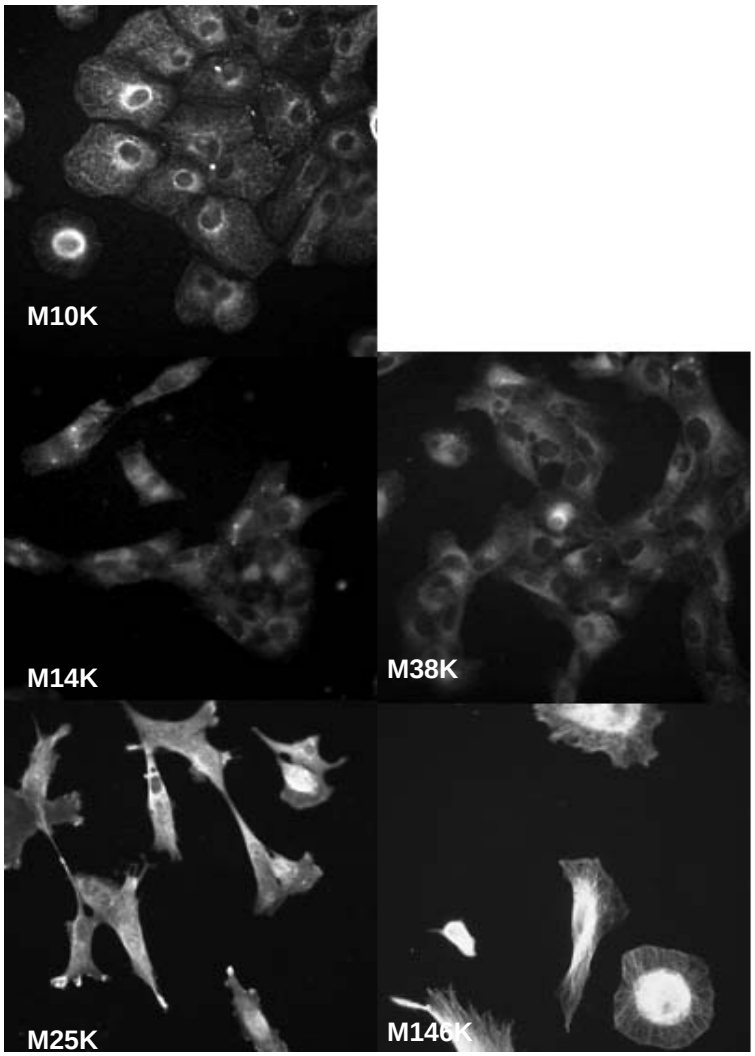

Figure 8.

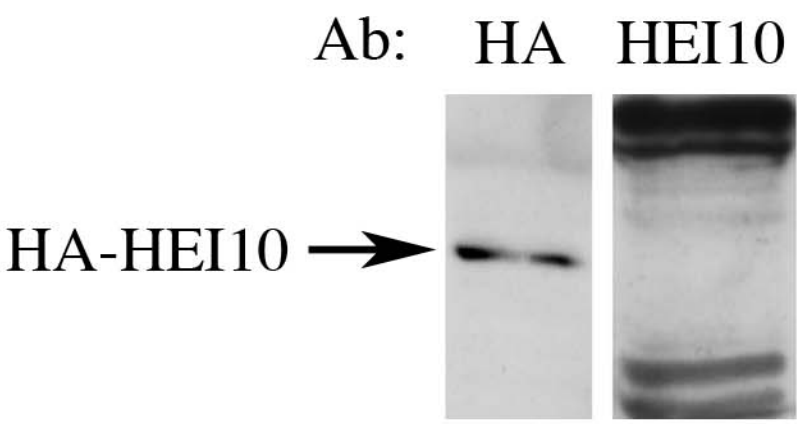

Figure 9.

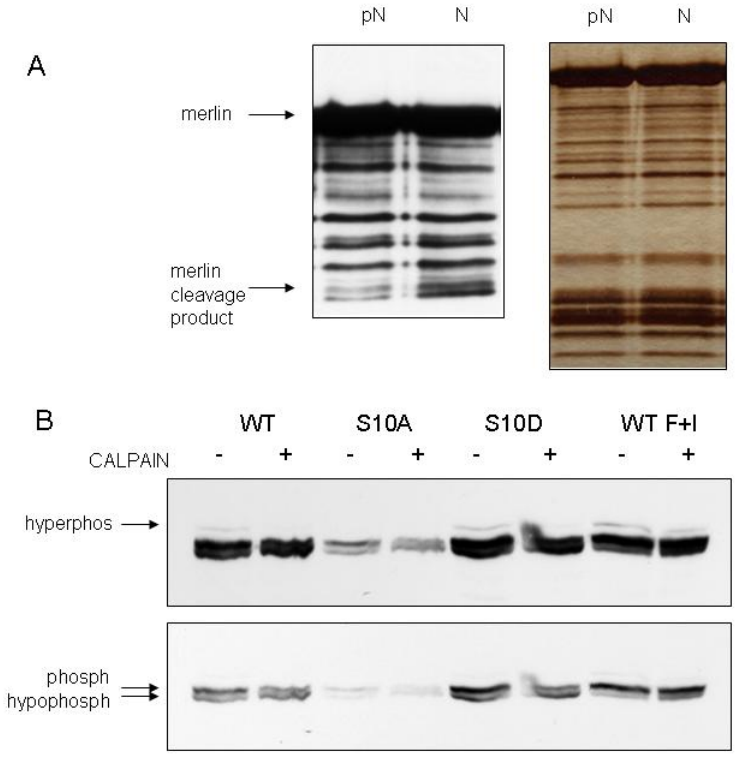
A
pN
N
pN
N
merlin
merlin
cleavage
product
B
WT
S10A
S10D
WT F+I
CALPAIN
- + - + - + - +
hyperphos
phosph
hypophosph

Figure 10

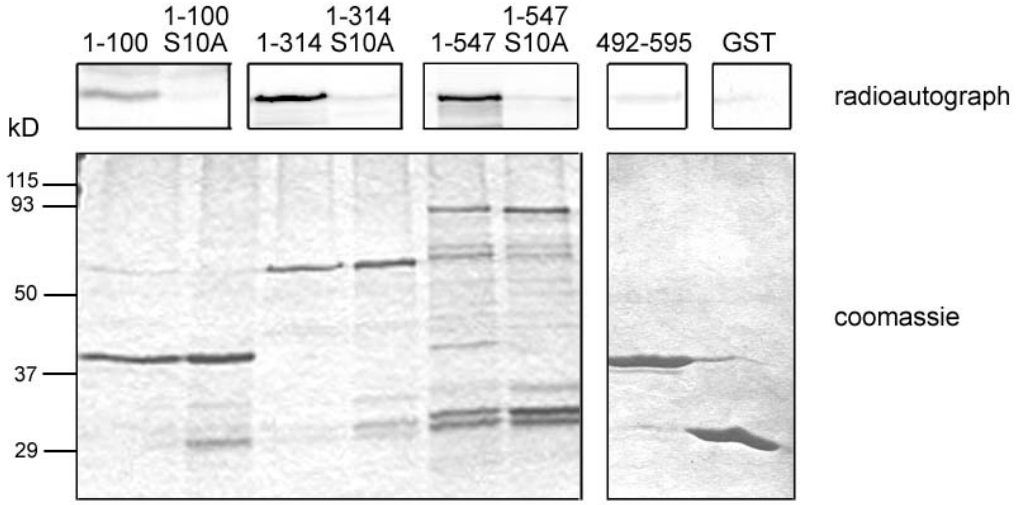

Figure 11

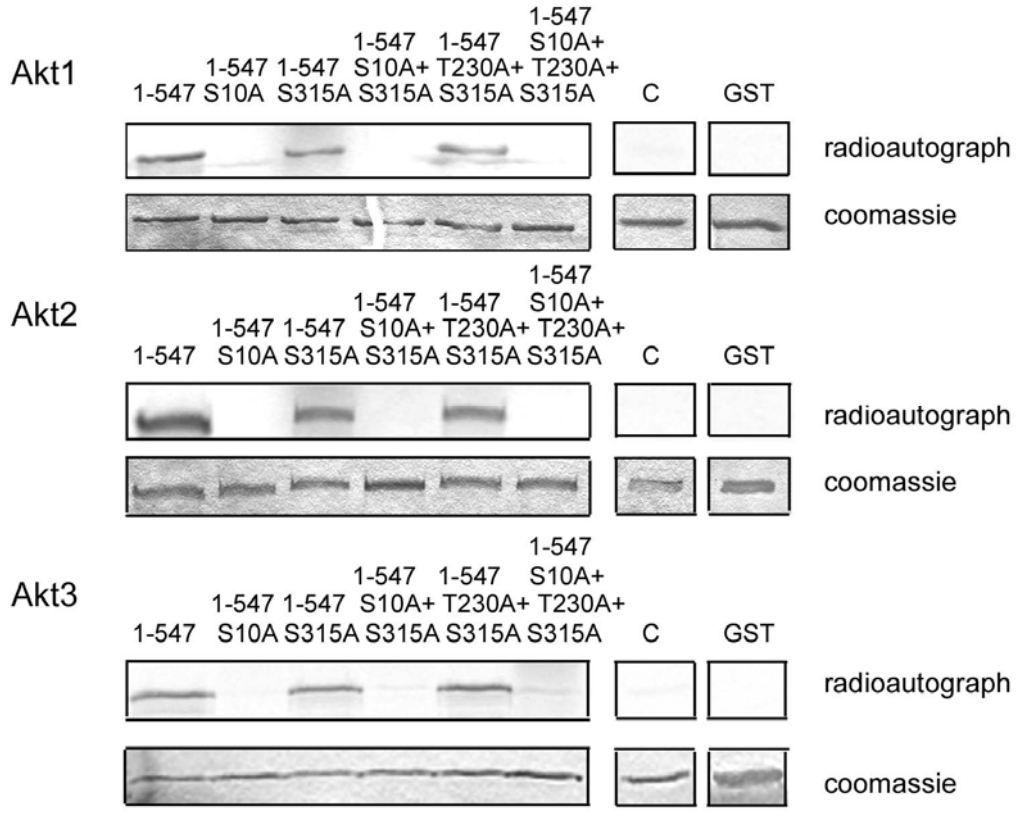

Figure 12

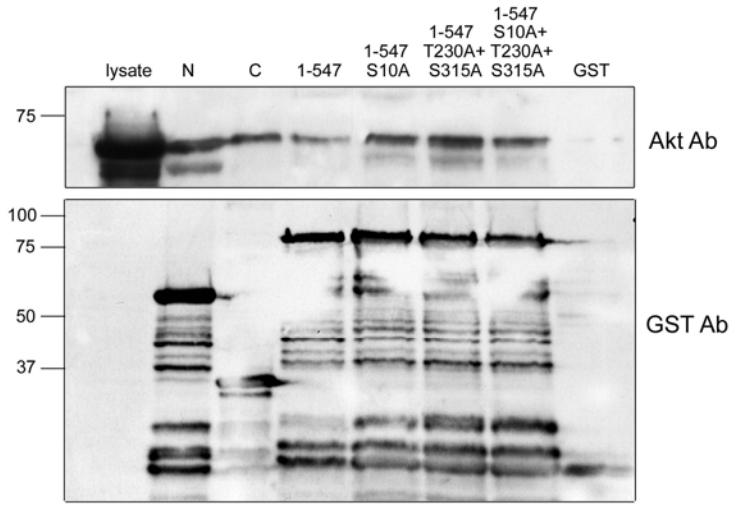

Figure 13

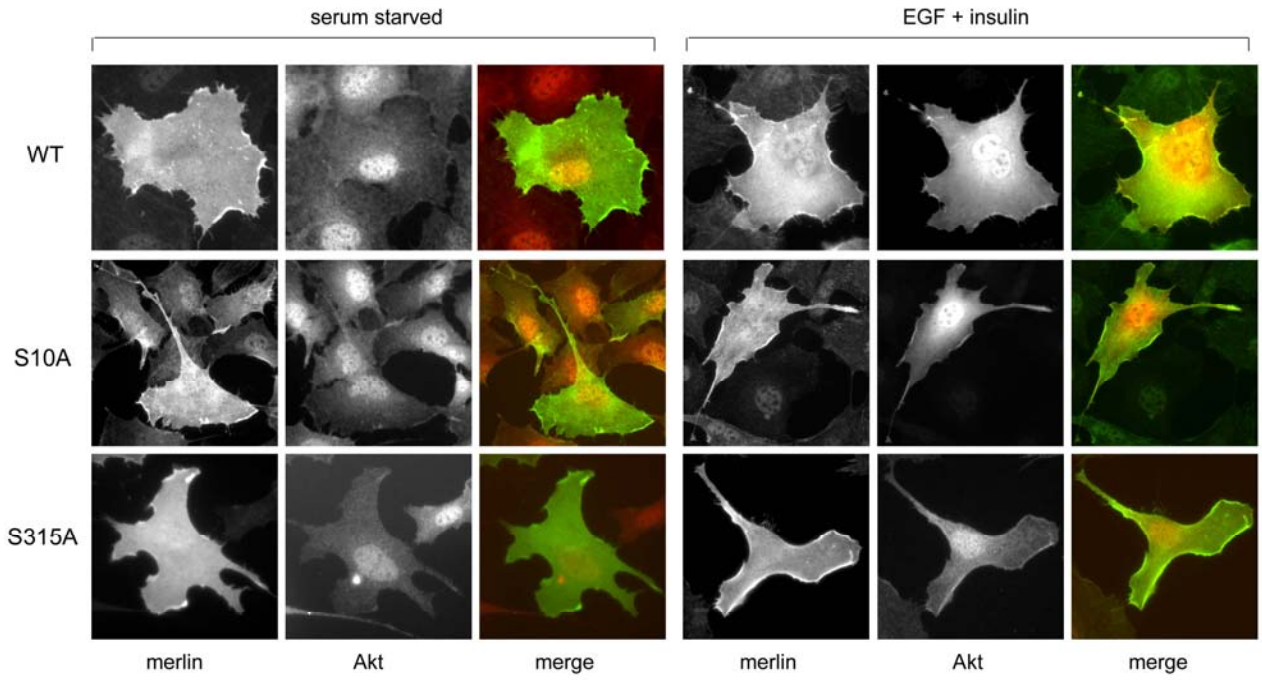

Figure 14

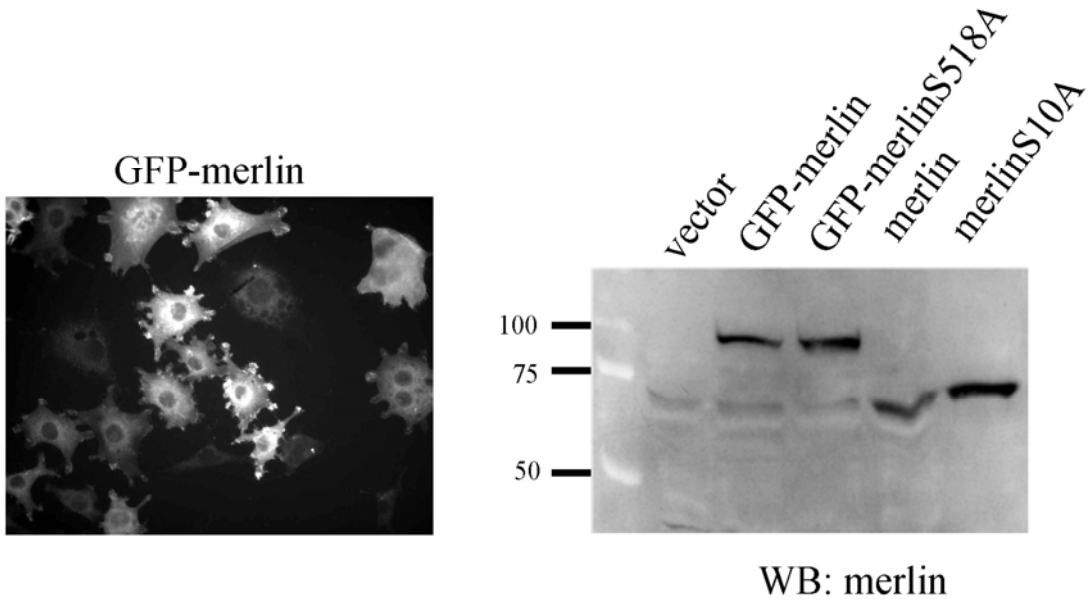

Figure 15

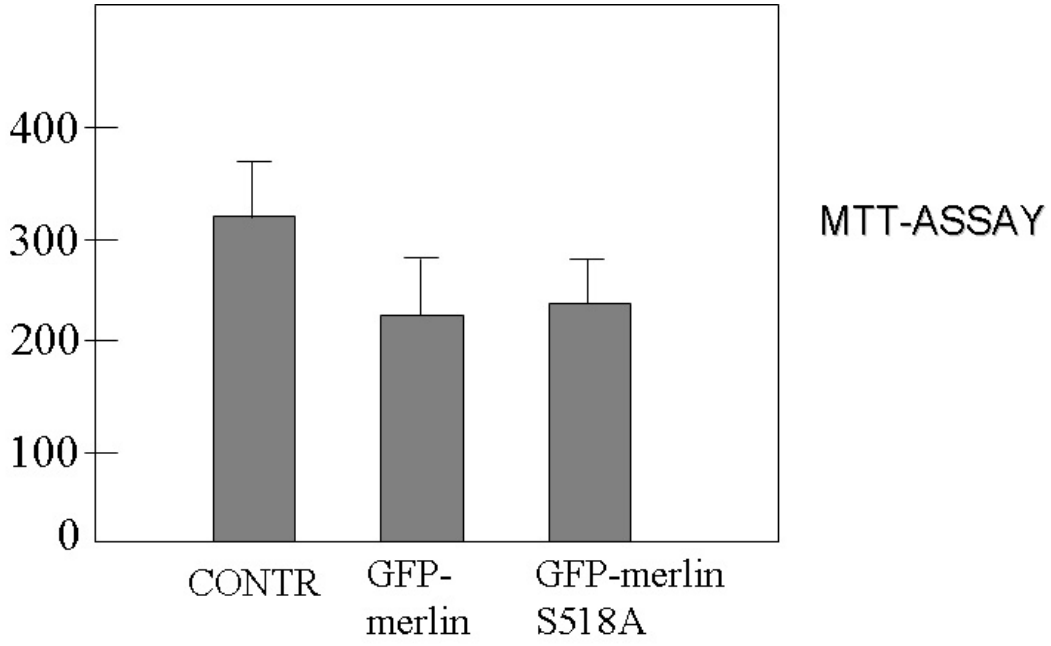

Figure 16

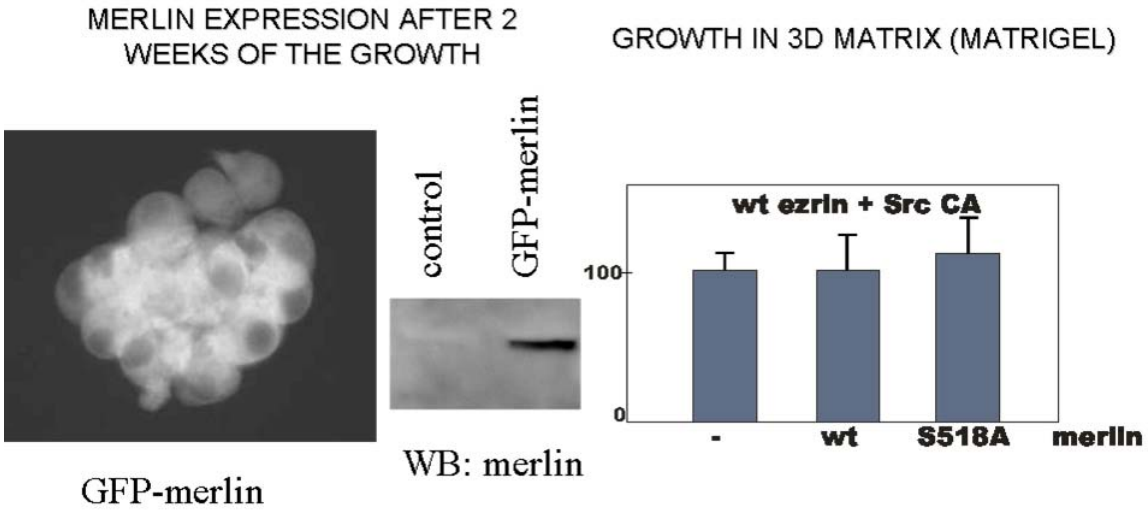

Figure 17

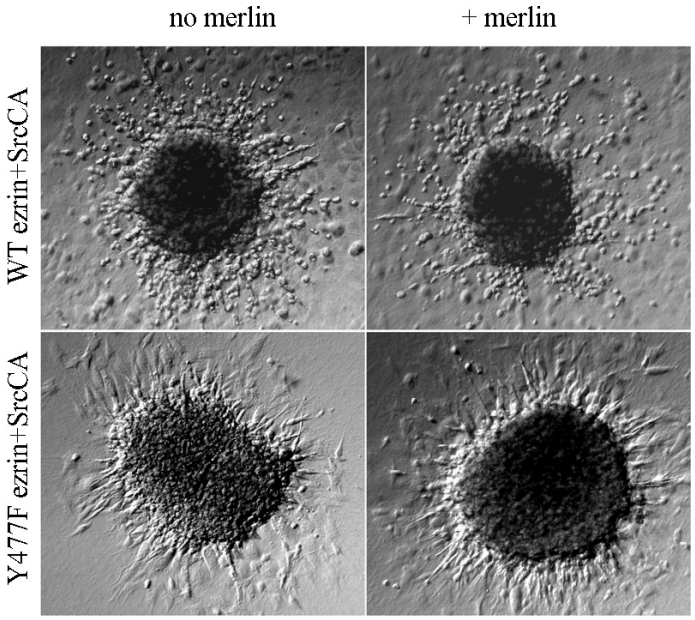

Figure 18

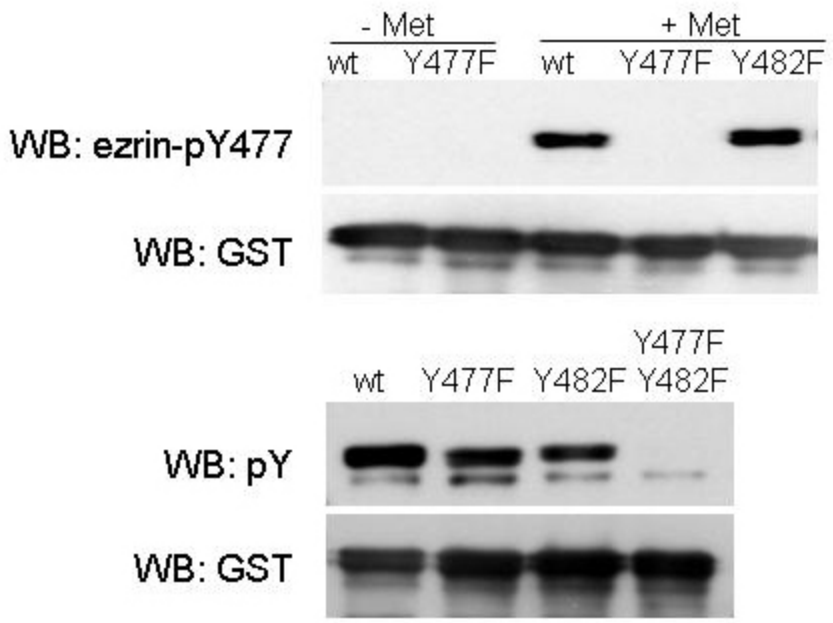
- Met
+ Met
wt
Y477F
wt
Y477F
Y482F
WB: ezrin-pY477
WB: GST
wt
Y477F
Y482F
Y477F
Y482F
WB: pY
WB: GST

Oncogene (2006) 25, 4389–4398

www.nature.com/onc

ORIGINAL ARTICLE

A functional association between merlin and HEI10, a cell cycle regulator

M Grönholm[1,6], T Muranen[1,6], GG Toby[2], T Utermark[3], CO Hanemann[4], EA Golemis[2] and O Carpén[1,5]

[1]*Neuroscience Program, Biomedicum Helsinki, Department of Pathology, University of Helsinki and Helsinki University Central Hospital, Helsinki, Finland;* [2]*Division of Basic Science, Fox Chase Cancer Center, Philadelphia, PA, USA;* [3]*Department of Neurology, University of Ulm, Ulm, Germany;* [4]*Clinical Neurobiology, Institute of Clinical and Biomedical Science, Peninsula Medical School, Plymouth, UK and* [5]*Department of Pathology, University of Turku and Turku University Hospital, Turku, Finland*

Merlin and ezrin are homologous proteins with opposite effects on neoplastic growth. Merlin is a tumor suppressor inactivated in the neurofibromatosis 2 disease, whereas upregulated ezrin expression is associated with increased malignancy. Merlin's tumor suppressor mechanism is not known, although participation in cell cycle regulation has been suggested. To characterize merlin's biological activities, we screened for molecules that would interact with merlin but not ezrin. We identified the cyclin B-binding protein and cell cycle regulator HEI10 as a novel merlin-binding partner. The interaction is mediated by the alpha-helical domain in merlin and the coiled-coil domain in HEI10 and requires conformational opening of merlin. The two proteins show partial subcellular colocalization, which depends on cell cycle stage and cell adhesion. Comparison of Schwann cells and schwannoma cultures demonstrated that the distribution of HEI10 depends on merlin expression. In transfected cells, a constitutively open merlin construct affected HEI10 protein integrity. These results link merlin to the cell cycle control machinery and may help to understand its tumor suppressor function.
Oncogene (2006) **25,** 4389–4398. doi:10.1038/sj.onc.1209475; published online 13 March 2006

Keywords: NF2; ERM; HEI10

Introduction

Inherited mutations of the neurofibromatosis 2 (*NF2*) gene, which encodes for merlin, result in the development of numerous nervous system tumors; schwannomas, meningiomas and ependymomas, in the dominantly inherited NF2 disease (Louis *et al*., 1995). Biallelic *NF2* gene inactivation has also been demonstrated in other tumor types, especially mesotheliomas (Arakawa *et al*., 1994; Pineau *et al*., 2003). The NF2 tumor suppressor protein merlin (schwannomin) is related to the ezrin–radixin–moesin (ERM) protein family. Ezrin–radixin–moesin proteins are associated with the actin cytoskeleton and cell membrane components and are involved in membrane structure morphogenesis, cell adhesion, membrane traffic, cell signaling and the regulation of cell growth (Bretscher *et al*., 2002).

Inter- and intramolecular associations regulate merlin's functions and interactions with other proteins (Gonzalez-Agosti *et al*., 1999; Grönholm *et al*., 1999). Two types of kinases, PAK-1/2 and PKA have been shown to phosphorylate merlin at serine 518 and regulate its activity (Kissil *et al*., 2002; Xiao *et al*., 2002; Alfthan *et al*., 2004), but it is still unclear, whether the phosphorylation is sufficient to release the intramolecular bond between the N-terminal FERM domain and the C-terminus.

In spite of many studies, the tumor suppressor function of merlin is not yet understood. Some evidence indicates that merlin is involved in cell cycle control. Overexpression of merlin can inhibit cell proliferation (Lutchman and Rouleau, 1995; Sherman *et al*., 1997; Gutmann *et al*. 1999) and transfection of merlin into primary schwannoma and mesothelioma cells reduces proliferation and promotes G0/G1 arrest (Schulze *et al*., 2002; Xiao *et al*., 2005). Conversely, suppression of merlin in tumor cells induces proliferation (Huynh and Pulst, 1996) and a targeted disruption of the *NF2* gene results in increased cell proliferation and tumor formation (McClatchey, 2003). In accordance with a role for merlin in cell cycle regulation, we recently demonstrated cell cycle-dependent nucleo-cytoplasmic shuttling of merlin (Muranen *et al*., 2005). To get insight into merlin's mechanism of action in cell cycle control we exploited the fact, that in spite of structural homology, overlapping subcellular distribution, direct association and partially overlapping protein interactions, merlin and ezrin exert opposite effects on cell growth. Indeed, increased expression of ezrin is associated with enhanced cell growth and poor prognosis of malignant tumors (Geiger *et al*., 2000; Mäkitie *et al*., 2001; Khanna *et al*., 2004; Tynninen *et al*., 2004; Ilmonen *et al*., 2005). To provide clues on how merlin exerts its growth regulatory activity, we therefore sought to identify binding partners which are specific for merlin or ezrin.

Correspondence: Dr M Grönholm, Neuroscience Program, Biomedicum Helsinki, Haartmanink. 8, PB 63, Helsinki 00014, Finland.
E-mail: mikaela.gronholm@helsinki.fi
[6]These authors contributed equally to this work.
Received 4 October 2005; revised 16 December 2005; accepted 10 January 2006; published online 13 March 2006

HEI10 is a recently identified cell cycle regulator in both yeast and vertebrate cells (Toby *et al*., 2003). HEI10 encodes a 277 amino-acid protein, which consists of an N-terminal RING-finger motif characteristic of E3 ubiquitin ligase, a coiled-coil domain and a C-terminal domain with a VSPSR motif, which is phosphorylated by cyclin B/cdc2. The N-terminal part of HEI10 interacts with the UbcH7 E2 ubiquitin conjugating enzyme and both interacts with and controls the accumulation of cyclin B, a key protein in cell cycle control (Toby *et al*., 2003). The *HEI10* gene is a component of a translocation fusion to the *HMG1C* gene in uterine leiomyoma (Mine *et al*., 2001) and altered HEI10 expression has been seen in melanomas (Smith *et al*., 2004). These results imply that the deregulation of HEI10 may have consequences for tumor development. Here, we provide *in vitro* and *in vivo* evidence of a direct interaction between merlin and HEI10 and a role for merlin in regulation of HEI10 expression.

Results

Interaction of merlin and HEI10

To identify novel interaction partners specific for merlin but not ezrin we performed a yeast two-hybrid screen of a HeLa cell library using merlin 252–595 as bait. This construct was chosen instead of the full-length protein, since previous studies have shown that N- or C-terminally truncated merlin mimics an open conformation, where binding sites to other proteins are accessible (Grönholm *et al*., 1999). The screen identified HEI10 as a novel binding partner for merlin. In a mating assay merlin constructs 1–546 and 252–595, but not ezrin constructs 1–309 and 278–585, interacted with HEI10 (Figure 1a). To further study the interaction, *in vitro* binding assays were performed. *In vitro* translation (IVT)-produced merlin 1–595 (wt) or merlin 1–547, which have previously been shown to mimic a constitutively open conformation (Grönholm *et al*., 1999), was mixed with glutathione-coupled glutathione *S*-transferase (GST)-HEI10 46–277 or GST and bound proteins detected with SDS–PAGE and autoradiography. Glutathione *S*-transferase-HEI10 46–277 but not GST alone pulled down merlin 1–547 and merlin 1–595. In a reciprocal experiment, GST-merlin 1–547 but not GST alone pulled down IVT-produced HEI10 1–277 (wt) (Figure 1b).

In an additional interaction test, HA-tagged merlin and ezrin constructs were produced in yeast and yeast lysates were used for pull down assays with glutathione-bound GST-HEI10 46–277. Glutathione *S*-transferase-HEI10 46–277 pulled down merlin constructs 1–546 and 252–595, both of which contain the alpha-helical part of merlin. Full-length merlin or merlin constructs containing only the N-terminal domain 1–314 or the C-terminal domain 492–595, were not precipitated by GST-HEI10 46–277 (Figure 1c, for domain structure see Figure 3). Again, no association was seen between ezrin and HEI10.

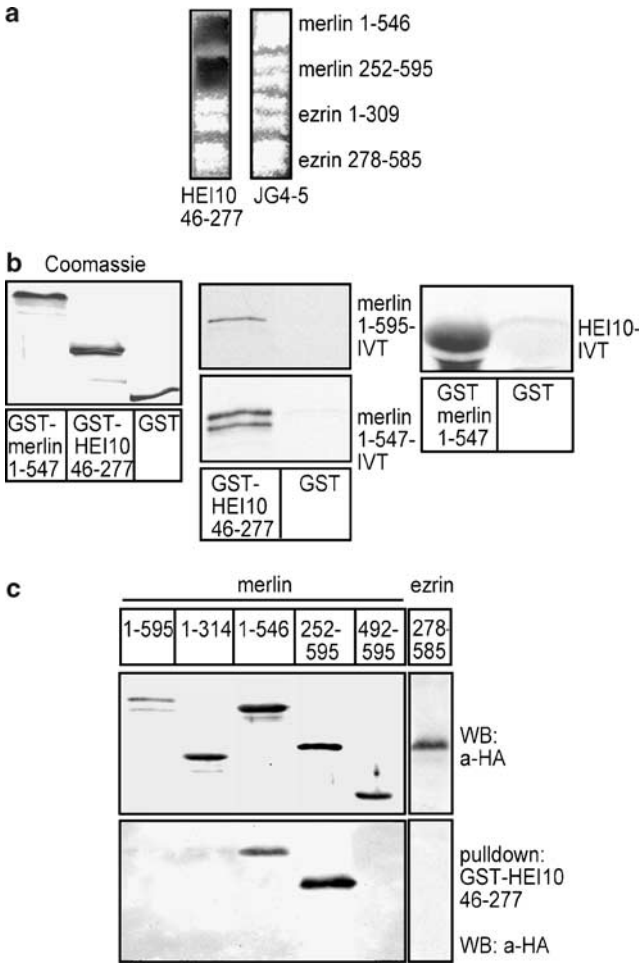

Figure 1 Interaction studies of merlin and HEI10. (**a**) A yeast two-hybrid analysis of the interaction between merlin and HEI10. Both merlin baits interact with HEI10 46–277, whereas ezrin baits show no reactivity. The empty vector JG4-5 was used as a control. (**b**) Interaction between glutathione *S*-transferase (GST)-fusion constructs and *in vitro* translated proteins. Left panel shows Coomassie blue staining of purified GST-tagged merlin 1–547 and HEI10 46–277 constructs. In middle panel, *in vitro* translated merlin 1–595 (wt) or 1–547 were incubated with glutathione agarose-coupled GST-HEI 46–277 or GST alone. Bound protein was detected with autoradiography. Right panel, shows a reciprocal experiment in which *in vitro* translated HEI10 1–277 was allowed to bind GST-merlin 1–547 or GST containing beads. (**c**) HA-tagged merlin and ezrin constructs were produced in yeast and their expression verified with anti-HA monoclonal antibody (mAb) (left panel). Lysates from yeast expressing HA-tagged merlin and ezrin constructs were incubated with glutathione agarose-coupled GST-HEI10 46–277. Bound proteins were detected using the anti-HA mAb (right panel).

The HEI10 rabbit antiserum is not functional in immunoprecipitations. Therefore, to study whether merlin and HEI10 interact in cells, 293HEK cells stably expressing merlin 1–595 (wt) or merlin 1–547 were transfected with HA-tagged HEI10. Cells were lysed 24 h after transfection and lysates immunoprecipitated with anti-HA monoclonal antibody (mAb). Filters were immunoblotted with merlin antibody or with anti-HA mAb. Merlin 1–547 (Figure 2b), but not merlin wild type (wt) (Figure 2a), could be coprecipitated with HA-HEI10.

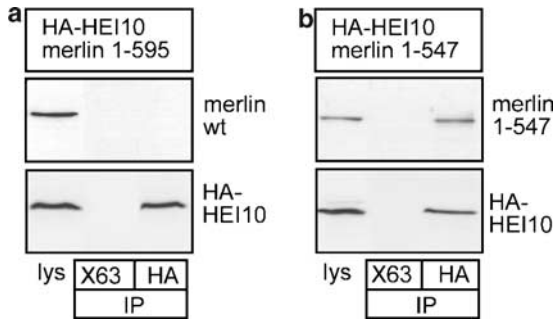

Figure 2 Coimmunoprecipitation of merlin and HEI10 from 293HEK cells. 293HEK cells stably expressing merlin wild type (wt) (**a**) or merlin 1–547 (**b**) were transfected with HA-HEI10. 24 h after transfection cells were lysed (lys) and used for immunoprecipitation with X63 control monoclonal antibody (mAb) or HA mAb. Precipitated proteins were detected with merlin A19 rabbit antiserum or anti-HA mAb.

Mapping of the merlin and HEI10 interaction sites

The yeast two-hybrid method and various merlin and HEI10 deletion constructs and mutants were used to further map the interaction sites in merlin and HEI10. Only constructs containing the alpha-helical region of merlin interacted with HEI10 (Figure 3a). The region between merlin 306 and 339 contained critical residues, since the alpha-helical sequence 306–478 bound HEI10, but the N-terminal construct 1–314 or C-terminal construct 339–595 did not. A HEI10 construct containing the coiled-coil domain (residues 116–200) was sufficient for the interaction, while neither the N-terminal RING-finger domain nor the C-terminal domain containing the cyclin B/cdc2 phosphorylation site bound merlin. Binding was retained in merlin 252–595 with patient missense mutations L316T or L316W, or an amino-acid substitution (A468P), which completely disrupts the PKA-RIβ-binding site (Grönholm *et al*., 2003).

To further map the interaction site we created a transposon mutation library of merlin 1–546 with randomly introduced 15 bp in-frame insertions, each encoding five extra amino acids. Constructs were tested against HEI10 1–200 binding in the yeast two-hybrid system. Seven independent insertions within amino acids 275–326 disrupted binding of merlin to HEI10. Four of these insertions; at amino acids 306, 307, 318 and 326 localized within the previously mapped critical region, while two (275 and 283) were localized immediately before the interaction domain. One insertion within this region, at amino acid 277, did not affect binding. None of the other insertions prior to amino acid 275 at the end of the FERM-domain or the more C-terminal part of the alpha-helix affected HEI10 binding (Figure 3b).

Distribution of merlin and HEI10 in osteosarcoma cells

We recently demonstrated that the subcellular distribution of merlin is altered during adhesion and cell cycle progression in many cell types including U2OS osteosarcoma cells, which express both merlin (Muranen *et al*., 2005) and HEI10 (Toby *et al*., 2003). To evaluate

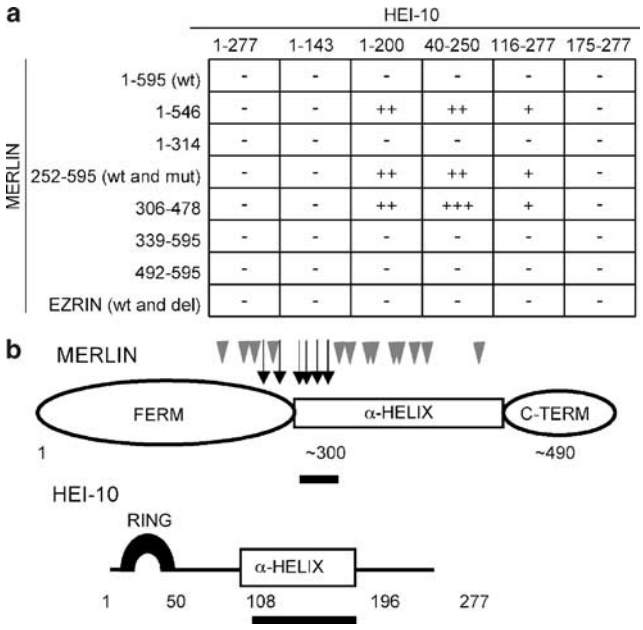

Figure 3 Interaction analysis of merlin and HEI10 using the yeast two-hybrid system. (**a**) Merlin bait constructs were tested against HEI10 prey constructs for interactions in a yeast two-hybrid mating assay. Numbers represent amino acids, + − +++ indicate weak to strong color reaction, a marker of an interaction and − indicates lack of interaction. Merlin 252–595 includes the normal construct and one with an introduced PKA-binding site mutation A468P as well as known patient mutations L316W and L316F, which all bound with identical strength. Ezrin represents 1–585 (wt) and deletion constructs (del) 1–309 and 278–585. (**b**) A mutation library of merlin two-hybrid construct 1–546 with randomly introduced 5 amino-acid insertions was used to test the interaction with HEI10 1–200 in a yeast two-hybrid mating assay. Insertions in positions indicated by black arrows abolished the interaction with HEI10 and grey arrowheads represent insertions that do not alter the interaction. Black bars underneath merlin and HEI10 represent the critical residues required for binding; merlin amino acids 306–339 and HEI10 116–200, based on the constructs used.

whether merlin and HEI10 are targeted in a similar fashion, cells were trypsinized and allowed to reattach. During early reattachment, both merlin and HEI10 were localized to the nucleus (Figure 4a). However, as cells started to spread, merlin and HEI10 could be seen in punctuate structures at the plasma membrane. At this stage, a significant fraction of HEI10 was still present in the nucleus but most of the merlin immunoreactivity had exited the nucleus (Figure 4b). When the cells were more fully spread, merlin and HEI10 could be seen in the submembranous compartment and diffusely in the cytoplasm (Figure 4c).

The colocalization of merlin and HEI10 in U2OS cells is dependent on cell cycle stage

In order to study the localization of HEI10 at different phases of the cell cycle, subconfluent U2OS cells were synchronized using nocodazole or mimosine treatment. FACS analysis was used to confirm the efficiency of synchronization and to monitor the cell cycle phase after block release (not shown). This experiment revealed that

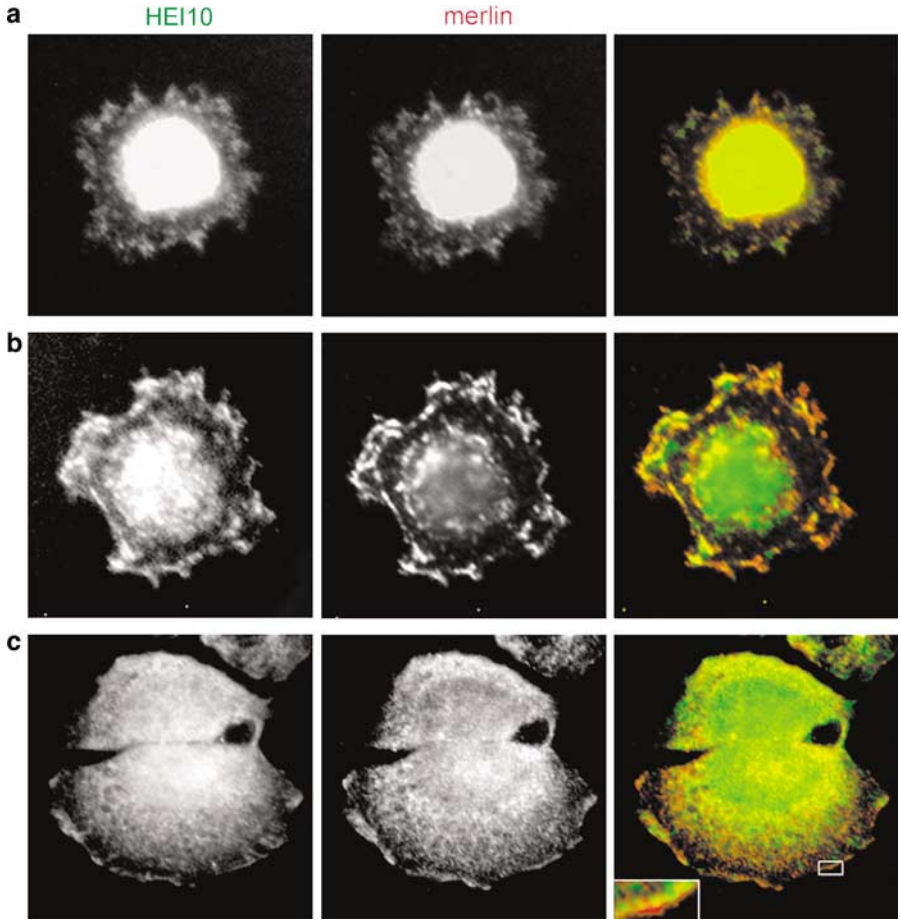

Figure 4 Localization of merlin and HEI10 in osteosarcoma cells. U2OS cells expressing endogenous merlin and HEI10 were trypsinated and allowed to reattach for 30 min (**a**), 1 h (**b**) or 2 h (**c**). Cells were fixed and stained with merlin IC4 monoclonal antibody (mAb) and HEI10 rabbit antiserum and images taken with an epifluorescence microscope. Both proteins are present primarily in the nucleus as cells are attaching. HEI10 persists in the nucleus longer than merlin during reattachment and spreading. A partial colocalization, particularly at the membrane (inset), can be seen in fully spread cells.

HEI10 localization varied in a cell cycle-specific manner. HEI10 colocalized with merlin in some but not all stages of the cell cycle (Figure 5). In early G1 merlin and HEI10 were present in the nucleus but both proteins rapidly disappeared from the nucleus as cells progressed in G1. HEI10 returned to the nucleus in S-phase, remaining in this compartment until mitosis. In contrast, merlin remained at the cell periphery until late G2, at which state the protein accumulated in the perinuclear region. During the entire cell cycle a fraction of both proteins could also be found at the membrane. We recently showed that merlin is concentrated in the mitotic spindle of dividing cells and to the midbody during cytokinesis (Muranen *et al*., 2005). In U2OS cells stained for HEI10, tubulin and DNA, also HEI10 associated with microtubules at the mitotic spindle and the contractile ring (Figure 5).

The localization of HEI10 is dependent on merlin expression level

To study if the distribution of HEI10 is dependent on the expression level of merlin, we compared the RT4 rat schwannoma cell line with a merlin-inducible RT4-5-4 variant (Figure 6). RT4 cells express very low amounts of merlin, but expression of merlin can be induced with doxycycline in RT4-5-4 cells. In RT4 cells, HEI10 was seen in nuclei and diffusely in the cytoplasm, while weak merlin reactivity was detected underneath the cell membrane. RT4-5-4 cells with induced merlin expression showed a different HEI10 staining pattern. In some cells merlin and HEI10 colocalized in extensions and at the membrane (Figure 6f). In around 10% of RT4-5-4 cells (an estimation from 500 counted cells) the nucleus was completely devoid of merlin and HEI10 (Figure 6f and f′). Cells, in which merlin expression was not induced demonstrated strong nuclear HEI10 reactivity (Figure 6f and f″).

HEI10 localization was also studied in primary human schwannoma and Schwann cell cultures, which by immunoblotting were verified to express HEI10 (not shown). In schwannoma cells, which do not express merlin due to biallelic *NF2* gene inactivation, HEI10 was frequently localized the nucleus (Figure 6h) in line with rat schwannoma cells. On the other hand, in Schwann cells, which express merlin (not shown) HEI10

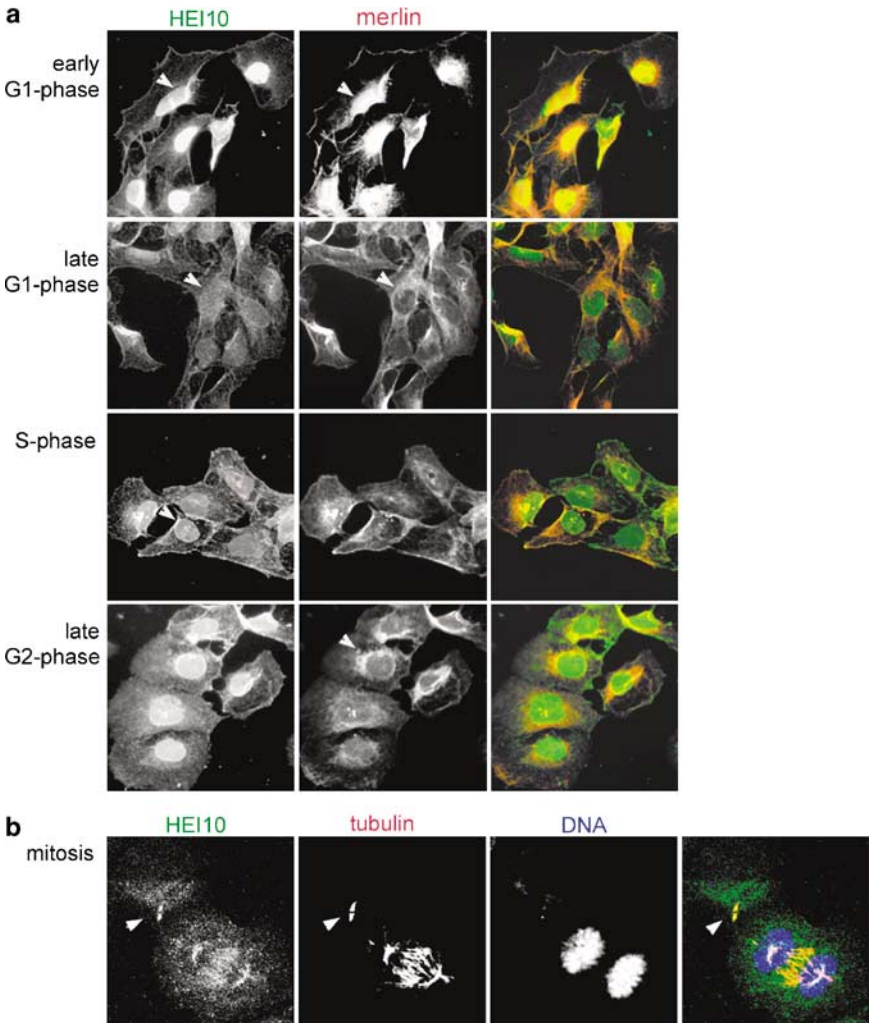

Figure 5 Localization of merlin and HEI10 at different stages of the cell cycle. (**a**) U2OS cells were synchronized using nocodazole or mimosine treatment and the block was released. Cells in early and late G1, S and late G2 phase were stained with merlin 1C4 monoclonal antibody (mAb) and HEI10 rabbit antiserum and images taken with an epifluorescence microscope. Nuclear merlin and HEI10 can be seen at early G1 (arrows) after which nuclear merlin and most nuclear HEI10 disappear (arrows). HEI10 shuttles into the nucleus at the onset of S phase (arrow) where it is present until mitosis, while merlin accumulates perinuclearly at late G2 phase (arrow). (**b**) Mitotic cells were stained with HEI10 rabbit antiserum, tubulin mAb and DAPI to detect DNA and images taken with a confocal microscope. HEI10 can be seen in the mitotic spindle of a dividing cell and the contractile ring in a cell undergoing cytokinesis (arrow).

mainly localized to the submembranous region (Figure 6g).

The interaction with merlin affects HEI10 protein levels

In order to gain insight into the potential functional interplay between merlin and HEI10, 293HEK cells were transfected with HA-HEI10 and merlin constructs 1–595 (wt), 1–547, 1–314 or 492–595, and expression levels of HEI10 and merlin assessed 72 h after transfections (Figure 7a). Similar amounts of HEI10 were detected in cells coexpressing an empty pcDNA3 vector, merlin 1–314 or 492–595. However, cells coexpressing merlin 1–547 demonstrated a significantly reduced amount of HEI10 ($P = 0.0004$), and a minor decrease was seen in cells coexpressing merlin 1–595 (wt) ($P = 0.019$). Quantification of five experiments indicated an average 59% reduction of HEI10 in cells coexpressing merlin 1–547 in comparison to control cells, and a 23% reduction in cells coexpressing merlin 1–595 (wt). To study whether binding to merlin is a requirement for the decrease, we tested the merlin 1–547 construct with an insertion at position 307, 1–547/ins307, which abolished HEI10 binding in the yeast two-hybrid experiment. Merlin 1–547/ins307, 1–547 or 1–595 (wt) was co-transfected with HEI10. In contrast to merlin 1–547, which resulted in a significant decrease of the HEI10 protein, the effect of 1–547/ins307 on HEI10 protein levels was much weaker, but comparable to that of merlin 1–595 (wt) (Figure 7b), although all merlin constructs were expressed at similar levels.

To study the time dependence of merlin-induced degradation of HEI10, 293HEK cells were transfected with merlin 1–547 and HA-HEI10, and lysed at various

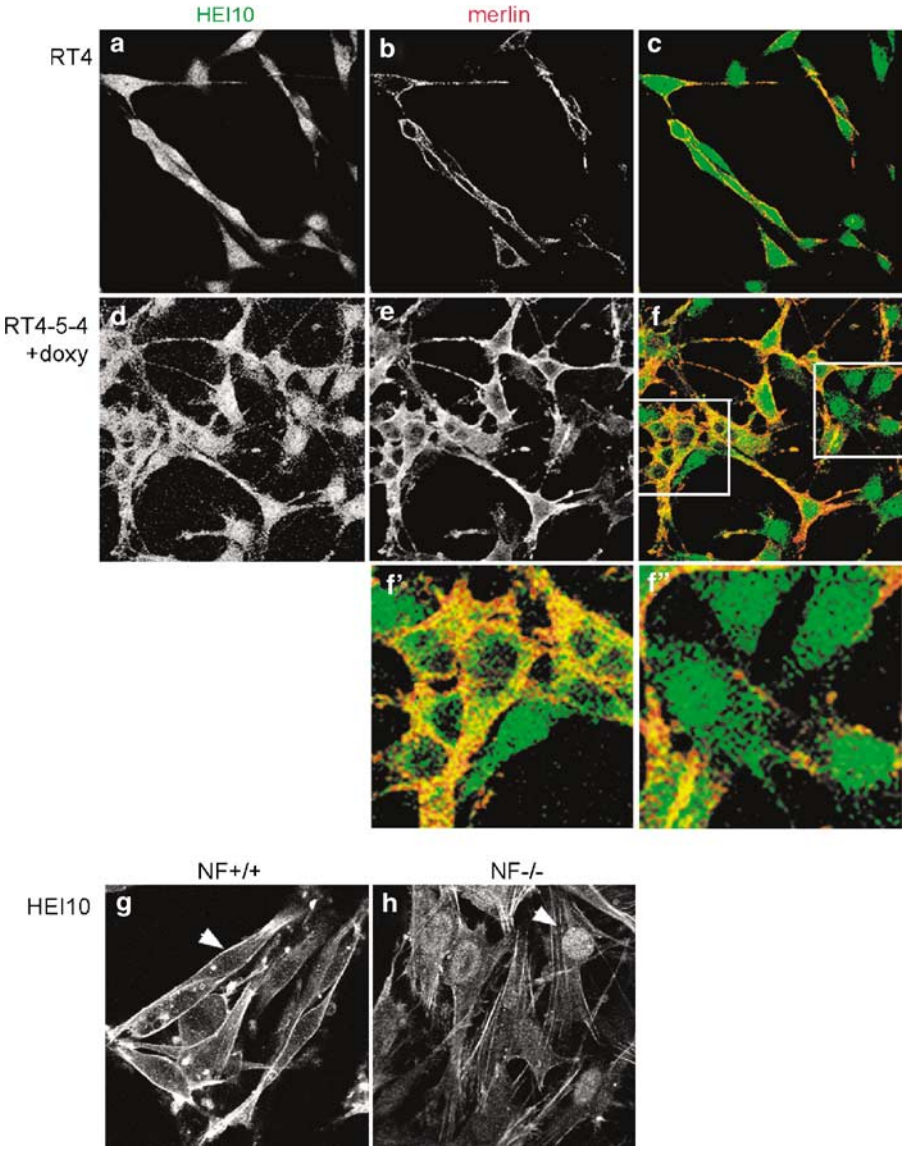

Figure 6 Expression of merlin changes the subcellular localization of HEI10 in Schwann cell derivatives. RT4 rat schwannoma cells, expressing low amounts of merlin (**a**–**c**) and RT4-5-4 schwannoma cells induced to express merlin with doxycyclin (**d**–**f**) were stained for merlin with 1C4 monoclonal antibody (mAb) and HEI10 with rabbit antiserum and images taken with a confocal microscope. HEI10 is present in the nucleus of all cells with low merlin expression (**c**). Cells with high merlin expression are devoid of nuclear HEI10 (**f** and **f′**), whereas those RT4-5-4 cells, which express very little merlin, show strong nuclear HEI10 staining (**f** and **f″**). Merlin-positive primary human Schwann cells (**g**) and merlin-negative schwannoma cells (**h**) were stained for HEI10 with HEI10 rabbit antiserum. Nuclear HEI10 is seen in NF−/− cells but not in NF+/+ cells (arrows).

intervals (Figure 7c). For up to 60 h after transfection, the levels of HA-HEI10 remained constant. However, at 72 and 90 h, a markedly reduced amount of HEI10 was seen, while the level of merlin 1–547 remained unaffected.

In additional experiments, 293HEK cells stably expressing merlin 1–547 or vector only, were transiently transfected with HA-HEI10 or untagged HEI10. Cells were lysed after 60 h, HA-HEI10 detected with anti-HA mAb and untagged HEI10 with the HEI10 rabbit antiserum (Figure 7d). In cells expressing the constitutively open merlin 1–547, the level of HEI10 was reduced compared to empty vector. Interestingly, in these cells a smaller ~22 kDa protein band could be detected by the HEI10 Ab. This was apparently a degradation product, which was not detected with anti-HA mAb in HA-HEI10-transfected cells.

Discussion

Resolution of the tumor suppressor mechanism of the *NF2* gene product merlin requires knowledge of its molecular interactions. In this respect, molecules that link merlin to cell cycle regulation are of special interest. In order to find explanations for the opposite effects merlin and ezrin play on cell proliferation we have

focused on molecular interactions that would be specific for either protein. With this approach, we identified the cell cycle regulator HEI10 as a protein that binds merlin but not ezrin.

The interaction, which was verified by yeast two-hybrid, affinity precipitation, and coimmunoprecipitation experiments is mediated between coiled-coil domains on both proteins. Such domains are frequently involved in protein interactions, in particular during protein oligomerization (Burkhard *et al*., 2001). Interestingly, although the sequence in ezrin is very similar (~90% identity) to the corresponding region in merlin, ezrin does not bind HEI10. Only few interaction partners are known to bind the alpha-helical part of merlin. One of them is the regulatory subunit RIβ of PKA (Grönholm *et al*., 2003). An amphipatic helix disrupting mutation, which inhibits merlin-PKA-RIβ binding, did not affect HEI10 interaction suggesting that the interactions do not compete with each other. Two NF2 patient missense mutations, L316W and L316F (http://uwcmml1s.uwcm.ac.uk/uwcm/mg/nf2/, 2005) have been identified within residues 306–339, which is the critical sequence in merlin. These mutations did not, however, affect binding to HEI10, which indicates that disruption of the interaction is not the likely cause of NF2 in these patients. The PAK1 kinase, which is essential for the malignant growth of *NF2* gene-deficient cells, is controlled by merlin through two separate binding domains (Hirokawa *et al*., 2004). Interestingly, the HEI10 binding domain lies within one of them, comprising of amino acids 288–359. Our results also indicate that the association between merlin and HEI10 needs conformational activation of merlin. In yeast two-hybrid and coimmunoprecipitation experiments of transfected 293HEK cells, merlin wt did not bind HEI10. However, merlin 1–547 could be coprecipitated with HEI10 from transfected cells and an N- or C-terminally truncated merlin construct, interacted with HEI10 in the two-hybrid experiment. We have previously shown that N- and C-terminal merlin constructs, including merlin 1–546, mimic an open conformation of merlin, and interact with proteins, which *in vivo* need conformational activation of merlin (Grönholm *et al*., 1999, 2003). *In vitro* translation-produced merlin 1–595 could be pulled down by GST-HEI10, but this product might not represent the full-length protein, as the C-terminus of recombinant ERM proteins is easily degraded, and such degradation results in loss of the

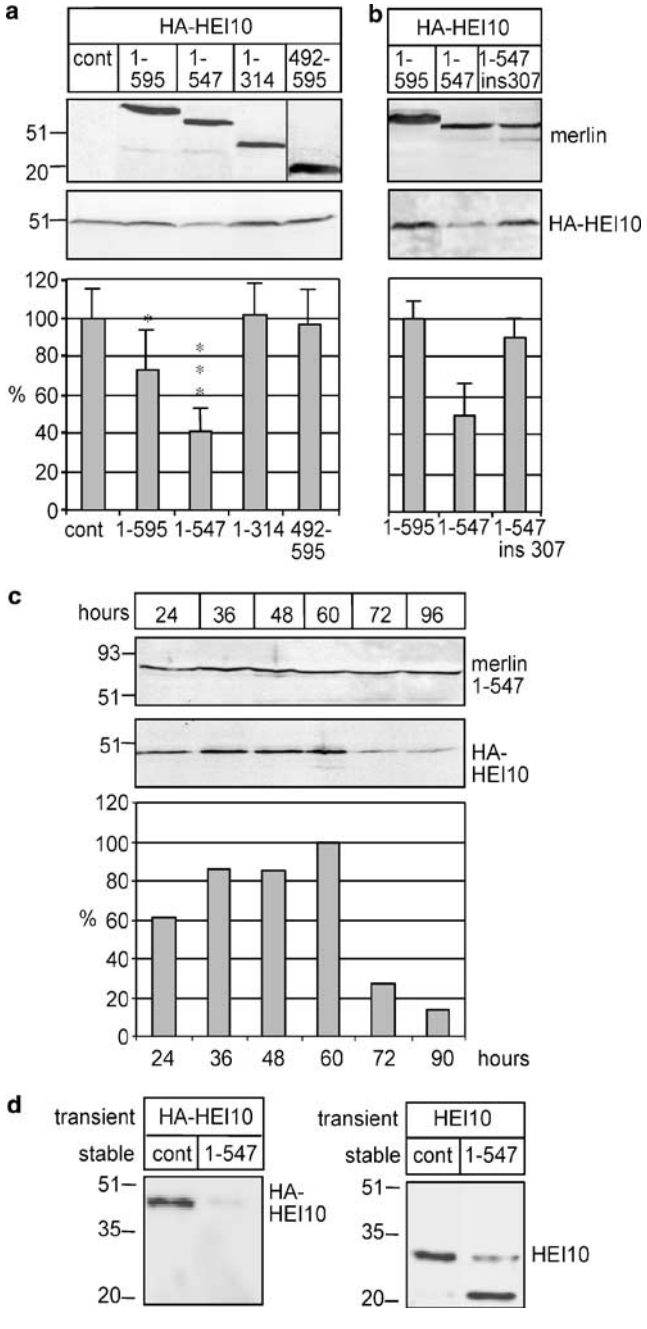

Figure 7 Constitutively open merlin regulates HEI10 protein levels. (**a**) 293HEK cells were transiently transfected with HA-HEI10 and different merlin constructs or an empty pcDNA3 vector (cont). Cells were lysed after 72 h, samples normalized for protein concentration, and detected with A19 rabbit antiserum for N-terminal merlin constructs, C18 to detect merlin 492–595, anti-HA monoclonal antibody (mAb) to detect HA-HEI10 (~45 kDa) and HEI10 rabbit antiserum to detect untagged HEI10 (32 kDa). In cells expressing merlin 1–547 and 1–595 (wt) a decreased amount of HEI10 can be seen. The bottom panel shows quantified intensity of the HEI10 band in cells expressing various merlin constructs. Mean values and standard deviation of five experiments. Bars represent percentage compared to control cells (100%). $*P<0.05$, $***P<0.01$. (**b**) The same experiment as above performed with merlin 1–547 with a five amino-acid insertion at position 307, 1–547/ins307. Less decrease in the HEI10 amount could be seen with this construct. Bars represent percentage compared to merlin 1–595 (100%). $***P<0.01$. (**c**) 293HEK cells co-transfected with HA-HEI10 and merlin 1–547 were lysed after 24, 36, 48, 60, 72 and 96 h and detected as above. Bars represent percentage compared to the highest expression level at 60 h (100%). (**d**) The same experiment as in A was performed with cells stably expressing merlin 1–547 or empty vector and transiently transfected with HA-HEI10 or untagged HEI10. A decrease of the ~45 kDa HA-HEI10 band can be seen with the anti-HA mAb and of the HEI10 32 kDa band with the HEI10 rabbit antiserum. An additional band around 22 kDa can be seen with the HEI10 rabbit antiserum but not with anti-HA mAb.

intramolecular bond between N- and C-terminus (Chambers and Bretscher, 2005).

Many of the known tumor suppressors undergo nucleo-cytoplasmic shuttling as an efficient, simple and rapid way to control cell growth (Fabbro and Henderson, 2003). Merlin is typically localized to cortical actin structures in patterns that partly overlap with ERM proteins (Gonzalez-Agosti *et al*., 1996; Sainio *et al*., 1997; Shaw *et al*., 1998). However, it can also be targeted to the nucleus dependent on the cell cycle phase, cell density and adhesive state (Muranen *et al*., 2005). In this study we show that also HEI10 localizes to the nucleus in a cell cycle-dependent manner and to the cortical actin cytoskeleton. The partial colocalization between merlin and HEI10 can indicate functional interplay between merlin and HEI10 in certain cell cycle phases. Nucleo-cytoplasmic shuttling may provide means for merlin and HEI10 to affect cell growth, although no nuclear function for either protein has been identified yet.

In a recent report, expression of merlin in a *NF2* gene-deficient mesothelioma cell lines caused accumulation of cells in G1 concomitant with a decreased expression of cyclin D1, inhibition of Cdk4 activity and dephosphorylation of Rb, which are important steps for G1/S transtition. This decrease was caused by merlin's inhibitory effect on PAK, a known upstream activator of cyclin D1 transcription (Xiao *et al*., 2005). The current results link merlin to cyclin B and thus to another control point of the cell cycle. Further studies are needed to find out, whether the pathways are regulated independently or in parallel.

Schwannomas are the primary manifestation of NF2. Therefore, it is of interest that Schwann cells express HEI10 and that its distribution depends on the expression of merlin. In human and rat schwannoma cells deficient for merlin expression, HEI10 was targeted to the nucleus, whereas in human Schwann cells and in rat schwannoma cells expressing increased levels of merlin, HEI10 was cytoplasmic. The results indicate that merlin is, either directly or indirectly, involved in targeting of HEI10. An indirect effect might result from the fact that merlin expressing cells are more frequently in G1 than merlin-negative cells (Schulze *et al*., 2002), and during G1 HEI10 was shown to have mainly cytoplasmic location. Since both proteins are exported from the nucleus at a similar time frame during G1, it is also possible that merlin contributes to the transport of HEI10 from the nucleus. Our interpretation is that in cells deficient for merlin, the function of HEI10 is compromised due to inappropriate targeting.

Interestingly, the constitutively open form of merlin affected the integrity of the HEI10 protein. Coexpression of merlin 1–547 with HEI10 resulted in degradation of HEI10 with a mechanism that required binding between the two proteins. The mechanism of degradation is not yet clear. HEI10 can be ubiquitinated and can function as an E3 ubiquitin ligase (Toby *et al*., 2003). However, preliminary experiments with proteasome inhibitors did not affect the degradation induced by constitutively open merlin.

Previously, models for the tumor suppressor role of merlin at the membrane–cytoskeleton interphase have been proposed. We have shown a more versatile localization of merlin, which is regulated by cell cycle phase, and demonstrate here an association between merlin and the cell cycle regulator. This suggests that merlin performs several functions in cells, which may all be linked to its function as a tumor suppressor.

Materials and methods

Antibodies and probes

1C4 mAb (Gonzalez-Agosti *et al*., 1996), KF10 mAb (den Bakker *et al*., 1995) and A19 or C18 rabbit antiserum (Santa Cruz Biotechnology Inc., Santa Cruz, CA, USA) were used to detect merlin. The anti-HEI10 antibody has been described (Toby *et al*., 2003). In addition, we used anti-HA antibody (Covance Inc., Princeton, NJ, USA), anti-α-tubulin mAb N356 (Amersham Pharmacia Biotech, Buckinghamshire, UK), DAPI to stain DNA (Sigma, St Louis, MO, USA) and propidium iodide (Sigma).

Cell cultures and stainings

U2OS human osteosarcoma cells were cultured in McCoy's medium supplemented with 15% fetal bovine serum, and 293HEK cells in RPMI medium with 10% FBS and RT4 and RT4-5-4 rat schwannoma cells (Morrison *et al*., 2001) in DMEM medium with 10% FBS. Expression of merlin in RT4-5-4 cells was induced by 1 μg/ml doxycycline (Orion Pharma, Espoo, Finland) for 24 h. Since merlin expression affects RT4-5-4 cell proliferation in confluent cells (Morrison *et al*., 2001), cells were not allowed to grow to confluency. 293HEK cultures stably expressing full-length merlin (1–595, wt), merlin 1–547 or empty pcDNA3 vector (Invitrogen, Carlsbad, CA, USA) were produced by selection in 100 μg/ml hygromycin (Gibco). Cells were fixed in 3.5% paraformaldehyde (PFA), pH 7.4, and stained with 1C4 mAb (1:100) or A19 rabbit antiserum (1:200) to detect merlin and with anti-HEI10 rabbit antiserum (1:50) to detect HEI10 followed by Alexa488 anti-mouse or Alexa594 anti-rabbit antibodies (Molecular Probes, Eugene, OR, USA). Coverslips were mounted in DABCO (Sigma) and Mowiol (Calbiochem, San Diego, CA, USA) and examined by confocal microscopy (Leica SP2, Leica Microsystems, Heerbrugg, Switzerland) using the sequential scanning mode, or by immunofluorescence microscopy (Zeiss Axiophot epifluorescence microscope equipped with AxioCam cooled CCD-camera, Carl Zeiss, Esslingen, Germany).

Normal human Schwann and schwannoma cells were isolated as previously described (Hanemann *et al*., 1998; Rosenbaum *et al*., 1998). Following collection, cells were resuspended in proliferation medium (DMEM, 10% fetal calf serum, 500 U/ml penicillin/streptomycin (Gibco), 0.5 μM forskolin (Sigma), 10 nM β1-heregulin177–244 (Mark Sliwkowski, Genentech, San Francisco, CA, USA), 0.5 mM 3-isobutyl-1-methylxanthine (Sigma), 2.5 μg/ml insulin (Sigma)). Cells were seeded on plates pre-coated with 1 mg/ml poly-L-lysine (Sigma) and 4 μg/ml natural mouse laminin (Gibco). Cells were fixed by 4% PFA, permeabilized with 0.2% Triton X-100 for 5 min and blocked in 10% goat serum/1% bovine serum albumin in phosphate-buffered saline, before incubation with the HEI10 rabbit antiserum overnight at 4°C and goat-anti-rabbit Cy3 1:800 (Dianova) for 40 min. Cells were analysed on a confocal scanning microscope (LSM510, Leica), and experiments were repeated three times using cell cultures from different donors each.

Production of glutathione S*-transferase-fusion proteins*
Glutathione *S*-transferase-fusion proteins were expressed in *Escherichia coli* (DH5α) and purified following standard protocols. Fusion proteins were eluted from glutathione-Sepharose (G-Sepharose) beads by 5 mM reduced glutathione in 50 mM Tris-HCl, pH 8 over night at 4°C.

In vitro *translation*
Merlin pcDNA3 plasmids were used as a template for a T7-coupled rabbit reticulocyte transcription-translation system (Promega, Madison, WI, USA) in the presence of ^{35}S-methionine (Sigma). Of 50 μl reaction, 5 μl were separated in SDS–PAGE, the gel was dried and exposed on film to determine the size and amount of labelled protein. Fusion proteins on glutathione beads (~1 μg) were mixed with IVT-produced protein. Bound proteins were separated in SDS–PAGE, and detected with autoradiography.

Affinity precipitation
Yeast expressing HA-tagged merlin constructs were lysed with a mini beadbeater (BioSpec Products Inc., Bartlesville, OK, USA) in the presence of 1 ml acid-washed glass beads (Sigma) in 200 μl of ELB-buffer (50 mM Hepes, pH 7.4, 150 mM NaCl, 5 mM EDTA), 1% NP-40 and protease inhibitors. Debris was removed by centrifugation, and supernatant diluted to ELB-0.5% NP-40. Total protein (200 μg) from lysates were incubated with purified GST-fusion protein bound to G-Sepharose beads (0.5–1 μg) for 45 min. Beads were washed in ELB-0.1% NP-40 buffer and bound proteins eluted by boiling in non-reducing Laemmli sample buffer, separated in SDS–PAGE and analysed by immunoblotting. Bound proteins were detected with anti-HA antibody (1:3000).

Yeast two hybrid
A yeast two-hybrid screen was performed with merlin amino acids 252–595 cloned in the EG202 vector as bait using a HeLa cDNA library in the JG4-5 vector as described (Gyuris *et al*., 1993). Merlin, ezrin and HEI10 constructs were cloned into EG202 and JG4-5 vectors. Mutations were introduced in merlin constructs using the QuickChange Kit (Stratagene, La Jolla, CA, USA) and their authenticity verified by sequencing. Yeast two-hybrid mating assays and detection of interactions were performed as described (Grönholm *et al*., 1999). Identification of the merlin coiled-coil domain was performed with COILS-prediction program (www.ch.embnet.org/software/COILS_form.html).

Merlin transposon mutation library
Merlin mutation library with random pentapetide insertions was constructed in the yeast two-hybrid vector pYesTrp2 (Invitrogen) containing merlin 1–546 using an *in vitro* DNA transposition-based peptide insertion mutagenesis system (Finnzymes Oy, Espoo, Finland). The library was transformed into yeast and interaction with HEI10 1–200 in the EG202 vector tested with the yeast two-hybrid mating assay (Grönholm *et al*., 1999).

Cell transfections and Western blot analysis
293HEK cells were grown as above and transfected with a pcDNA3 vector expressing HA-HEI10, which contains 6 inserted HA-tags adding ~90 amino acids to the expressed protein, or untagged HEI10 and different pcDNA3/merlin constructs using the Fugene transfection reagent (Roche, Mannheim, Germany). Transfected subconfluent cells were lysed after 24–90 h in 500 μl ELB-buffer (50 mM Hepes, pH 7.4, 150 mM NaCl, 5 mM EDTA), supplemented with 0.5% NP-40, protease and phosphatase inhibitors, and lysates normalized for protein concentration. Samples were separated in SDS–PAGE and analysed by immunoblotting using the anti-HA antibody (1:3000), HEI10 rabbit antiserum (1:50) or merlin A19 rabbit antiserum (1:1500). Proteins were detected with enhanced chemiluminescence. Western blot bands from five different experiments were analysed using the Image J imaging program and the mean values and standard deviation calculated.

Coimmunoprecipitation
293HEK cells stably expressing merlin 1–595 (wt), 1–547 or empty vector were transfected with the pcDNA3/HA-HEI10 construct, and lysed as above. Lysates were centrifuged at 15 000 *g* for 1 h at 4°C. The supernatant was incubated with KF10 mAb, anti-HA mAb or X63, together with protein G-Sepharose beads (Amersham Biosciences, Uppsala, Sweden) for 4 h at 4°C. Immunoprecipitates were washed with ELB-0.1% NP-40 and bound proteins were eluted from the beads by boiling in non-reducing Laemmli sample buffer. Precipitated proteins were detected as above.

Cell cycle studies
For cell cycle synchronization, U2OS cells were treated with nocodazole (200–400 ng/ml, Calbiochem) or L-mimosine (200–400 μM, Calbiochem). After 18–24 h, the block was released. At various time points after release, samples were taken for immunofluorescence analysis as described.

Acknowledgements

We thank V Ramesh for the merlin 1C4 mAb, L Sherman for the RT4 and RT4-5-4 cell lines, and H Ahola, S Blomqvist, T Halmesvaara, A Partanen and M Schoultz for skillful technical assistance. This work was supported by United States Army Neurofibromatosis Research Grant DAMD17-00-0550, The Finnish Cancer Society, the Pennsylvania Tobacco Settlement Fund, Finsk-Norska Medicinska Stiftelsen and Svenska kulturfonden.

References

Alfthan K, Heiska L, Grönholm M, Renkema GH, Carpén O. (2004). *J Biol Chem* **279**: 18559–18566.
Arakawa H, Hayashi N, Nagase H, Ogawa M, Nakamura Y. (1994). *Hum Mol Gen* **3**: 565–568.
Bretscher A, Edwards K, Fehon RG. (2002). *Nat Rev Mol Cell Biol* **3**: 586–599.
Burkhard P, Stetefeld J, , Strelkov SV. (2001). *Trends Cell Biol* **11**: 82–88.
Chambers DN, Bretscher A. (2005). *Biochemistry* **44**: 3926–3932.
den Bakker MA, Tascilar M, Riegman PH, Hekman AC, Boersma W, Janssen PJ *et al*. (1995). *Am J Pathol* **147**: 1339–1349.
Fabbro M, Henderson BR. (2003). *Exp Cell Res* **282**: 59–69.
Geiger KD, Stoldt P, Schlote W, Derouiche A. (2000). *Am J Pathol* **157**: 1785–1793.
Gonzalez-Agosti C, Wiederhold T, Herndon ME, Gusella J, Ramesh V. (1999). *J Biol Chem* **274**: 34438–34442.
Gonzalez-Agosti C, Xu L, Pinney D, Beauchamp R, Hobbs W, Gusella J *et al*. (1996). *Oncogene* **13**: 1239–1247.

Grönholm M, Sainio M, Zhao F, Heiska L, Vaheri A, Carpén O. (1999). *J Cell Sci* **112**: 895–904.
Grönholm M, Vossebein L, Carlson CR, Kuja-Panula J, Teesalu T, Alfthan K *et al*. (2003). *J Biol Chem* **278**: 41167–41172.
Gutmann DH, Sherman L, Seftor L, Haipek C, Hoang Lu K, Hendrix M. (1999). *Hum Mol Genet* **8**: 267–275.
Gyuris J, Golemis E, Chertkov H, Brent R. (1993). *Cell* **75**: 791–803.
Hanemann CO, Rosenbaum C, Kupfer S, Wosch S, Stoegbauer F, Muller HW. (1998). *Glia* **23**: 89–98.
Hirokawa Y, Tikoo A, Huynh J, Utermark T, Hanemann CO, Giovannini M *et al*. (2004). *Cancer J* **10**: 20–26.
Huynh DP, Pulst SM. (1996). *Oncogene* **13**: 73–84.
Ilmonen S, Vaheri A, Asko-Seljavaara S, Carpén O. (2005). *Mod Pathol* **18**: 872.
Khanna C, Wan XL, Bose S, Cassaday R, Olomu O, Mendoza A *et al*. (2004). *Nat Med* **10**: 182–186.
Kissil JL, Johnson KC, Eckman MS, Jacks T. (2002). *J Biol Chem* **277**: 10394–10399.
Louis DN, Ramesh V, Gusella JF. (1995). *Brain Pathol* **5**: 163–172.
Lutchman M, Rouleau GA. (1995). *Cancer Res* **55**: 2270–2274.
Mäkitie T, Carpén O, Vaheri A, Kivelä T. (2001). *Invest Ophthalmol Vis Sci* **42**: 2442–2449.
McClatchey AI. (2003). *Nat Rev Cancer* **3**: 877–883.
Mine N, Kurose K, Konishi H, Araki T, Nagai H, Emi M. (2001). *Jpn J Cancer Res* **92**: 135–139.
Morrison H, Sherman LS, Legg J, Banine F, Isacke C, Haipek CA *et al*. (2001). *Gene Dev* **15**: 968–980.
Muranen T, Grönholm M, Renkema GH, Carpén O. (2005). *Oncogene* **24**: 1150–1158.
Pineau P, Marchio A, Cordina E, Tiollais P, Dejean A. (2003). *Int J Cancer* **106**: 216–223.
Rosenbaum C, Kluwe L, Mautner VF, Friedrich RE, Muller HW, Hanemann CO. (1998). *Neurobiol Dis* **5**: 55–64.
Sainio M, Zhao F, Heiska L, Turunen O, den Bakker M, Zwarthoff E *et al*. (1997). *J Cell Sci* **110**: 2249–2260.
Schulze KM, Hanemann CO, Muller HW, Hanenberg H. (2002). *Hum Mol Genet* **11**: 69–76.
Shaw RJ, McClatchey AI, Jacks T. (1998). *J Biol Chem* **273**: 7757–7764.
Sherman L, Xu HM, Geist RT, Saporito-Irwin S, Howells N, Ponta H *et al*. (1997). *Oncogene* **15**: 2505–2509.
Smith AP, Weeraratna AT, Spears JR, Meltzer PS, Becker D. (2004). *Cancer Biol Ther* **3**: 104–109.
Toby GG, Gherraby W, Coleman TR, Golemis EA. (2003). *Mol Cell Biol* **23**: 2109–2122.
Tynninen O, Carpén O, Jääskeläinen J, Paavonen T, Paetau A. (2004). *Neuropathol Appl Neurobiol* **30**: 472–477.
Xiao GH, Beeser A, Chernoff J, Testa JR. (2002). *J Biol Chem* **277**: 883–886.
Xiao GH, Gallagher R, Shetler J, Skele K, Altomare DA, Pestell RG *et al*. (2005). *Mol Cell Biol* **25**: 2384–2394.

Human Molecular Genetics, 2007, Vol. 16, No. 14 **1742–1751**
doi:10.1093/hmg/ddm122
Advance Access published on June 12, 2007

The tumor suppressor merlin interacts with microtubules and modulates Schwann cell microtubule cytoskeleton

Taru Muranen[1,*], Mikaela Grönholm[1], Aurelie Lampin[2], Dominique Lallemand[2], Fang Zhao[1], Marco Giovannini[2] and Olli Carpén[1,3]

[1]Program of Neuroscience, Department of Pathology, University of Helsinki, Biomedicum Helsinki C511, PL 63, 0014 Finland, [2]Inserm U674, Fondation Jean Dausset-CEPH et Institut Universitaire d'Hématologie, 75010 Paris, France and [3]Department of Pathology, University of Turku and Turku University Central Hospital, 20520 Turku, Finland

Received March 09, 2007; Revised and Accepted April 30, 2007

The lack of neurofibromatosis 2 tumor suppressor protein merlin leads to the formation of nervous system tumors, specifically schwannomas and meningiomas. Merlin is considered to act as a tumor suppressor at the cell membrane, where it links transmembrane receptors to the actin cytoskeleton. Several tumor suppressors interact with another component of the cytoskeleton, the microtubules, in a regulated manner and control their dynamics. In this work, we identify merlin as a novel microtubule-organizing protein. We identify two tubulin-binding sites in merlin, one residing at the N-terminal FERM-domain and another at the C-terminal domain. Merlin's intramolecular association and phosphorylation of serine 518 regulate the interaction between merlin and tubulin. Analysis of cultured glioma cells indicates colocalization between merlin and microtubules especially during cell division. In primary mouse Schwann cells only minor colocalization at the cell periphery of interphase cells is seen. However, these cells drastically change their microtubule organization upon loss of merlin indicating a functional association of the proteins. Both *in vitro* assays and *in vivo* studies in Schwann cells indicate that merlin promotes tubulin polymerization. The results show that merlin plays a key role in the regulation of the Schwann cell microtubule cytoskeleton and suggest a mechanism by which loss of merlin leads to cytoskeletal defects observed in human schwannomas.

INTRODUCTION

Inactivation of the neurofibromatosis 2 (*NF2*) tumor suppressor gene leads to the development of multiple benign tumors of the nervous system, particularly meningiomas and schwannomas (1). The *NF2* gene encodes a 595-amino acid protein merlin (schwannomin), which is related to the ezrin–radixin–moesin (ERM) protein family. Merlin and ERM proteins are located primarily underneath the cell membrane where they anchor transmembrane proteins to the actin cytoskeleton (2,3). They form homo- and heterotypic interactions (4) which in turn regulate their binding to other proteins (5–7). Head-to-tail binding leads to a closed conformation of the ERM proteins (4); for merlin, the closed form is thought to act as a tumor suppressor, whereas the open protein is unable to regulate growth. Phosphorylation of a C-terminal serine (S518) by p21-activated kinase (PAK) or cAMP-dependent protein kinase A (PKA) weakens merlin's self-association and is believed to inactivate the growth-suppressing activity of merlin (8,9). However, the functional regulation of merlin is still not completely understood.

Merlin is also involved in receptor recycling and endocytosis. It inhibits platelet-derived growth factor receptor degradation (10) and binds hepatocyte growth factor-regulated tyrosine kinase substrate (HRS) (11), which is known to regulate receptor tyrosine kinase trafficking to the degradation pathway (12). Recently, merlin was shown to regulate EGF receptor recycling and turnover in *Drosophila* (13). Thus, increasing evidence positions merlin at the membrane where it can bind membrane receptors and regulate their expression and localization.

A common feature of many tumor suppressors is their ability to interact with microtubules and regulate microtubule

*To whom correspondence should be addressed. Tel: +358 9 19125651; Fax: +358 9 4717194; Email: taru.muranen@helsinki.fi

stability (14,15). Microtubules, themselves, are also known to regulate cell growth. They, for instance, control cell division and regulate endocytosis and recycling of growth factor receptors (16). We set out to study merlin–tubulin interaction when we noticed that endogenous merlin colocalizes with tubulin in mitotic structures of U251 glioma cells (17). Although merlin has previously been suggested to bind tubulin *in vitro* (3,18), no further evidence has been provided to support the binding. Here, we have studied the association between merlin and tubulin, the regulation of the interaction, the effects of merlin on microtubule dynamics and the consequences of loss of merlin on microtubules in Schwann cells. Our results show that merlin plays an important role in regulating microtubule cytoskeleton of mouse primary Schwann cells.

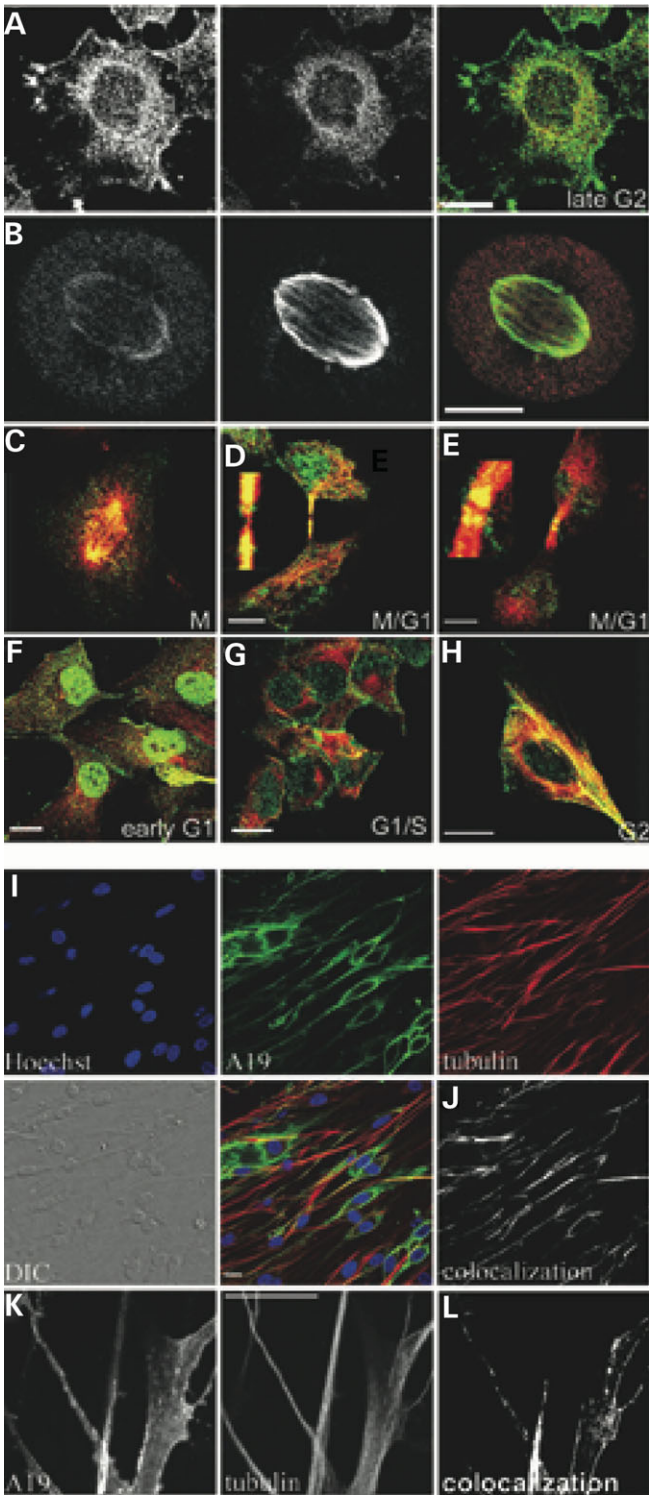

RESULTS

Merlin associates with microtubules

We have previously shown that in synchronized U251 glioma cells merlin localizes to mitotic structures (17,19). This led us to analyze the distribution of endogenous merlin and tubulin at various cell cycle stages in U251 glioma cells (Fig. 1A–H). We noticed parallel accumulation of merlin and tubulin around the nucleus in interphase cells before mitosis (A). During mitosis, merlin colocalized with microtubules at the mitotic spindles, although some diffuse merlin staining was also noticed in the cytoplasm (B and C). During cytokinesis especially the midbody demonstrated high degree of colocalization between merlin and tubulin (D and E). The colocalization was lost at early G1, when merlin accumulated in the nucleus (F). The staining patterns remained separate during the entire G1 and S phase (G). At G2, a partial colocalization was seen (H). We also studied cultured primary mouse Schwann cells, whose purity was verified by a Schwann cell-specific marker p75 (Supplementary Material, Fig. S1). In interphase cells merlin had a predominantly submembraneous localization, whereas tubulin was localized at the cytoplasm. Areas of potential colocalization were identified from confocal sections using image analysis software. The analysis revealed occasional sub-plasmalemmal regions and (I and J) and cell extensions (K and L) (colocalized points shown in white in Fig. 1J, L), in which codistribution was seen. In mitotic Schwann cells staining was mostly diffuse.

Merlin binds polymerized microtubules *in vitro*

We then wanted to identify the tubulin-binding regions in merlin. We mapped the interaction sites with a tubulin pull-down assay using various purified glutathione *S*-transferase

Figure 1. Distribution of merlin and microtubules in U251 glioma and primary mouse Schwann cells. (**A–H**) U251 glioma cells were synchronized and stained for merlin (green, A19) and tubulin (red, α-tubulin). The cells were fixed at different points of the cell cycle, the cell cycle phase was verified by FACS analysis and the localization of the two proteins was analyzed by confocal microscopy. Merlin and tubulin start to colocalize already in interphase cells when cells are approaching mitosis (**A**). During mitosis merlin localizes to mitotic spindles (**B, C**) and during cytokinesis at the midbody (**D, E** and insets). After mitosis the two proteins have separate staining patterns (**F, G**). At late G2, some colocalization can be seen again (**H**). (**I–L**) In the primary mouse Schwann cells merlin (green, A19) shows a predominantly submembraneous distribution, whereas microtubules (red, β-tubulin) are distributed within the cells body. Analysis of confocal sections with Image J analysis software demonstrates occasional submembraneous regions, where the two proteins colocalize (white areas in J and L). Scale bar 10 μm.

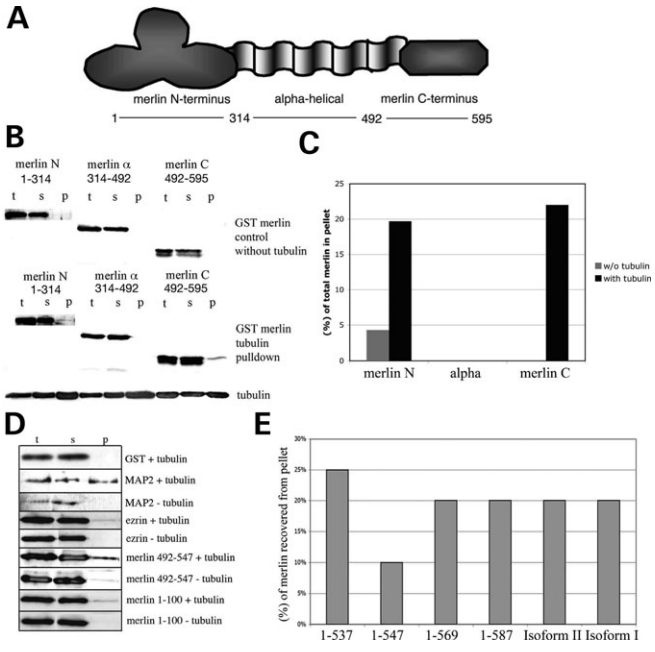

Figure 2. Merlin binds polymerized tubulin *in vitro*. (**A**) A schematic drawing on merlin's domains. (**B**) Tubulin binding sites in merlin were mapped by a tubulin pull-down assay, in which recombinant GST-merlin was pulled down with polymerized microtubules by ultracentrifugation. Merlin N (amino acids 1–314), α-helical merlin (amino acids 314–492) and merlin C (amino acids 492–595) constructs were used in the assay. Total (t), supernatant (s) and pellet (p) fractions with or without tubulin were run into SDS–PAGE, blotted either with merlin (A19 or C18) or GST-antibody and analyzed. (**C**) The amount of merlin in the pellet fraction was quantified by western blots by Typhoon Imager and compared to the total amount of merlin. (**D**) The binding sites in merlin were further mapped with merlin constructs 1–100 and 492–547. GST alone, MAP2 and ezrin N (1–309) were used as controls in the pull-down assay. The tubulin blots can be found from Supplementary Material, Figure S2. (**E**) *In vitro* translated ^{35}S methionine labeled merlin was produced and used for *in vitro* tubulin pull-down experiments. Merlin was pulled down with polymerized microtubules and the amount of merlin in the pellet was analyzed and compared with total amount of merlin (%). Merlin isoforms 1 and 2 and C-terminally deleted merlin constructs associated with microtubules. A patient mutation construct, merlin 1–547, did not associate with microtubules equally well. The graph represents the average of five experiments.

(GST)-merlin constructs. Tubulin was incubated with different GST-constructs after which polymerized tubulin was pulled down by centrifugation and quantified. Both the N-terminal FERM- (amino acids 1–314) and the C-terminal (amino acids 492–595) domain were recovered from the tubulin pellet, whereas the α-helical region (amino acids 314–492) of merlin or GST alone (quantification not shown) did not bind tubulin (Fig. 2B, C). We further mapped the N-terminal binding site to amino acids 1–100 and the C-terminal binding site to residues 492–547 (Fig. 2D). As a positive control we used microtubule-associated protein 2 (MAP2), a well-characterized tubulin interacting protein. As an additional control, we tested the N-terminus of ezrin, a FERM-domain protein homologous to merlin. Similar to merlin, the N-terminus of ezrin could be found in the tubulin pellet (Fig. 2D).

In addition, we produced *in vitro*-translated methionine-labeled merlin constructs and pulled them down with polymerized tubulin. With this assay we could see an interaction between tubulin and merlin isoforms I and II (Fig. 2E). C-terminal deletion constructs 1–569 and 1–587 bound tubulin similar to isoform I. As truncating mutations around amino acid 547 cause NF2 (http://neurosurgery.mgh.harvard.edu/NFclinic/NFresearch.htm), we tested whether merlin 1–547 would show altered binding to tubulin. Indeed, this construct demonstrated reduced binding in comparison with isoform I. However, a further truncation of 10 residues returned the binding activity (Fig. 2E) showing the complexity of the binding interphase.

Intramolecular association and phosphorylation of merlin regulate its binding to microtubules

Merlin undergoes conformational regulation and can form intramolecular association with its N- and C-terminal domains (6). This intramolecular association can mask many of the binding sites in merlin. Therefore, we studied whether intramolecular binding affects merlin–tubulin binding. Purified C-terminal GST-merlin was incubated together with increasing amounts of N-terminal merlin in order to saturate the C-terminal binding site. When C-terminus was saturated with the N-terminus it could no longer bind tubulin (Fig. 3A). GST alone incubated with the C-terminus was used as a negative control.

The C-terminal S518 of merlin can be phosphorylated by PAKs and cAMP-dependent PKA (8,9,20). This phosphorylation is thought to affect merlin's growth-regulating activity (21–23). We studied whether the phosphorylation plays a role in merlin–tubulin binding. We treated the C-terminus (492–595) of wild-type merlin or non-phosphorylatable merlin S518A mutant *in vitro* with PKA and performed the tubulin pull-down assay (Fig. 3B). Phosphorylation was verified by ^{32}P ATP labeling (not shown). Significantly lower amount of merlin was pulled down after PKA treatment indicating that the phosphorylation of the serine 518 decreases the *in vitro* binding of merlin to tubulin.

Merlin enhances microtubule polymerization *in vitro*

Many tumor suppressor proteins have been reported to affect tubulin polymerization (14) and therefore we studied whether merlin has an effect on tubulin polymerization. Purified tubulin was polymerized *in vitro* and the polymerization was monitored at OD_{350}. Microtubule-associated proteins (MAPs) and Taxol were used as positive controls and GST alone as a zero control. Nocodazole was used to control tubulin depolymerization (not shown). When recombinant merlin was added to the polymerization reaction, the rate of tubulin polymerization was increased (Fig. 4). Merlin N-, α- or C alone were not able to induce tubulin polymerization (not shown) and merlin 1–547, which has reduced affinity for tubulin, was also unable to induce tubulin polymerization.

Merlin affects the structure of Schwann cell microtubule cytoskeleton

As schwannomas, the hallmark of Neurofibromatosis 2, originate from Schwann cells, we studied merlin's effect on microtubule cytoskeleton in this cell type. We used primary mouse Schwann cells lacking merlin ($Nf2^{flox2/flox2}$, after addition of

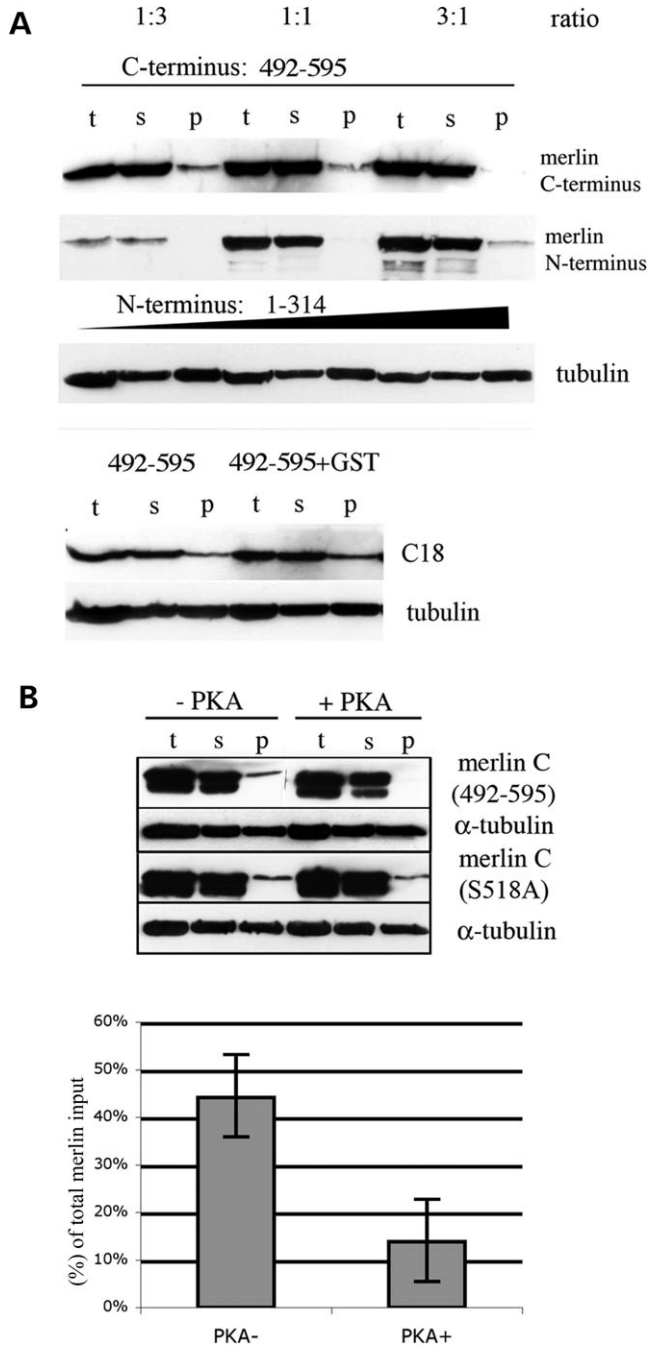

Figure 3. Intramolecular association and phosphorylation of S518 in merlin inhibits its binding to tubulin. (**A**) *In vitro* tubulin pull-down assay was performed with purified GST-merlin constructs. C-terminal merlin (amino acids 492–595) was incubated with increasing amounts of N-terminal merlin (1–314). Total (t), supernatant (s) and pellet (p) samples were analyzed by western blot with an antibody recognizing N- or C-terminal merlin (A19 or C18). When the C-terminus was saturated with the N-terminus, it could no longer bind tubulin. As a control, the C-terminus was incubated with plain GST. (**B**) The C-terminus of GST-merlin (wild-type or with S518A mutant) was phosphorylated *in vitro* with PKA and tubulin pull-down assay was performed. The amount of merlin in pellet was analyzed and compared with the total amount of merlin (%). PKA activity decreased markedly ($P = 0.006$) the binding of wild-type merlin to tubulin, but did not affect binding of the S518A mutant. The graph shows average $\pm$SD of six experiments.

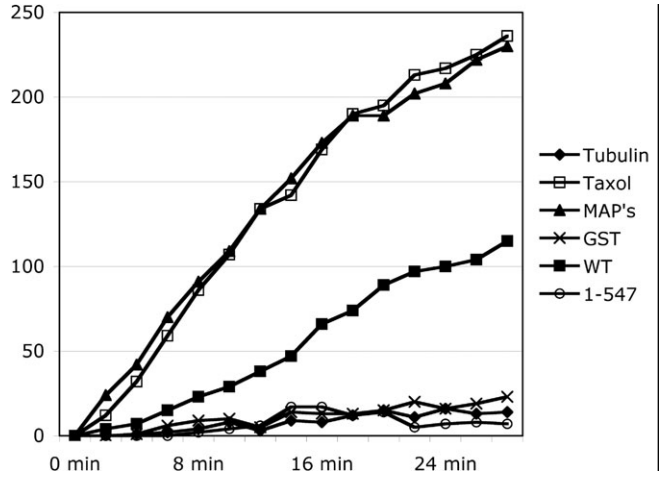

Figure 4. Merlin enhances tubulin polymerization *in vitro*. Purified tubulin from bovine brain was polymerized *in vitro* at +37°C and the polymerization was monitored at OD_{350}. Merlin GST-fusion proteins were incubated together with tubulin. Taxol and MAP2 were used as positive controls for tubulin polymerization, tubulin alone and tubulin together with GST were used as zero controls. When full-length merlin (WT) was added to the polymerization reaction, tubulin polymerized more rapidly. Merlin 1–547 was not able to induce tubulin polymerization. The graph shows an average of three experiments.

Cre-recombinase leading to genotype $Nf2^{\Delta 2/\Delta 2}$, from now on marked as Nf2 −/−, see also discussion) (24) and re-introduced wild-type merlin via adenovirus infection (Nf2 add-back). The microtubule cytoskeleton of the Nf2 −/− mouse Schwann cells differed markedly from cells re-expressing merlin via adeno-infection (Nf2 add-back). In the Nf2 add-back cells, microtubules were assembled as dense cables reaching from one end of the cell to the other and the cells displayed a normal spindle-like structure (Fig. 5A, D). Instead, the microtubules of the Nf2 −/− cells were disorganized, and the overall cell shape was more spread (Fig. 5B, D). Similar morphological differences have also been described in cultured human Schwann cells versus schwannoma cells (25).

The amount of polymerized versus unpolymerized (i.e. soluble) tubulin was analyzed from Schwann cells extracted with Triton X-100. More soluble α- and β-tubulin were present in Nf2 −/− cells than in wild-type ($Nf2^{flox2/flox2}$, marked as Nf2 +/+) or add-back cells (MWT) (Fig. 5C). The amount of soluble tubulin was associated with the expression level of merlin; increasing merlin expression resulting in reduced soluble tubulin. The total amount of tubulin in Nf2 −/− and the add-back Schwann cells were evaluated after solubilization in 6 M urea buffer. When the urea-lysates were analyzed in SDS–PAGE the add-back (MWT) and the Nf2 +/+ cells appeared to contain at least equal amount of tubulin as the Nf2 −/− cells. From this data we concluded that the ratio of polymerized/unpolymerized tubulin differs between Nf2 −/− and add-back cells; i.e. in Nf2 −/− Schwann cells the proportion of free tubulin (α/β) is higher than in the wild-type cells.

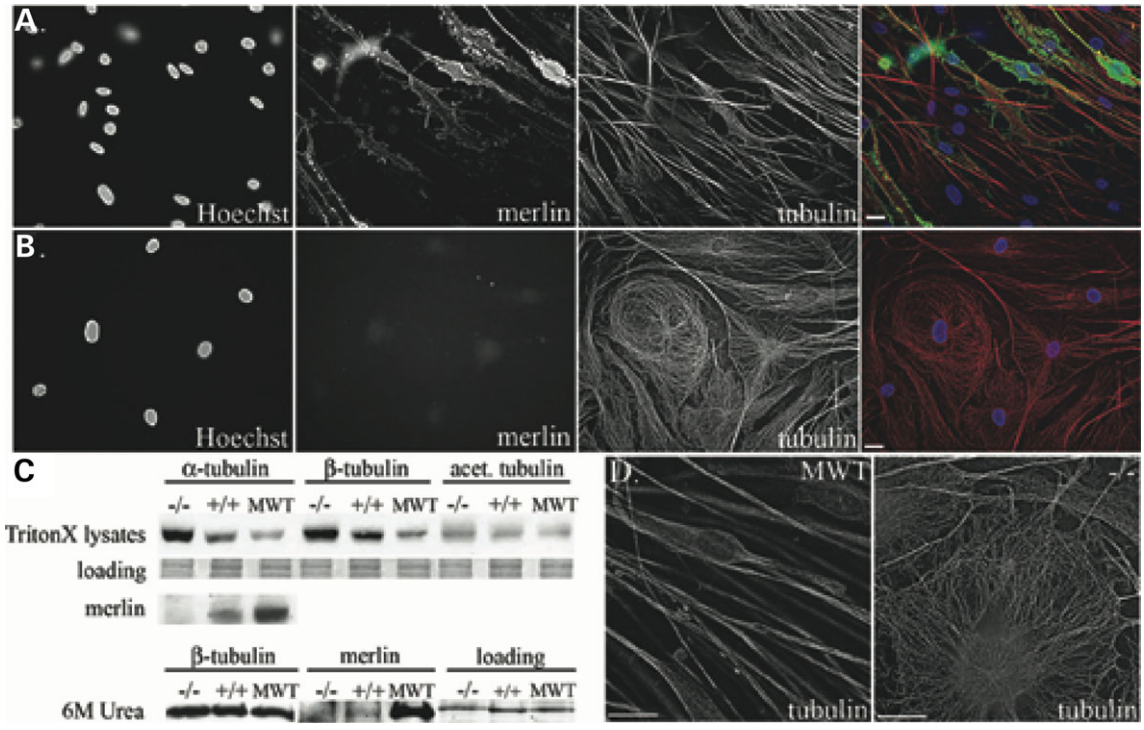

Figure 5. Microtubule cytoskeleton is altered in NF2 −/− Schwann cells. Primary mouse Schwann cells with merlin null background (NF2Δexon2, here marked as −/− (**B**) and the same cells with adeno-infected wild-type merlin (MWT) (**A**) were stained for merlin (green, A19) and β-tubulin (red) and imaged by fluorescence microscope and the images were deconvoluted. Microtubule organization is different in merlin −/− cells and in cells expressing merlin. Magnification ×630. (**C**) Triton X-100 lysates made from the −/−, +/+ and add-back (MWT) cells. Protein amounts were analyzed by Bradford assay and equal protein amounts used. As an additional loading control, the membranes were stained with Ponceau red. The lysates were probed for merlin (A-19), α-, β- and acetylated-tubulin by western blot. Total lysates of the −/−, +/+ and merlin add-back cells (MWT) were solubilized in 6 M Urea buffer and probed for β-tubulin and merlin (A-19). (**D**) A high-magnification image of tubulin in MWT and −/− cells. Scale bar 10 μm.

Tubulin polymerization dynamics differ in −/− and Nf2 add-back Schwann cells

The difference in the integrity of the tubulin cytoskeleton in −/− and add-back Schwann cells led us to test whether a difference in the polymerization rates of tubulin is also seen *in vivo*. We treated the Schwann cells with Nocodazole, which sequesters tubulin monomers and thereby depolymerizes microtubules. Incubation with Nocodazole reversed the normal morphology of Schwann cells and the cells obtained more fibroblast-like morphology (Fig. 6A, B; Supplementary video 1 and 2, for add-back and −/− cells, respectively). After 5 min of Nocodazole block release both cell types began to regain their normal shape by loosing the flattened morphology. The add-back Schwann cells began to obtain their normal morphology (i.e. long extensions) 2 h after the block release, whereas the −/− cells had only unorganized microtubules at this time-point (Fig. 6C, D; 120 min). After 4 h of block release both cell types had their microtubules re-grown. In addition, the add-back cells had regained their spindle-like shape (Fig. 6C, D; 240 min). This implies that the normal Schwann cell morphology is dependent on intact microtubule cytoskeleton and that merlin enhances microtubule organization in Schwann cells.

In addition, we used fluorescence recovery after photobleaching (FRAP) technology to study, whether tubulin dynamics were altered in primary Schwann cells lacking merlin. Schwann cells were transfected with EGFP-tubulin and 24 h after transfection the cells were analyzed by FRAP. Cells expressing merlin had a 25% faster tubulin recovery rate than the Nf2 −/− cells (Fig. 6E) ($P < 0.001$). The data suggest that merlin is able to enhance microtubule dynamics of Schwann cells *in vivo*.

DISCUSSION

In this study we describe a novel function for merlin in the regulation of microtubule organization and dynamics. We show that merlin directly binds tubulin and regulates microtubule dynamics *in vitro* and *in vivo*. Our results show that merlin contains two tubulin-binding sites, one in the FERM-domain and another in the C-terminal domain. The existence of two separate binding sites in merlin indicates that merlin could bind either laterally to the sides of the microtubules or cross-link individual microtubules to each other, this way bundling the microtubules to thicker entities. In addition, the entire protein is needed to induce tubulin polymerization, as shorter merlin fragments were not able to induce polymerization. Interestingly, the truncating patient mutation 1–547 showed reduced tubulin binding and did not induce polymerization, although it harbors the two identified tubulin binding sites. A further 10 residue deletion returned the binding activity indicating that mere loss of the binding site does not

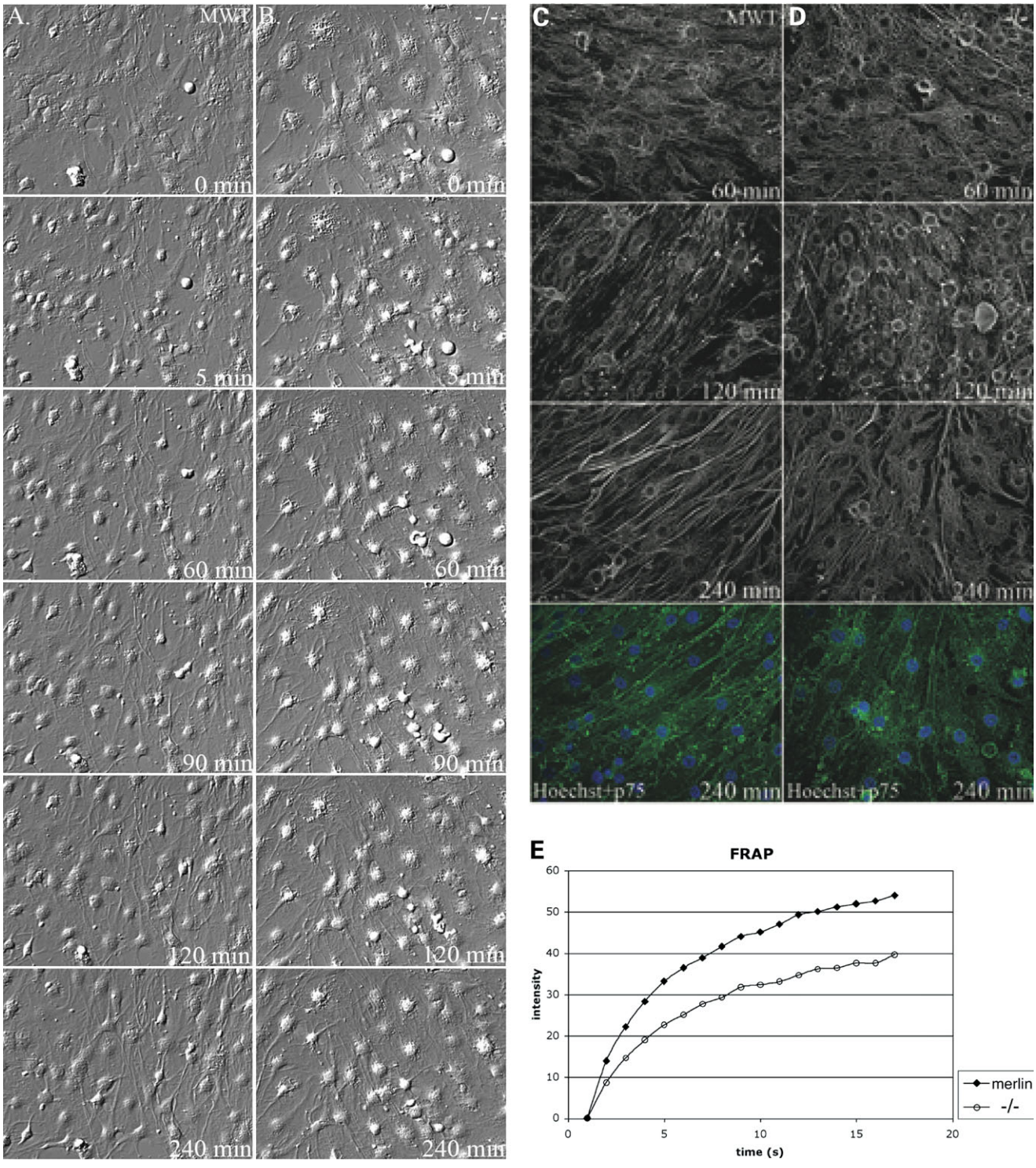

Figure 6. Microtubule recovery is faster in merlin-expressing primary Schwann cells. (**A, B**) Primary mouse Schwann cells lacking merlin (−/−) (**B**) or with adeno-infected merlin add-back (MWT) (**A**) were treated with Nocodazole to depolymerize microtubules. The block was released and cells were either imaged with DIC filter for 4 h once every 30 s (Supplementary videos 1 and 2, 200× magnification) or still images were captured from the indicated time points. Alternatively add-back MWT (**C**) and −/− (**D**) cells were fixed at indicated time points after which cells were stained with β-tubulin and a Schwann cell marker p75 and imaged with fluorescence microscope (magnification 630×) after which the images were deconvoluted. Nuclei were stained with Hoechst (blue). (**E**) For FRAP experiments primary Schwann cells (−/− and add-back) were transfected with EGFP-tubulin and 24 h after transfection the cells were imaged for FRAP with confocal microscope. Pre-bleach images were obtained and the region of interest (equal size region of interest was used with all the cells) was bleached. Post-bleach images were acquired at 2 s intervals. From the data, background was subtracted and normalized similarly for all the samples. Eight cells of each construct (−/− and add-back/MWT) were imaged and the averaged data was used for data analysis. Cells that were expressing merlin had a faster recovery rate of tubulin than the −/− cells ($P < 0.001$).

explain the result. It is possible that the 1–547 mutation leads to an altered folding of the protein and thereby prevents the interaction with tubulin.

An intramolecular association and phosphorylation of S518 in merlin can regulate its binding to microtubules. The binding of several other proteins to microtubules is regulated by phosphorylation. For example a major phosphoprotein in the brain, MAP2, is phosphorylated by PKA and upon phosphorylation dissociates from microtubules (26). Both MAP2 and merlin function as PKA-anchoring proteins (AKAPs) (27,28) and therefore merlin might have a similar function as MAP2, targeting PKA to microtubules. It is of interest that both kinases, PKA and PAK, known to regulate merlin phosphorylation, localize to centrosomes at mitosis and affect microtubule formation, in analogy with merlin (8,9,20,29,30). Previous results have suggested that phosphorylation of merlin results in the conformational opening of the molecule allowing it to interact with other proteins (23). However, in light of our study (and our unpublished observations from other interaction studies) it seems that the regulation is more complex than previously thought. We hypothesize that merlin can be 'open' but non-phosphorylated at S518 since in our results only the open but S518 non-phosphorylated merlin binds tubulin.

To study the role of merlin on microtubule dynamics *in vivo*, we used cells from genetically engineered mouse, in which wild-type *Nf2* gene has been replaced with a $NF2^{flox2/flox2}$ variant. Addition of Cre-recombinase to the cell cultures leads to deletion of exon 2 ($Nf2^{\Delta exon2/\Delta exon2}$ genotype) and to complete loss of merlin (Fig. 5). Overexpression of a Δexon 2 mutant in cultured cells is known to disturb cell adhesion (31). However, in our model, replacement of the wild-type allele with the Nf2Δexon2 leads to a greatly reduced merlin expression, when compared with the wild-type *Nf2* gene as shown in mouse tissues (24). Indeed, Cre-recombinase treated MEF cells from the same mice have previously been used as a model of genetically engineered Nf2 −/− cells (32).

Our data suggest that merlin plays an important role in regulating Schwann cell microtubule cytoskeleton. Loss of merlin in Schwann cells results in a change of the spindle-like morphology and alteration in microtubule organization. Also the ratio of polymerized versus unpolymerized tubulin is affected by merlin, i.e. Schwann cells that lack merlin have more unpolymerized tubulin than cells expressing merlin. The Nf2 −/− cells contain more acetylated tubulin, which is regarded as a marker of older and more stable structures. This might imply that tubulin polymerization/turn-over is not as efficient in the Nf2 −/− cells as in merlin-expressing cells. The results from the Nocodazole-repolymerization experiment confirm these data. Our FRAP data further supports this finding as tubulin turnover appears to be higher in merlin-expressing Schwann cells. Unfortunately, in our experimental FRAP set-up, it was not possible to monitor the dynamics of individual microtubules due to the thickness of the cells and to the high amount of free tubulin dimers. Therefore, by FRAP we have only analyzed tubulin recovery as a tubulin pool and not as individual microtubule polymers. The difference might have been even greater if we were able to study individual microtubule polymers. It also seems that microtubules are a major contributor to the Schwann cell morphology, since Schwann cell morphology resembled that of fibroblasts after depolymerization of microtubules.

Microtubules regulate endocytic pathways (16,33). Recent papers have linked merlin to endocytic events and receptor recycling (10–13). It has been shown that cells use a specific sorting mechanism of fast and slow maturation of the endocytic vesicles. Certain receptors, such as EGFR, are recycled through a dynamic pool of early endosomes that are highly mobile on microtubules and that mature rapidly towards the late endosomes. This rapid movement and maturation is completely dependent on microtubules; if microtubules are disrupted, the dynamic vesicles will non-selectively join all early endosomes and are less-efficiently degraded (34). Two papers have localized merlin to early endosomes (11,13). Thus, merlin may function as a linker at the plasma membrane, helping receptor-containing endocytosed vesicles to attach to microtubules. If cells lack merlin, this receptor recycling might be slower, and the receptors would be cleared from the membrane less efficiently. We propose that merlin plays a dual role at the membrane of Schwann cells, partly by transferring early endocytic vesicles to rapidly growing microtubules with the help of its interaction partner HRS and partly by increasing the microtubule polymerization rate, thus enhancing the vesicle maturation process.

In the past years several tumor suppressor proteins, including p53, APC, VHL and BRCA1 have been shown to bind and regulate microtubules (14). In line with merlin, also APC and VHL show only limited colocalization with microtubules, but yet affect their dynamics *in vivo* (35,36). Here, we show that also merlin binds microtubules, regulates their polymerization and has an important role in the establishment of normal Schwann cell morphology. Schwannoma cells from NF2 patients display altered morphology with long, multiple extensions (37). Based on our study this altered morphology may be associated with a disturbed microtubule cytoskeleton due to the lack of merlin, thus linking the interplay of merlin and tubulin to normal Schwann cell development and possibly to schwannoma formation.

MATERIALS AND METHODS

Cell lines and antibodies

U251 glioma cells were maintained in Dulbecco's Minimum Essential Medium (MEM), supplemented with 10% fetal calf serum (FCS) (PromoCell, Heidelberg, Germany), 1% L-glutamine and 50 μg/ml gentamycin (Invitrogen). Cells were fixed in 3.5% paraformaldehyde, pH 7.5. Primary Schwann cells were isolated and cultured as previously described (38) from NF2 knock-out mice with both alleles of the NF2 exon 2 loxed, thus producing after Cre recombination the $NF2^{\Delta 2/\Delta 2}$ genotype (24). The cells were used either at passage two or three. Anti-merlin polyclonal rabbit antibodies A-19 sc-331 (epitope 2-21), C-18 sc-332 (Santa Cruz Biotechnology, Santa Cruz, CA, USA), 1398 NF2 (39), anti-schwannomin (40) and mouse mAb KF10 (39) were used. TO-PRO 3-iodide probe (Invitrogen, Molecular Probes) was used for DNA staining. Monoclonal anti-α-, -β- and -acetylated-tubulin antibodies (Sigma–Aldrich) were used to detect tubulin. Anti-GST polyclonal

goat antibody (GE Healthcare) was used to detect GST proteins. p75 antibody (41) was used as a Schwann cell marker. Alexa 488-, 568-, 594- and 633-conjugated goat anti-mouse and goat anti-rabbit antibodies (Invitrogen, Molecular Probes) were used as secondary antibodies in immunofluorescence and HRP-conjugated rabbit anti-mouse and swine anti-rabbit and anti-goat (Santa Cruz) secondary antibodies (DAKO A/S, Glostrup, Denmark) in western blot analysis.

Plasmids and protein expression constructs

The following merlin constructs: isoform I (amino acids 1–595), isoform II and isoform I variants S518A, S518D, 1-314, 1-537 and 1-547) in pcDNA3 (Invitrogen) were used for *in vitro* translation. Luciferase cDNA was used as a negative control. For expression of recombinant GST-merlin fusion proteins, the following constructs were used: merlin N-terminus (amino acids 1–100 and 1–309), merlin a-helical domain (amino acids 314–477), C-terminus (amino acids 492–595) and C-terminus with S518A mutation as described previously (9), merlin 1–537 and merlin 1–547.

Adenovirus construct were made using Stratagene's AdEasy system. Full-length merlin was cloned into the adeno vector and the virus was produced according to manufacturer's instructions in 293A cells. The infection titer was optimized to have 100% efficiency and verified by immunofluorescence staining. Schwann cells lacking merlin were infected with adenoviruses 3 days before the experiments were conducted. EGFP-tubulin construct was obtained from Invitrogen, and transfection to primary Schwann cells was done with Lipofectamine PLUS (Invitrogen).

In vitro translation and quantification of labeled proteins

Merlin pcDNA3 plasmids (Invitrogen) were used as a template for a T7-coupled rabbit reticulocyte transcription–translation system (Promega, Madison, WI, USA) in the presence of ^{35}S-methionine. Five microlitres of 50 μl reaction were run in to SDS–PAGE, gel was dried and exposed to film to determine the size and amount of the labeled protein. For quantification the gel was also exposed to PhosphoImager low energy-plate (GE Healthcare), read by TyphoonImager 9400 (GE Healthcare) and analyzed by ImageQuantTL2003 software (GE Healthcare).

GST-fusion protein production

GST-fusion proteins were expressed in *Escherichia coli* DH5α and purified following standard protocol. Fusion protein was eluted from the Glutathione Sepharose beads (GE Healthcare) by 5 mM reduced glutathione in 50 mM Tris–HCl pH 8.0, over night at +4°C. Before some tubulin pull-down assays different amounts of N- and C-terminus were incubated in 50 mM Tris–HCl, 150 mM NaCl (pH 8.0) for 30 min at room temperature. The eluted fusion proteins for the PKA assay were dialyzed against 20 mM Tris–HCl, 10 mM $MgCl_2$, pH 7.4 at +4°C o/n. Wild-type merlin was produced in Sf9 insect cell line. Merlin with an N-terminal GST-tag was cloned into a baculovirus transfer vector pAcG2T (BD Biosciences) and then produced with the BaculoGOLD system (BD Biosciences). Sf9 cells were used to produce recombinant merlin according to user's manual (Invitrogen). Full-length merlin was purified after 1 day of infection following standard GST-purification protocol. The proteins were used immediately after purification.

In vitro phosphorylation

GST-proteins were dialyzed against the reaction buffer and run into SDS–PAGE, protein amounts estimated and equal amounts of each construct were used in the *in vitro* phosphorylation assay. Total volume of the reaction was 40 μl including PKA reaction buffer (20 mM Tris–HCl, 10 mM $MgCl_2$, pH 7.4), 200 mM ATP and purified human or bovine catalytic subunit of PKA (Sigma–Aldrich). Reaction was incubated 30 min at +30°C and was stopped by adding 20 mM PKA inhibitor H89 (Sigma–Aldrich).

Tubulin pull-down assay

Tubulin pull-down was performed with ^{35}S-labeled *in vitro* translated protein, eluted GST-fusion protein or with *in vitro* PKA phosphorylated eluted GST-fusion protein. Equal protein amounts were used in all experiments. Purified bovine tubulin (Cytoskeleton) (70 μg) was added to tubulin polymerization buffer (80 mM PIPES, 0.5 mM MgCl, 1 mM ethylene glycol-bis, 1 mM GTP, pH 6.9, 10% glycerol, 10 mM Taxol) to a final volume of 200 μl and the microtubules were allowed to polymerize at +37°C for 30 min in the presence of different merlin constructs. After this 50 μl were removed and labeled as 'total' fraction and the remaining 150 μl were centrifuged at 11 503 *g* for 30 min at +30°C to collect the polymerized microtubules. Supernatant was removed and the pellet was resuspended in 150 μl of polymerization buffer. Twelve microlitres of each fraction were analyzed on SDS–PAGE.

Western blot

Primary Schwann cells were lysed in ice-cold ELB buffer (150 mM NaCl, 50 mM Hepes pH 7.4, 5 mM EDTA, 0.5% NP40 and complete protease inhibitor cocktail tablet, Roche) or in mild Triton-X buffer (50 mM Tris pH 7.4, 150 mM NaCl, 1 mM EDTA, 1% Triton-X 100, 1 mM PMSF) including protease inhibitors (Complete), cells were incubated on ice for 15 min and centrifuged at full speed in +4°C for 15 min. Alternatively, cells were scraped in ice-cold PBS, centrifuged briefly and the cell pellet was suspended into Urea-buffer (50 mM Tris, 6 M Urea, pH 7.4). The cells were lysed for 15 min and briefly sonicated. The protein amounts were analyzed either by the Bradford assay or by Coomassie staining. Equal amounts of proteins were run into gel transferred into nitrocellulose membrane and blotted with antibodies. As an additional loading control, loading was verified after western blot by staining the filters with Ponceau red. A representative band of the whole filter of approximately 150 kD was chosen as the loading band for Figure 5C.

Immunofluorescence, laser scanning confocal microscopy, live cell imaging and fluorescence recovery after photobleaching

U251 and Schwann cells were fixed in 3.5% PFA for 10 min, washed in PBS and permeabilized for 5 min in 0.1% Triton X-100/PBS and blocked at 5% BSA in PBS. Cells were stained with merlin and tubulin antibodies (diluted 1:100 and 1:200, respectively) followed by secondary antibodies or TO-PRO 3-iodide or DAPI nuclear stain. Double stainings were performed sequentially. Coverslips were mounted in DABCO (Sigma) and Mowiol (Calbiochem) or Vectashield (Vector Laboratories, Burlingame, CA, USA). Cells were examined by confocal microscope: U251 cells with Leica SP2 equipped with Ar and Kr lasers (Leica Microsystems, Heerbrugg, Switzerland) and Schwann cells with Zeiss LSM 510 META (Fig. 1) using the sequential scanning mode. Schwann cell images (Figs 5 and 6D) were acquired by immunofluorescence microscope (Zeiss Axiophot equipped with AxioCam cooled CCD-camera, Carl Zeiss, Esslingen, Germany).

Live cell imaging was performed in pre-warmed microscope chambers at +37°C with 20 mM Hepes as a buffering agent in the medium. Cells were plated on LabTek borosilicate no. 1.5 imaging chambers (Nunc, Naperville, IL, USA) and imaged either with Olympus inverted IX81 microscope (supplemented with 5% CO_2, for the Nocodazole experiment) and CellR program or with confocal Zeiss LSM 510 META microscope. For videos, cells were imaged once every 30 s for 4 h (exposure 122 ms). FRAP analysis was performed with the Zeiss confocal microscope, pre-bleach images were obtained after which lasers were turned to full power and region of interest was bleached 50 times, the same settings were used for all FRAP experiments including the region of interest. Data analysis was performed in Zeiss META and in Microsoft Excel.

Statistical and image analysis

All statistical analyses were performed in Excel with Student's *t*-test using two-tailed distribution and image analysis was performed with Image J 1.36b. Images were processed with Adobe Photoshop, or with Image J 1.36b. Background was subtracted from DIC images with FFT bandpass filter and with Pseudo flat-field filter in Image J. Wide-field immunofluorescence images (Figs 5A, B and 6C, D) were deconvoluted with Huygens Deconvolution software (Scientific Volume Imaging), 30 iterations for each channel.

In vitro tubulin polymerization and other experiments

In vitro tubulin polymerization was performed on UV-permeable 96-well plates. Tubulin was purified from bovine brain as previously described (42) and recombinant merlin was produced in Sf9 insect cells as described in the GST-fusion protein section. Nocodazole 20 μM, Taxol 20 μM (Sigma) and MAP's (purified from bovine brain) were used as controls in the polymerization reaction. The polymerization buffer (80 mM PIPES, 0.5 mM MgCl, 1 mM Ethylene glycol-bis, 1 mM GTP, pH 6.9, 10% glycerol) was mixed with tubulin (25 μM) and merlin constructs (different amounts) were added on ice. At the beginning of the experiment the 96-well plate was transferred to pre-warmed 96-well plate reader that measured the OD at 350 nm every 5 min at +37°C for 60 min. The Nocodazole experiment was performed on primary Schwann cells with or without the re-expression of merlin via adeno-infection. Cells were incubated with 8 μM Nocodazole overnight after which the block was released and the cells were fixed at indicated time points. The cells were stained for tubulin and merlin.

SUPPLEMENTARY MATERIAL

Supplementary Material is available at HMG Online.

ACKNOWLEDGEMENTS

We would like to thank Niclas Setterblad at the Imaging Department of the Institut Universitaire d'Hématologie IFR105 for valuable help in confocal microscopy and FRAP experiments. The imaging department is supported by grants from the Conseil Regional d'Ile-de-France and the Ministère de la Recherche. In addition we would like to thank all the personnel in Dr Giovannini's laboratory for the help with Schwann cell experiments. We also thank M. Hukkanen and M. Liljeström from Molecular Imaging Unit in Biomedicum Helsinki for their help with the image analysis, H. Ahola for her skillful technical assistance and L. Heiska for her comments and critical reading of the manuscript. This study was supported by the grants of Department of Defense DAMD17-00-0550 and W81XWH-05-1-0469, the Finnish Cancer Organizations, Helsinki Graduate School of Biotechnology and Molecular Biology, French embassy in Helsinki, Centre for International Mobility (CIMO), Emil Aaltonen Foundation, Ida Montin Foundation, Maire Taponen Foundation, Svenska kulturfonden and Biomedicum Helsinki Foundation.

Conflict of Interest statement. None declared.

REFERENCES

1. Gutmann, D.H. (1997) Molecular insights into neurofibromatosis 2. *Neurobiol. Dis.*, **3**, 247–261.
2. den Bakker, M.A., Riegman, P.H., Suurmeijer, A.P., Vissers, C.J., Sainio, M., Carpen, O. and Zwarthoff, E.C. (2000) Evidence for a cytoskeleton attachment domain at the N-terminus of the NF2 protein. *J. Neurosci. Res.*, **62**, 764–771.
3. Xu, H.M. and Gutmann, D.H. (1998) Merlin differentially associates with the microtubule and actin cytoskeleton. *J. Neurosci. Res.*, **51**, 403–415.
4. Bretscher, A., Chambers, D., Nguyen, R. and Reczek, D. (2000) ERM-merlin and EBP50 protein families in plasma membrane organization and function. *Annu. Rev. Cell Dev. Biol.*, **16**, 113–143.
5. Gonzalez-Agosti, C., Wiederhold, T., Herndon, M.E., Gusella, J. and Ramesh, V. (1999) Interdomain interaction of merlin isoforms and its influence on intermolecular binding to NHE-RF. *J. Biol. Chem.*, **274**, 34438–34442.
6. Grönholm, M., Sainio, M., Zhao, F., Heiska, L., Vaheri, A. and Carpen, O. (1999) Homotypic and heterotypic interaction of the neurofibromatosis 2 tumor suppressor protein merlin and the ERM protein ezrin. *J. Cell. Sci.*, **112**, 895–904.
7. Nguyen, R., Reczek, D. and Bretscher, A. (2001) Hierarchy of merlin and ezrin N- and C-terminal domain interactions in homo- and heterotypic associations and their relationship to binding of scaffolding proteins EBP50 and E3KARP. *J. Biol. Chem.*, **276**, 7621–7629.

8. Shaw, R.J., Paez, J.G., Curto, M., Yaktine, A., Pruitt, W.M., Saotome, I., O'Bryan, J.P., Gupta, V., Ratner, N., Der, C.J. *et al.* (2001) The Nf2 tumor suppressor, merlin, functions in rac-dependent signaling. *Dev. Cell*, **1**, 63–72.
9. Alfthan, K., Heiska, L., Grönholm, M., Renkema, G.H. and Carpen, O. (2004) Cyclic AMP-dependent protein kinase phosphorylates merlin at serine 518 independently of P21-activated kinase and promotes merlin-ezrin heterodimerization. *J. Biol. Chem.*, **279**, 18559–18566.
10. Fraenzer, J.T., Pan, H., Minimo, L., Jr, Smith, G.M., Knauer, D. and Hung, G. (2003) Overexpression of the *NF2* gene inhibits schwannoma cell proliferation through promoting PDGFR degradation. *Int. J. Oncol.*, **23**, 1493–1500.
11. Scoles, D.R., Huynh, D.P., Chen, M.S., Burke, S.P., Gutmann, D.H. and Pulst, S.M. (2000) The neurofibromatosis 2 tumor suppressor protein interacts with hepatocyte growth factor-regulated tyrosine kinase substrate. *Hum. Mol. Genet.*, **9**, 1567–1574.
12. Lloyd, T.E., Atkinson, R., Wu, M.N., Zhou, Y., Pennetta, G. and Bellen, H.J. (2002) Hrs regulates endosome membrane invagination and tyrosine kinase receptor signaling in *Drosophila*. *Cell*, **108**, 261–269.
13. Maitra, S., Kulikauskas, R.M., Gavilan, H. and Fehon, R.G. (2006) The tumor suppressors merlin and expanded function cooperatively to modulate receptor endocytosis and signaling. *Curr. Biol.*, **16**, 702–709.
14. Fisk, H.A., Mattison, C.P. and Winey, M. (2002) Centrosomes and tumour suppressors. *Curr. Opin. Cell Biol.*, **14**, 700–705.
15. Hergovich, A., Lisztwan, J., Barry, R., Ballschmieter, P. and Krek, W. (2003) Regulation of microtubule stability by the von hippel-lindau tumour suppressor protein pVHL. *Nat. Cell Biol.*, **5**, 64–70.
16. Murray, J.W. and Wolkoff, A.W. (2003) Roles of the cytoskeleton and motor proteins in endocytic sorting. *Adv. Drug Deliv. Rev.*, **55**, 1385–1403.
17. Muranen, T., Grönholm, M., Renkema, G.H. and Carpen, O. (2005) Cell cycle-dependent nucleocytoplasmic shuttling of the neurofibromatosis 2 tumour suppressor merlin. *Oncogene*, **24**, 1150–1158.
18. Stokowski, R.P. and Cox, D.R. (2000) Functional analysis of the neurofibromatosis type 2 protein by means of disease-causing point mutations. *Am. J. Hum. Genet.*, **66**, 873–891.
19. Grönholm, M., Muranen, T., Toby, G.G., Utermark, T., Hanemann, C.O., Golemis, E.A. and Carpen, O. (2006) A functional association between merlin and HEI10, a cell cycle regulator. *Oncogene*, **25**, 4389–4398.
20. Kissil, J.L., Johnson, K.C., Eckman, M.S. and Jacks, T. (2002) Merlin phosphorylation by p21-activated kinase 2 and effects of phosphorylation on merlin localization. *J. Biol. Chem.*, **277**, 10394–10399.
21. Morrison, H., Sherman, L.S., Legg, J., Banine, F., Isacke, C., Haipek, C.A., Gutmann, D.H., Ponta, H. and Herrlich, P. (2001) The NF2 tumor suppressor gene product, merlin, mediates contact inhibition of growth through interactions with CD44. *Genes Dev.*, **15**, 968–980.
22. Xiao, G.H., Beeser, A., Chernoff, J. and Testa, J.R. (2002) p21-activated kinase links Rac/Cdc42 signaling to merlin. *J. Biol. Chem.*, **277**, 883–886.
23. Rong, R., Surace, E.I., Haipek, C.A., Gutmann, D.H. and Ye, K. (2004) Serine 518 phosphorylation modulates merlin intramolecular association and binding to critical effectors important for NF2 growth suppression. *Oncogene*, **23**, 8447–8454.
24. Giovannini, M., Robanus-Maandag, E., van der Valk, M., Niwa-Kawakita, M., Abramowski, V., Goutebroze, L., Woodruff, J.M., Berns, A. and Thomas, G. (2000) Conditional biallelic Nf2 mutation in the mouse promotes manifestations of human neurofibromatosis type 2. *Gene Dev.*, **14**, 1617–1630.
25. Utemark, T., Schubert, S.J. and Hanemann, C.O. (2005) Rearrangements of the intermediate filament GFAP in primary human schwannoma cells. *Neurobiol. Dis.*, **19**, 1–9.
26. Ozer, R.S. and Halpain, S. (2000) Phosphorylation-dependent localization of microtubule-associated protein MAP2c to the actin cytoskeleton. *Mol. Biol. Cell*, **11**, 3573–3587.
27. Rubino, H.M., Dammerman, M., Shafit-Zagardo, B. and Erlichman, J. (1989) Localization and characterization of the binding site for the regulatory subunit of type II cAMP-dependent protein kinase on MAP2. *Neuron*, **3**, 631–638.
28. Grönholm, M., Vossebein, L., Carlson, C.R., Kuja-Panula, J., Teesalu, T., Alfthan, K., Vaheri, A., Rauvala, H., Herberg, F.W., Tasken, K. *et al.* (2003) Merlin links to the cAMP neuronal signaling pathway by anchoring the RIbeta subunit of protein kinase A. *J. Biol. Chem.*, **278**, 41167–41172.
29. Lamb, N.J., Cavadore, J.C., Labbe, J.C., Maurer, R.A. and Fernandez, A. (1991) Inhibition of cAMP-dependent protein kinase plays a key role in the induction of mitosis and nuclear envelope breakdown in mammalian cells. *EMBO J.*, **10**, 1523–1533.
30. Banerjee, M., Worth, D., Prowse, D.M. and Nikolic, M. (2002) Pak1 phosphorylation on t212 affects microtubules in cells undergoing mitosis. *Curr. Biol.*, **12**, 1233–1239.
31. Koga, H., Araki, N., Takeshima, H., Nishi, T., Hirota, T., Kimura, Y., Nakao, M. and Saya, H. (1998) Impairment of cell adhesion by expression of the mutant neurofibromatosis type 2 (NF2) genes which lack exons in the ERM-homology domain. *Oncogene*, **20**, 801–810.
32. Lallemand, D., Curto, M., Saotome, I., Giovannini, M. and McClatchey, A.I. (2003) NF2 deficiency promotes tumorigenesis and metastasis by destabilizing adherens junctions. *Genes Dev.*, **17**, 1090–1100.
33. Petiot, A., Faure, J., Stenmark, H. and Gruenberg, J. (2003) PI3P signaling regulates receptor sorting but not transport in the endosomal pathway. *J. Cell Biol.*, **162**, 971–979.
34. Lakadamyali, M., Rust, M.J. and Zhuang, X. (2006) Ligands for clathrin-mediated endocytosis are differentially sorted into distinct populations of early endosomes. *Cell*, **124**, 997–1009.
35. Kita, K., Wittmann, T., Nathke, I.S. and Waterman-Storer, C.M. (2006) Adenomatous polyposis coli on microtubule plus ends in cell extensions can promote microtubule net growth with or without EB1. *Mol. Biol. Cell*, **17**, 2331–2345.
36. Lolkema, M.P., Mehra, N., Jorna, A.S., van Beest, M., Giles, R.H. and Voest, E.E. (2004) The von Hippel-Lindau tumor suppressor protein influences microtubule dynamics at the cell periphery. *Exp. Cell Res.*, **301**, 139–146.
37. Rosenbaum, C., Kluwe, L., Mautner, V.F., Friedrich, R.E., Muller, H.W. and Hanemann, C.O. (1998) Isolation and characterization of schwann cells from neurofibromatosis type 2 patients. *Neurobiol. Dis.*, **5**, 55–64.
38. Manent, J., Oguievetskaia, K., Bayer, J., Ratner, N. and Giovannini, M. (2003) Magnetic cell sorting for enriching schwann cells from adult mouse peripheral nerves. *J. Neurosci. Methods*, **123**, 167–173.
39. den Bakker, M.A., Riegman, P.H., Hekman, R.A., Boersma, W., Janssen, P.J., van der Kwast, T.H. and Zwarthoff, E.C. (1995) The product of the NF2 tumour suppressor gene localizes near the plasma membrane and is highly expressed in muscle cells. *Oncogene*, **10**, 757–763.
40. Lutchman, M. and Rouleau, G.A. (1995) The neurofibromatosis type 2 gene product, schwannomin, suppresses growth of NIH 3T3 cells. *Cancer Res.*, **55**, 2270–2274.
41. Huber, L.J. and Chao, M.V. (1995) Mesenchymal and neuronal cell expression of the p75 neurotrophin receptor gene occur by different mechanisms. *Dev. Biol.*, **167**, 227–238.
42. Hyman, A.A., Drexel, D., Kellog, D., Salser, S., Sawin, K., Steffen, P., Wordeman, L. and Mitchison, T.J. (1991) Preparation of modified tubulins. *Meth. Enzymol.*, **196**, 478–486.

Oncogene (2008) 27, 3233–3243

www.nature.com/onc

ORIGINAL ARTICLE

Protein kinase A-mediated phosphorylation of the NF2 tumor suppressor protein merlin at serine 10 affects the actin cytoskeleton

M Laulajainen[1,3], T Muranen[1,3], O Carpén[1,2] and M Grönholm[1]

[1]Department of Pathology, Biomedicum Helsinki, University of Helsinki, Helsinki, Finland and [2]Department of Pathology, University of Turku and Turku University Central Hospital, Turku, Finland

Mutations in the neurofibromatosis 2 tumor suppressor gene (*NF2*) encoding merlin (moesin–ezrin–radixin like-protein) induce tumors of the nervous system. Merlin localizes to the cell membrane where it links the actin cytoskeleton to membrane proteins. Cell proliferation is regulated by merlin in many cell types, but merlin's tumor suppressor function still remains unclear. Phosphorylation has been suggested to regulate merlin's activity. The C-terminal serine 518 is phosphorylated both by p21-activated kinases (PAKs) and protein kinase A (PKA). In this work, we identify a novel PKA phosphorylation site, serine 10, in the N terminus of merlin. We show that a non-phosphorylatable form of serine 10 (S10A) affects cellular morphology. Regulation of this site also influences actin cytoskeleton organization and dynamics *in vivo*, as merlin S10A reduces the amount of cellular F-actin and merlin S10D stabilizes F-actin filaments. By using a wound-healing assay and live cell imaging, we demonstrate that dephosphorylation of serine 10 leads to defects in migration, possibly through altered ability of the cells to form lamellipodia. This study suggests a role for merlin in mediating PKA-induced changes of the actin cytoskeleton.
Oncogene (2008) **27,** 3233–3243; doi:10.1038/sj.onc.1210988; published online 10 December 2007

Keywords: NF2; merlin; PKA; phosphorylation; actin

Introduction

Mutations in the *NF2* gene predispose to tumors of the nervous system, mainly schwannomas and meningiomas (Baser *et al*., 2003). The *NF2* gene encodes the tumor suppressor protein merlin (or schwannomin), which shares overall structural similarity with the highly conserved ERM (ezrin–radixin–moesin) family of proteins (Rouleau *et al*., 1993; Trofatter *et al*., 1993). Merlin and the ERM proteins function as linkers between the plasma membrane and cytoskeleton, where they modulate the morphology, growth and migration of cells (Bretscher *et al*., 2002). The proteins have an overall homology of 75–80% at the amino-acid level, and their structure consists of a large N-terminal FERM (Four-point-one, Ezrin, Radixin, Moesin) domain (amino acids 19–314 in merlin), an α-helical region (amino acids 315–491) and a small globular C terminus (amino acids 492–595) (Turunen *et al*., 1998).

Merlin exists as two major isoforms, I and II, as a result of alternative splicing of exon 16 (Rouleau *et al*., 1993). The two isoforms differ in their C-terminal sequences, but are identical over the first 579 residues. Merlin isoform I is capable of head-to-tail interactions, whereas isoform II is predicted to exist in a constitutively open conformation since it lacks the C-terminal residues implicated in the intramolecular binding (Sherman *et al*., 1997; Gonzalez-Agosti *et al*., 1999; Grönholm *et al*., 1999).

It has been suggested that phosphorylation regulates merlin's tumor suppressor activity. Shaw *et al*. (1998) demonstrated that merlin is phosphorylated on several serine and threonine residues, and that the phosphorylation status of merlin varies in response to different growth conditions. Three merlin species with different electrophoretic mobilities have been observed, suggesting that at least three differentially phosphorylated forms of merlin exist. Merlin contains a C-terminal serine 518, which is phosphorylated both by p21-activated kinase (PAK) and protein kinase A (PKA) (Shaw *et al*., 2001; Kissil *et al*., 2002; Xiao *et al*., 2002; Alfthan *et al*., 2004). Phosphorylation at this site is predicted to result in a more open conformation incapable of inhibiting cell growth, but instead allowing the activation of Ras signaling pathways leading to cell division (Morrison *et al*., 2001; Xiao *et al*., 2002). When serine 518 is dephosphorylated by the myosin phosphatase MYPT-1-PP1δ, the tumor suppressor function of merlin is activated, inhibiting the Ras signaling pathway and leading to growth arrest (Morrison *et al*., 2001; Jin *et al*., 2006). Recently, also two Akt phosphorylation sites, threonine 230 and serine 315, were identified in the N terminus of merlin (Tang *et al*., 2007).

Phosphorylation of serine 518 has been shown to enhance merlin–ezrin binding (Alfthan *et al*., 2004; Rong *et al*., 2004) and weaken merlin's association with the cytoskeleton (Shaw *et al*., 2001). Like ERM

Correspondence: M Laulajainen, Department of Pathology, Biomedicum Helsinki, Helsinki University, Haartmaninkatu 8, PL 63, Helsinki, Helsinki 14, Finland.
E-mail: minja.laulajainen@helsinki.fi
[3]These authors have contributed equally to this work.
Received 28 August 2007; revised 13 November 2007; accepted 15 November 2007; published online 10 December 2007

proteins, merlin interacts with F-actin, however, only through N-terminal sites (Xu and Gutmann, 1998; Brault *et al*., 2001). Even though the FERM domain of merlin is highly similar to the ERM proteins, the first 18 amino acids that precede the FERM domain (Brault *et al*., 2001; Shimizu *et al*., 2002) are unique to merlin (Golovnina *et al*., 2005). Interestingly, these 18 amino acids have been indicated in the actin binding of merlin (Brault *et al*., 2001).

We have previously shown that PKA binds to and phosphorylates merlin (Grönholm *et al*., 2003; Alfthan *et al*., 2004). PKA is a serine/threonine kinase that regulates the activity of several proteins, including the ERM family member ezrin (Zhou *et al*., 2003). The cyclic AMP–PKA pathway plays a role in cell division and actin cytoskeleton remodeling (Howe, 2004), and activation of PKA promotes cell growth and cell cycle progression in Schwann cells (Kim *et al*., 1997), the cells susceptible to tumor formation in the NF2 disease. The previously described binding between the α-helical domain of merlin and RIβ, one of the four regulatory subunits of PKA, suggests that merlin might function as a protein kinase A-anchoring protein (Grönholm *et al*., 2003).

Our previous study identified a PKA site in the N terminus of merlin in addition to the C-terminal serine 518 (Alfthan *et al*., 2004). We have now further characterized the N-terminal PKA-catalysed phosphorylation of merlin, and mapped the phosphorylation site to serine 10. In addition, we have studied the role of serine 10 in the regulation of actin cytoskeleton.

Results

Merlin contains two PKA phosphorylation sites, serine 10 in the FERM domain and serine 518 in the C-terminal domain

Our previous studies suggested that PKA phosphorylates the N-terminal domain of merlin (Alfthan *et al*., 2004). Metabolic labeling was performed to test whether this phosphorylation can be detected *in vivo*. 293A HEK cells transfected with wild-type (WT) and S518A (mimicking the unphosphorylated residue) merlin-glutathione *S*-transferase (GST) constructs were incubated with ^{32}P-labeled orthophosphate together with forskolin and 3-isobutyl-1-methylxanthine (IBMX) to activate PKA or with H89 to inhibit PKA activity. The amount of bound orthophosphate in merlin was compared to the orthophosphate in GST. Forskolin- and IBMX-treated WT merlin showed pronounced phosphorylation, which was reduced but not completely abolished with the PKA inhibitor H89 (Figure 1b). The amount of bound orthophosphate in merlin S518A was lower than that in WT, but the construct was still phosphorylated. Treatment of S518A with the PKA inhibitor strongly reduced the amount of bound orthophosphate.

With deletion constructs, we further mapped the phosphorylated region *in vitro* to amino acids 1–100 (data not shown), which contains one serine (S10) and two threonines (T28 and T53). These potential kinase recognition motifs were mutated to non-phosphorylatable alanines and an *in vitro* phosphorylation reaction was performed with recombinant GST-merlin proteins. Incubation of the fusion proteins with [^{33}P]ATP and human recombinant PKA resulted in incorporation of

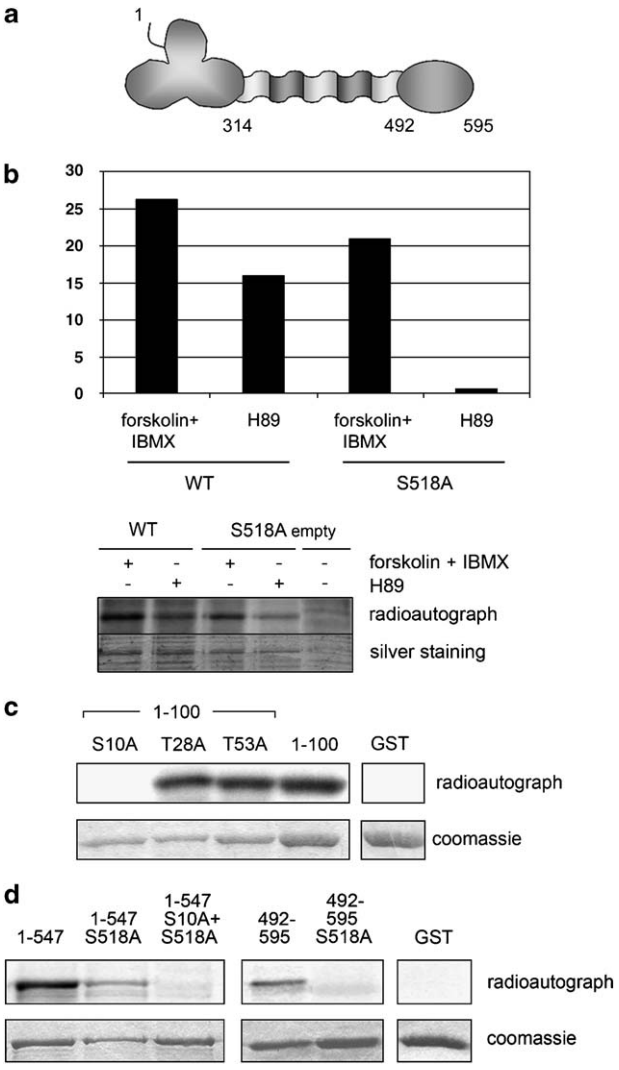

Figure 1 Merlin contains two PKA phosphorylation sites, serine 10 and serine 518. (**a**) Schematic overview of merlin's structural domains. Numbers indicate amino acids. (**b**) *In vivo* phosphorylation of merlin. Cells transfected with GST-merlin and treated with either forskolin and IBMX or with H89 were metabolically labeled with [^{32}P]orthophosphate. Merlin was pulled down, run on SDS–PAGE, silver stained (lower panel) and exposed (upper panel). The chart shows quantification of the orthophosphate signal. S518A is still phosphorylated in forskolin/IBMX-treated cells. (**c**) GST-merlin fusion proteins were phosphorylated *in vitro* using [^{33}P]ATP and human recombinant PKA. Proteins were separated on SDS–PAGE and exposed (upper panel). The Coomassie blue staining shows loading of the constructs (lower panel). Merlin 1–100 is phosphorylated by PKA and S10A mutation abolishes the phosphorylation. (**d**) Merlin 1–547 and merlin 492–595 constructs with serine 10 and/or serine 518 substituted with alanine were used to confirm the PKA phosphorylation of merlin. The double mutant (1–547 S10A + S518A) is not phosphorylated by PKA.

^{33}P into merlin constructs 1–100, 1–100 T28A and 1–100 T53A, but not into 1–100 S10A or GST (Figure 1c), indicating that the site phosphorylated by PKA is serine 10.

To verify that serine 10 functions as a substrate residue also in a longer merlin molecule, we mutated the phosphorylatable residues in merlin 1–547. WT merlin could not be used since it is degraded when produced as a GST fusion protein in bacteria. As shown in Figure 1d, incorporation of ^{33}P was detected both in merlin 1–547 and 1–547 S518A, although phosphorylation of merlin 1–547 S518A was reduced when compared to 1–547. However, when a double mutation (S10A + S518A) was introduced to merlin 1–547, no phosphorylation could be detected. As expected, the merlin C terminus (amino acids 492–595) was phosphorylated by PKA, but the S518A mutation abolished the phosphorylation. These results indicate that serines 10 and 518 are the only PKA phosphorylation sites present in merlin.

Mutation of serine 10 does not affect serine 518 phosphorylation or ezrin binding

Differentially phosphorylated forms of merlin differ in their electrophoretic mobility. Therefore, previous *in vivo* phosphorylation studies investigated the mobility of merlin mutants in SDS–polyacrylamide gel electrophoresis (PAGE). WT merlin migrates in the gel as a triplet, with the bands corresponding to hyperphosphorylated, phosphorylated and hypophosphorylated forms of the protein (Shaw *et al*., 1998; Alfthan *et al*., 2004). When serine 518 is dephosphorylated or mutated to alanine (S518A), the slowest migrating, hyperphosphorylated form of merlin disappears (Alfthan *et al*., 2004). To determine whether PKA phosphorylation of serine 10 induces similar changes in electrophoretic mobility, we generated mutations mimicking unphosphorylated (S10A or S518A) or phosphorylated (S10D or S518D) forms at both PKA phosphorylation sites. Lysates from 293 HEK cells, expressing these mutant proteins, were analysed by SDS–PAGE. Consistent with earlier studies, WT merlin migrated as a triplet in the gel (Figure 2a). As previously shown, the hyperphosphorylated merlin band was absent in the S518A mutants. However, we observed all three migrating species in both S10A and S10D, suggesting that phosphorylation of serine 10 does not induce a conformational change that would result in altered electrophoretic mobility. Substitution of serine 10 did not affect the band shift caused by serine 518 phosphorylation, since the slowest migrating merlin

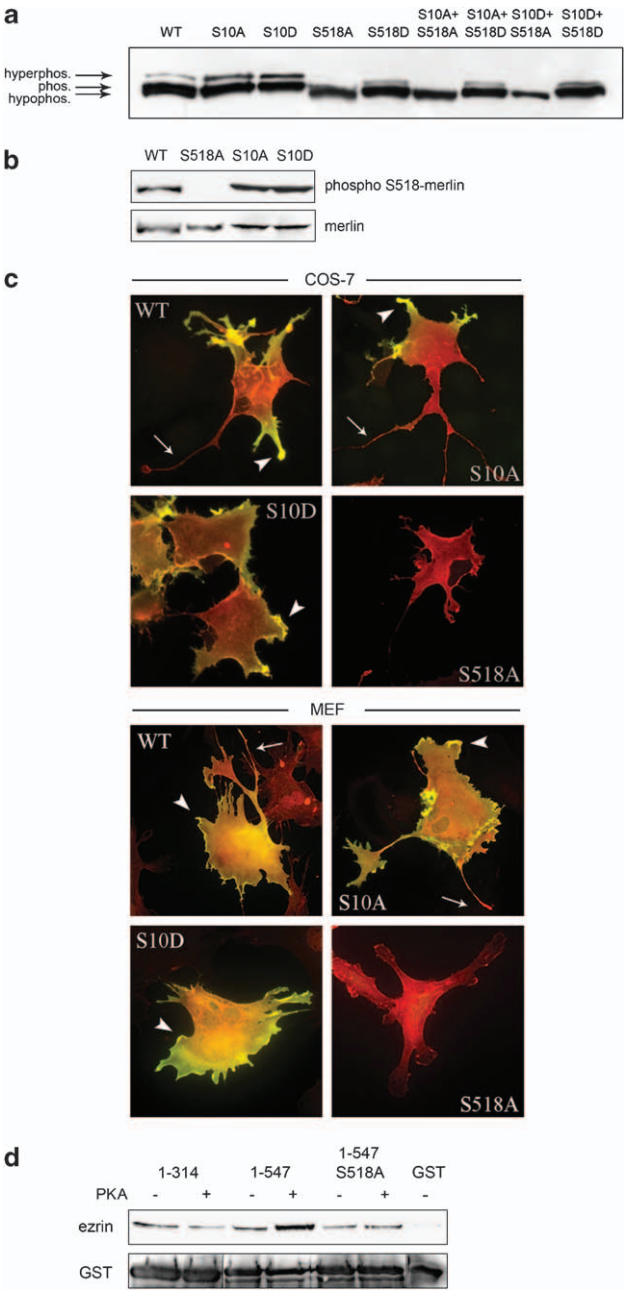

Figure 2 Electrophoretic mobility, ezrin binding and cellular localization of merlin mutants. (**a**) 293 HEK cells were transfected with merlin constructs and soluble fractions of cell lysates were immunoblotted. Wild-type (WT) merlin migrates as a triplet of hyperphosphorylated, phosphorylated and hypophosphorylated forms. Mutation of serine 10 does not affect the electrophoretic mobility of merlin. Merlin was detected with KF10 mAb. (**b**) Western blot analysis of lysates from transfected 293 HEK cells. WT, S10A and S10D merlin are recognized with the phosphoserine 518 (pS518) pAb, whereas S518A is not detected (upper panel). Expression levels of constructs are shown with merlin KF10 mAb (lower panel). (**c**) COS-7 cells and Nf2−/− MEFs transfected with WT, S10A, S10D and S518A merlin were stained with antibodies detecting merlin (KF10 mAb, red) and merlin phosphorylated at S518 (pS518 pAb, green). Long cell extensions in WT- and S10A-expressing cells are not stained by pS518 pAb (arrow). Serine 518 phosphorylated merlin is present in shorter protrusions observed in WT-, S10A- and S10D-transfected cells (arrowhead). pS518 Ab does not detect merlin S518A mutant. (**d**) Non-phosphorylated (−) or PKA phosphorylated (+) GST-merlin was incubated with purified full-length ezrin. Proteins were run in SDS–PAGE and detected with ezrin 3C12 mAb (upper panel) and merlin with GST pAb (lower panel). Phosphorylation of merlin 1–547 enhances ezrin binding whereas no difference in binding affinity is detected with phosphorylated merlin 1–314 or 1–547 S518A.

band was present in constructs with S10 mutations. Insoluble fractions of the lysates showed similar results and we could not detect any differences in the solubility of the constructs (data not shown), suggesting that S10 does not markedly regulate the association of merlin with detergent-insoluble cytoskeleton.

To further test whether PKA-induced phosphorylation of serine 10 is a prerequisite for serine 518 phosphorylation and to examine the possible link between the two sites, 293 HEK cells were transfected with the mutated merlin constructs and analysed with an antibody specifically recognizing S518 phosphorylated merlin (pS518 Ab). The expression levels of merlin constructs were verified using merlin KF10 Ab (antibody) (Figure 2b). Mutation of serine 10 did not reduce the reactivity of pS518 Ab, consistent with the results from the electrophoretic mobility assay. As expected, pS518 Ab did not detect the S518A construct.

To analyse serine 518 phosphorylation of merlin S10 mutants *in vivo*, COS-7 cells and mouse embryonic fibroblasts lacking merlin (Nf2−/− MEFs) were transfected with the mutants. Overexpression of WT and S10A merlin induced long thin cellular extensions that were not stained with the pS518 Ab. However, serine 518 phosphorylated merlin was present in shorter thicker protrusions observed in WT-, S10A- and S10D-transfected cells (Figure 2c). These findings suggest that phosphorylation of serine 10 does not directly affect serine 518 phosphorylation.

We have previously shown that PKA phosphorylation of serine 518 promotes merlin–ezrin heterodimerization (Alfthan *et al*., 2004). To determine whether serine 10 phosphorylation similarly regulates intermolecular binding with ezrin, we examined the interaction of phosphorylated and unphosphorylated merlin constructs with ezrin *in vitro* by GST pull-down assays. Equal amounts of merlin constructs were used and the loading was verified by GST antibody. We observed the previously reported effect of serine 518 phosphorylation on ezrin binding, as PKA-treated merlin 1–547 pulled down more full-length ezrin than unphosphorylated merlin 1–547 (Figure 2d). In contrast, PKA-mediated phosphorylation of the merlin N terminus (amino acids 1–314) or 1–547 S518A did not increase merlin–ezrin binding.

Serine 10 affects the morphological changes induced by merlin

Overexpressed WT merlin influences cell morphology (Sainio *et al*., 1997). To study whether the phenotypic effect of merlin is regulated by modification of serine 10, COS-7 cells and Nf2−/− MEFs were transiently transfected with WT, S10A or S10D merlin either in isoform I or II, and examined by immunofluorescence microscopy.

Overexpression of merlin isoform I (WT) affected cell morphology, leading to an increase in the amount of membrane extensions both in COS-7 cells and Nf2−/− MEFs (Figure 3). Merlin isoform II also induced cell projections, but they were often more abundant and longer than those observed with WT isoform I. Expression of merlin S10A resulted in long cellular extensions, and these extensions were even more pronounced in S10A isoform II. Interestingly, S10D expression induced a morphology with dense filopodia-like structures but only rarely long cellular projections. These data suggest that phosphorylation of serine 10 regulates merlin-induced cell morphology.

Serine 10 phosphorylation regulates F-actin organization

As serine 10 regulates cell morphology and the first 18 amino acids of merlin are involved in actin binding (Brault *et al*., 2001), we hypothesized that phosphorylation of serine 10 might affect the interplay between merlin and actin. To study the effect of phosphorylation mutants on actin cytoskeleton organization, Nf2−/− MEFs were transfected with WT, S10A, S10D or S518A merlin. Cells were stained for F-actin and merlin, and lamellipodial structures were analysed by confocal and immunofluorescence microscopy.

Untransfected cells displayed intense F-actin staining in stress fibers, whereas the actin filament staining in WT and S518A merlin-transfected cells showed less pronounced fibers and often a dense cytoplasmic actin network (Figure 4a). The intensity of cytoplasmic F-actin staining was weaker in cells expressing merlin S10A compared to untransfected cells or cells expressing other merlin constructs. S10A cells lacked both stress fibers and the actin filament network seen in cells expressing WT merlin. These cells were also irregularly shaped and made no lamellipodia. Cells transfected with the S10D mutant displayed stress fibers resembling those of untransfected cells.

The amount of F-actin of whole cells, visualized by phalloidin fluorescence intensity, was quantified from WT-, S10A- and S10D-expressing cells and analysed with Image J software (Figure 4b). The intensity of merlin-transfected cells was normalized to the intensity of untransfected cells. In cells expressing WT merlin, the phalloidin staining was significantly stronger than in untransfected cells, indicating that these cells contain more filamentous actin. A decrease of F-actin was observed in cells expressing S10A, whereas S10D-transfected cells displayed phalloidin intensity most by resembling the untransfected cells.

Merlin S10D protects the actin cytoskeleton from Latrunculin B-induced depolymerization

Based on our observation that differentially phosphorylated merlin constructs influence cell morphology and actin cytoskeleton organization, we studied actin dynamics in merlin-transfected cells. Nf2−/− MEFs, transfected with merlin WT, S10A or S10D, were incubated with Latrunculin B (LatB), used to dissociate F-actin. Cells were fixed before or 8 min after LatB treatment, stained for merlin and F-actin, and analysed by immunofluorescence microscopy.

Latrunculin B treatment caused actin depolymerization in WT-transfected cells, and in S10A cells the actin cytoskeleton was completely disrupted (Figure 5). However,

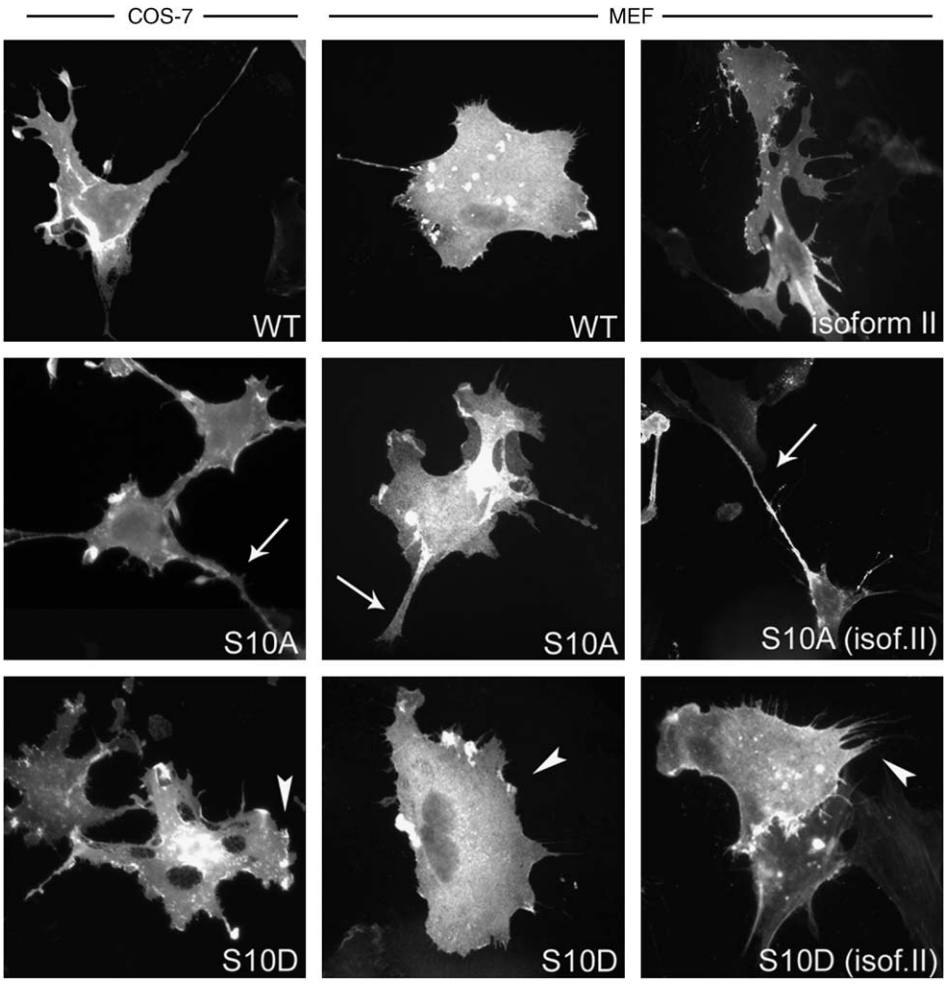

Figure 3 Phenotypic effect of serine 10 mutations. COS-7 cells and Nf2−/− MEFs were transfected with WT, S10A or S10D mutant merlin isoform I (WT) or isoform II and stained with merlin KF10 mAb (COS-7) or merlin pAb A-19 (Nf2−/− MEFs). WT and S10A merlin-expressing cells have long extensions (arrows) not seen in cells expressing S10D. S10D expression induces dense filopodia-like structures (arrowheads) not seen in WT-, isoform II- or S10A-transfected cells.

actin filaments in S10D-expressing cells depolymerized at a slower rate, indicating that this construct stabilizes actin filaments. All merlin constructs relocalized to the cytoplasm as a result of LatB treatment.

Serine 10 phosphorylation regulates cell migration and lamellipodia formation

Rapid actin polymerization at the leading edge of a moving cell results in the formation of filopodia and lamellipodia. Since we observed changes in both the morphology and actin organization of merlin-transfected cells, we hypothesized that also cell motility may be affected. Wound-healing assays were performed with Nf2−/− MEFs and Nf2−/− Schwann cells, infected with retro- and adenovirus constructs, respectively, analysed by phase contrast microscopy and wound widths quantified. Both MEFs and Schwann cells lacking merlin filled the wound in 24–48 h, whereas the migration of merlin-infected cells was slower (Figure 6a). Interestingly, S10A-expressing cells closed the wound even slower than their WT counterparts ($P<0.001$ in both MEFs and Schwann cells).

The movement of WT- and S10A-expressing cells was also studied by live cell imaging. Merlin constructs were co-transfected into Nf2−/− MEFs with a green fluorescent protein (GFP) vector to allow identification of the merlin-containing cells. S10A-expressing cells did not display lamellipodia seen in WT-transfected cells, but instead the expression promoted the formation of protrusions and extensions (Figure 6b, Supplementary Data). Thus, the migration rate of S10A merlin-transfected cells may be reduced because of alterations in lamellipodia formation.

Discussion

Post-translational modifications such as phosphorylation regulate the biological activity of merlin. At low cell density, merlin is phosphorylated and growth permissive,

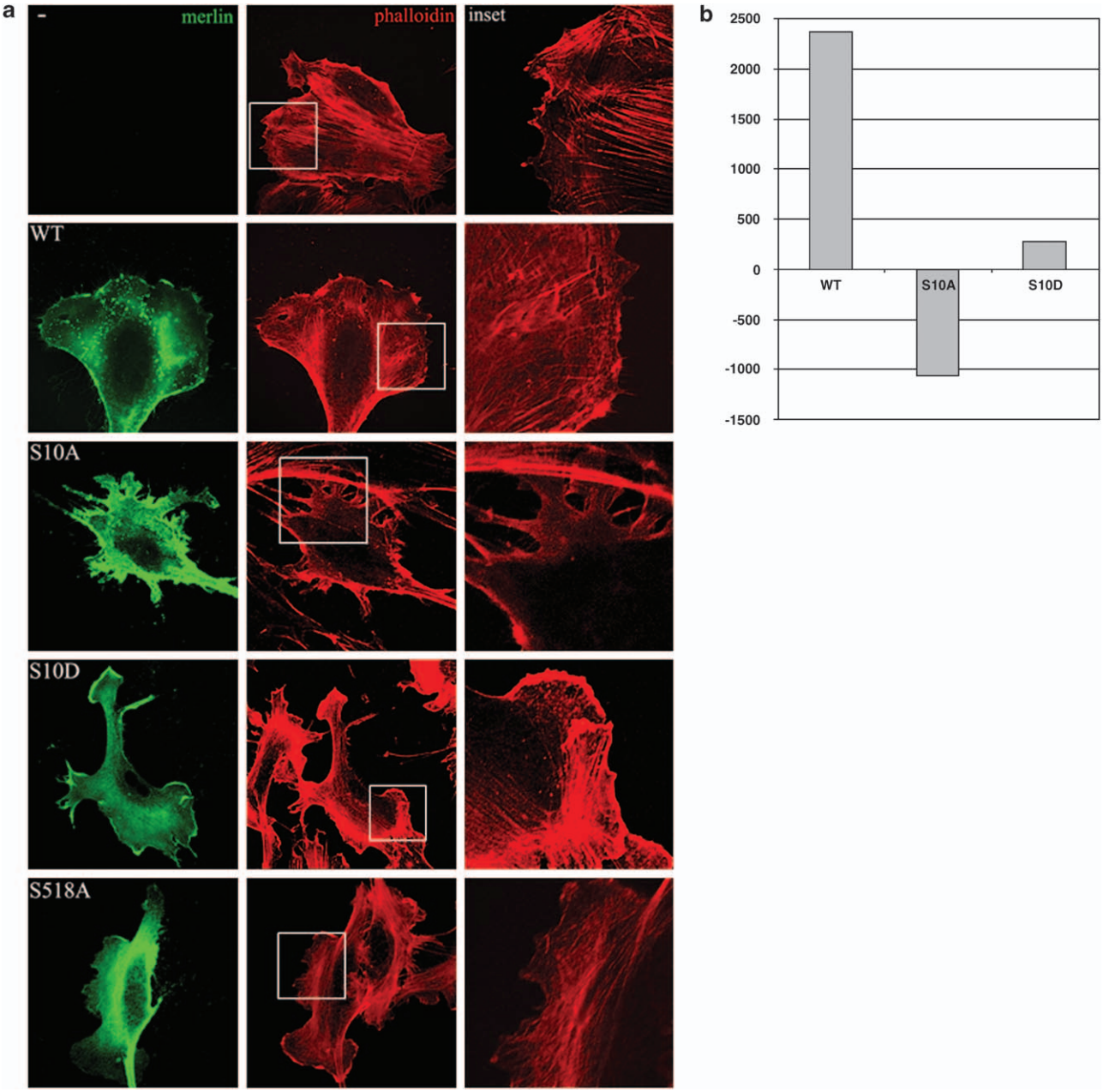

Figure 4 Altered F-actin organization in cells expressing merlin mutants. Nf2−/− MEFs transfected with WT, S10A, S10D or S518A were stained with merlin pAb A-19 (green) and phalloidin (red) and analysed with a confocal microscope. (**a**) Single confocal sections at the plane close to ventral surface are shown. The right panel shows a higher magnification of the marked area. (**b**) Intensity of phalloidin staining of whole WT-, S10A- and S10D-expressing cells analysed with Image J software after normalization against untransfected control cells. WT cells show increased and S10A cells display decreased phalloidin staining intensity compared to untransfected cells.

whereas merlin exists in a hypophosphorylated form as a result of serum deprivation, high cell density or loss of adhesion. The hypophosphorylated form of merlin is growth inhibitory and represents the functionally active tumor suppressor (Shaw *et al*., 1998; Morrison *et al*., 2001). We have previously shown that in addition to PAK, also PKA phosphorylates merlin at serine 518 (Alfthan *et al*., 2004). We now identify an additional PKA phosphorylation site in merlin, and present evidence that this phosphorylation site plays a role in merlin's ability to regulate the actin cytoskeleton. The identified PKA phosphorylation site, serine 10, is conserved in merlin homologs in mouse, rat and *Xenopus*, suggesting that the residue has important functions.

Merlin contains multiple phosphorylated residues, but the only well-characterized phosphorylation site is serine 518 (Shaw *et al*., 1998, 2001; Kissil *et al*., 2002;

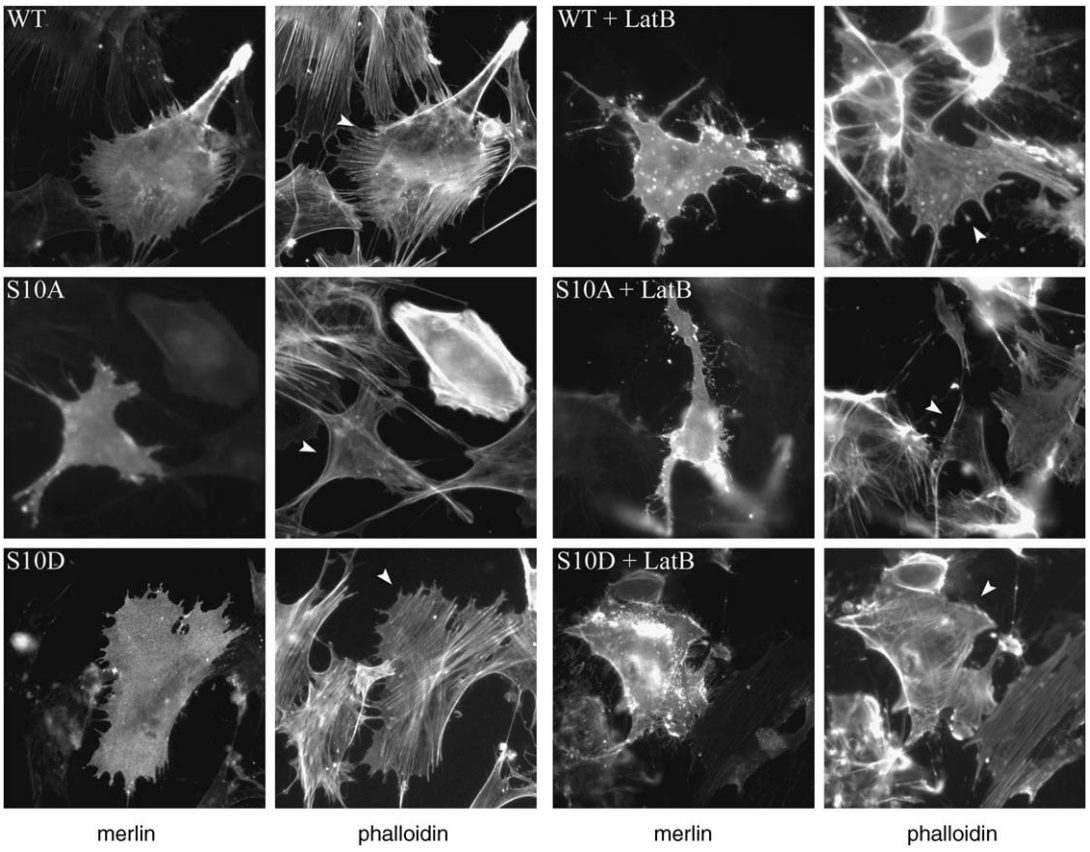

Figure 5 Actin depolymerization in merlin-expressing cells. Nf2−/− MEFs transfected with merlin WT, S10A or S10D were fixed before (left panel) or 8 min after (right panel) Latrunculin B (LatB) treatment. Cells were stained with merlin pAb A-19 and phalloidin; arrowheads indicate merlin-transfected cells. LatB treatment induces actin depolymerization in WT and S10A cells, whereas S10D cells are more resistant to the LatB effect.

Xiao *et al*., 2002; Alfthan *et al*., 2004). Phosphorylation of this site participates in the control of cell proliferation, morphology and motility, all important for the tumor suppressor function of merlin. Serine 518 phosphorylation impairs merlin's ability to self-associate and affects the binding of interacting proteins such as CD44, hepatocyte growth factor-regulated tyrosine kinase substrate, PKA regulatory subunit RIβ and tubulin (Grönholm *et al*., 2003; Rong *et al*., 2004; Muranen *et al*., 2007). To test whether phosphorylation of serine 10 similarly affects the activity of merlin, mutants mimicking both phosphorylated and unphosphorylated S10 were examined for their ability to mediate functions previously described for merlin. Neither form of serine 10 directly affected the phosphorylation of serine 518, and phosphorylation of serine 10 did not enhance binding to ezrin in contrast to phosphorylation of serine 518. These results suggest that phosphorylation of the two PKA sites have distinct functions and is regulated independently of each other.

Merlin is localized underneath the plasma membrane, especially at areas of membrane remodeling (Gonzalez-Agosti *et al*., 1996; Sainio *et al*., 1997). Phosphorylation of serine 518 promotes the appearance of multiple cell extensions in different cell types (Surace *et al*., 2004; Thaxton *et al*., 2007), and serine 518 phosphorylated merlin is present at the most peripheral regions of lamellipodia, microspikes and radial membrane protrusions in Schwann cells (Thaxton *et al*., 2007). Our data suggest that merlin's phosphorylation state, not only at serine 518 but also at serine 10, influences cell morphology. Merlin S10A expression resulted in the appearance of long cellular extensions. These structures lacked serine 518 phosphorylated merlin, which instead was present in cellular protrusions. In contrast, S10D merlin promoted the formation of multiple short filopodia-like protrusions where serine 518 phosphorylation was apparent. Our data show that only a subset of merlin molecules at specific membrane structures are hyperphosphorylated, suggesting that the phosphorylation status of merlin is tightly regulated. Interestingly, we detected a more prominent cell-extension effect with merlin isoform II containing the S10 mutations, indicating that phosphorylation of serine 10 in a more open merlin molecule is more efficient in promoting changes in cell morphology. This effect might be mediated through actin, since deformation of the cell membrane requires reorganization of actin filaments and merlin isoform II has a different affinity for actin than isoform I (James *et al*., 2001).

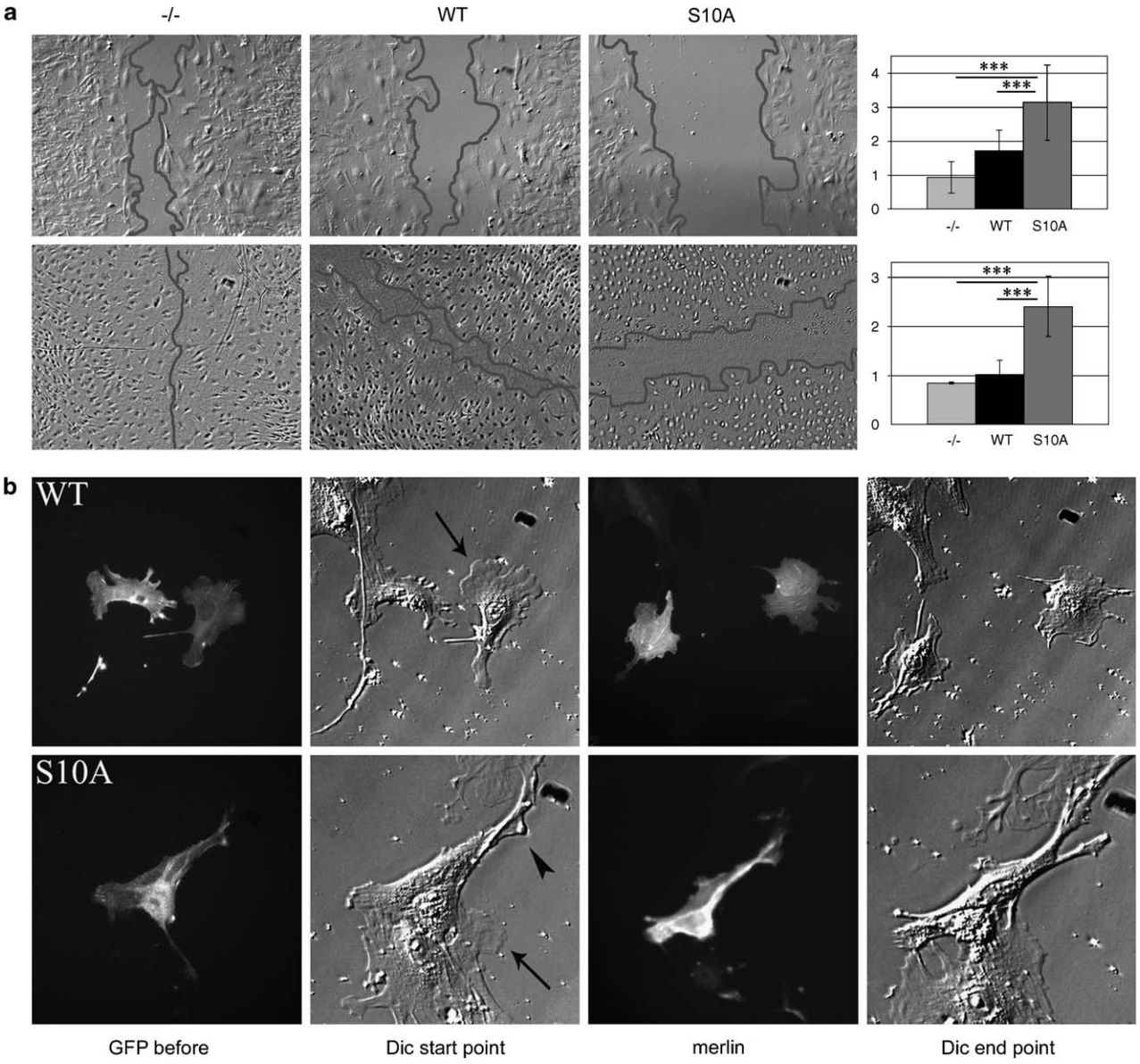

Figure 6 Mutation of S10 leads to defects in cell migration and lamellipodia formation. (**a**) Nf2−/− MEFs (upper panel) and Nf2−/− Schwann cells (lower panel) expressing empty vector, merlin WT or merlin S10A were wounded and examined by phase contrast microscopy. Cells lacking merlin filled the wound in 24–48h, whereas cells expressing WT and S10A merlin were slower in their migration. Gray lines show cell monolayer edges. The right panel shows quantification of wound width 24–48 h after wounding. WT- and S10A-expressing cells have a significant difference in their migration rate (***$P<0.001$ in both MEFs and Schwann cells). Mean values ± s.d. calculated from four experiments are shown in arbitrary units. (**b**) Nf2−/− MEFs were co-transfected with GFP-α-actinin and merlin WT or S10A. Live cells expressing merlin were chosen by their GFP expression and imaged for 5 h with a DIC filter (videos are provided as Supplementary Information). Still images from the videos are shown (second and fourth panels) together with the GFP expression (first panel) and merlin A-19 pAb staining (third panel). Arrows mark lamellipodia and arrowhead filopodia. Lamellipodia formation is impaired in S10A-expressing cells.

Cellular transformation is often associated with disorganization of the cell cytoskeleton, which links cytoskeletal alterations to tumor formation. Nf2-deficient schwannoma cells exhibit cytoskeletal abnormalities manifested by membrane ruffling, large surface areas and F-actin instability (Pelton *et al*., 1998). It has previously been shown that the merlin FERM domain and isoform II have the ability to stabilize actin filaments and reduce depolymerization rates (James *et al*., 2001), whereas PAK phosphorylation of serine 518 weakens merlin's association with the cytoskeleton (Shaw *et al*., 2001). Serine 10 appears to be involved in regulating some of the cytoskeletal changes observed, as both F-actin organization and the amount and depolymerization of F-actin were affected by S10 mutations. Interestingly, a drastic decrease of F-actin was detected in S10A-expressing cells, suggesting that dephosphorylation of serine 10 reduces actin filament formation,

while S10D merlin stabilizes the filaments. Therefore, serine 10 is important for actin filament dynamics *in vivo*. We could not, however, detect any differences in the solubility, actin binding or actin depolymerization effect of S10 mutants compared to WT *in vitro* (data not shown). Thus, we hypothesize that the observed effect of merlin on actin cytoskeleton is indirect through merlin interaction partners regulating actin cytoskeleton.

Cell movement is induced by protrusion of a leading edge, movement of the cell body and finally by retraction of the cell. Nf2-deficient primary fibroblasts migrate faster than WT cells expressing merlin in wound-healing assays (Shaw *et al*., 2001), which we also observed in our studies with Nf2-deficient MEFs and Schwann cells. However, S10A merlin-expressing cells migrated even slower than the WT-infected cells. S10D cells migrated at a reduced rate between WT- and S10A-expressing cells (data not shown), indicating that regulation of the phosphorylation state of serine 10 is important for cell motility. S10A-transfected cells also displayed altered lamellipodia formation. The lamellipodium is critical for cell motility since it localizes protein complexes needed for actin polymerization (Small *et al*., 2002). Thus, as proper formation of lamellipodia is impaired in S10A merlin-expressing cells, their ability to migrate may be altered.

It has been proposed that the very N-terminal sequence of merlin contains residues important for actin binding, and that this region may function as a common protein-binding motif (Brault *et al*., 2001; Golovnina *et al*., 2005). Interestingly, Bai *et al*. (2007) recently showed that the first 50 amino acids of merlin contain regulatory residues that affect the interplay between merlin, ezrin, actin and CD44. Phosphorylation of serine 10 could be involved in regulating the formation of these complexes.

The results described in this study indicate that phosphorylation of serine 10 is an important factor in the functional regulation of merlin and that PKA-dependent phosphorylation of serine 10 participates in cytoskeletal organization.

Materials and methods

Plasmids and antibodies

Human merlin isoform I (WT, amino acids 1–595) and isoform II (amino acids 1–590) in pcDNA3 vector (Invitrogen, Carlsbad, CA, USA) were used for transfection experiments. For expression of recombinant GST fusion proteins, the following constructs were used: merlin 1–100, merlin N terminus (amino acids 1–314), merlin 1–547, merlin C terminus (amino acids 492–595) and full-length ezrin, all in pGEX4T1 vector (Amersham Biosciences, Buckinghamshire, UK). Point mutations of merlin in all vectors were made by site-directed mutagenesis using the QuikChange Kit (Stratagene, La Jolla, CA, USA). WT or S518A merlin in pDEST27 vector (Invitrogen) containing an N-terminal GST tag was used for metabolic labeling. Merlin retro- and adenovirus constructs have been described previously (Schulze *et al*., 2002; Muranen *et al*., 2007). GFP-α-actinin used in live cell imaging has also been described before (Hotulainen and Lappalainen, 2006).

Anti-merlin pAb A-19 sc-331 (Santa Cruz Biotechnology, Santa Cruz, CA, USA) and mAb KF10 (den Bakker *et al*., 1995) were used to detect merlin. S518 phosphorylated merlin was detected with pS518 pAb (Biodesign, Saco, ME, USA). 3C12 mAb (Böhling *et al*., 1996) was used for ezrin detection, Alexa-568-conjugated phalloidin (Invitrogen-Molecular Probes, Carlsbad, CA, USA) to detect F-actin and anti-GST polyclonal goat antibody (GE Healthcare, Budapest, Hungary) to detect GST proteins. Alexa-488-, Alexa-568- and Alexa-594-conjugated goat anti-mouse and goat anti-rabbit antibodies (Invitrogen-Molecular Probes) were used as secondary antibodies in immunofluorescence and HRP-conjugated rabbit anti-mouse and swine anti-rabbit (both from DAKO A/S, Glostrup, Denmark) and swine anti-goat (Santa Cruz Biotechnology) secondary antibodies in western blot analysis.

Cell culture, transfections and immunoblotting

293 human embryonic kidney (HEK) cells were maintained in RPMI 1640 medium supplemented with 10% fetal calf serum (FCS) (PromoCell, Heidelberg, Germany). COS-7 cells, merlin−/− mouse embryonic fibroblasts (Nf2−/− MEFs) and 293A HEK cells were all grown in Dulbecco's minimum essential medium (DMEM, Gibco-Invitrogen, Carlsbad, CA, USA) with 10% FCS. Primary Nf2 knockout Schwann cells (Giovannini *et al*., 2000) were isolated and cultured as previously described (Manent *et al*., 2003). The cells were immortalized and used before passage 20.

Cells were transfected using Fu-GENE6 reagent (Roche, Basel, Switzerland) and incubated for 48 h before analysis. Cells grown on glass coverslips were fixed in 3.5% paraformaldehyde (pH 7.5) for immunofluorescence. For western blotting, cells were rinsed with phosphate-buffered saline and lysed in ELB buffer (50 mM HEPES, pH 7.4, 150 mM NaCl, 5 mM EDTA) containing 0.5% Nonidet P-40 (NP-40), 1.5 μM okadaic acid (Calbiochem, San Diego, CA, USA), HALT phosphatase inhibitors (Pierce, Rockford, IL, USA) and Complete protease inhibitors (Roche). Lysed cells were centrifuged at 20 000 *g* for 30 min at +4 °C. Protein concentrations were determined by Bio-Rad Protein Assay (Bio-Rad, Hercules, CA, USA). Equal amounts of proteins were analysed by SDS–PAGE and immunoblotting.

Metabolic labeling

Forty-eight hours after merlin transfection, 293A HEK cells were changed into serum- and phosphate-free DMEM, and 1 mCi ml^{-1} of ^{32}P-labeled orthophosphate (Amersham Biosciences) was added for 2 h. Cells were treated with 50 μM IBMX and 25 μM forskolin or 40 μM H89 (all from Sigma-Aldrich, St Louis, MO, USA) for 30 min or 2 h respectively. Cells were lysed in ELB buffer with 1% NP-40, phosphatase inhibitors (HALT, 1.5 μM Calyculin A (Calbiochem), Cocktail Set IV (Calbiochem), 1.5 μM okadaic acid) and protease inhibitors, and centrifuged at 14 000 *g* for 30 min at +4 °C. Samples were diluted to a final concentration of 0.5% NP-40, glutathione Sepharose (Amersham Biosciences) was added to the lysates to pull down merlin and the samples were incubated overnight at +4 °C. Beads were washed with ELB buffer containing inhibitors, reducing Laemmli buffer was added and samples were run in 8% SDS–PAGE. Gels were silver stained following standard protocol, dried and exposed on a PhosphoImager plate, read by TyphoonImager 9400 and analysed by ImageQuant TL2003 software (all by GE Healthcare). The amount of bound orthophosphate was normalized to the merlin amount, and the background radioactivity (empty GST plasmid) was subtracted.

In vitro *phosphorylation*
Glutathione *S*-transferase fusion proteins were expressed in *Escherichia coli* DH5α and purified. Glutathione-Sepharose beads to which 5 μg of fusion protein was conjugated were washed in PKA buffer (20 mM Tris–HCl, 10 mM $MgCl_2$, pH 7.4). The phosphorylation reaction was carried out in a 30 μl buffer volume, including 10 μCi of [γ-^{33}P]ATP (PerkinElmer, Waltham, MA, USA) and 2 ng of purified human recombinant PKA (Sigma-Aldrich) for 30 min at +30 °C. The reaction was stopped by washing the beads in PKA buffer and adding reducing Laemmli buffer. Samples were resolved by 12% SDS–PAGE. The gel was fixed and stained with Coomassie blue followed by exposure to a PhosphoImager plate and detection with Typhoon as previously described.

Merlin–Ezrin pull-down
Bacterially expressed full-length ezrin was cleaved from GST by thrombin (Sigma-Aldrich). Glutathione-Sepharose beads carrying 5 μg of merlin fusion proteins were washed in PKA buffer and phosphorylated by human recombinant PKA as described above except that 200 μM of cold ATP (Sigma-Aldrich) was used. After phosphorylation, beads were washed in binding buffer (50 mM HEPES, pH 7.4, 150 mM NaCl, protease inhibitors). Four micrograms of thrombin-cleaved ezrin was incubated with phosphorylated or unphosphorylated merlin constructs under rotation for 2 h at +4 °C. Beads were washed with binding buffer, reducing Laemmli buffer was added and bound proteins were resolved in SDS–PAGE. Proteins were detected with ezrin and GST antibodies.

Actin stainings and quantification
Nf2−/− MEFs, transfected with WT, S10A, S10D or S518A, were stained with merlin pAb A-19 and phalloidin. Images were taken with Leica SP2 confocal microscope, equipped with Ar and Kr lasers (Leica Microsystems, Heerbrugg, Switzerland). For quantification of actin, cells were imaged with immunofluorescence microscopy (Zeiss Axiophot equipped with AxioCam cooled CCD camera, Carl Zeiss, Esslingen, Germany) using a fixed exposure of 900 ms for phalloidin. The intensity of the actin staining was measured from whole cells by Image J (v10.2) software. Total fluorescence from 20 merlin-transfected cells and untransfected cells from the same slides was analysed separately, and the staining intensities were normalized to the untransfected cells. The experiment was repeated three times with similar results.

Latrunculin B assay
Forty-eight hours after transfection, Nf2−/− MEFs were fixed (zero time point) or treated with 2.5 μM Latrunculin B (Sigma-Aldrich) for 8 min. Cells were stained for merlin and phalloidin and analysed with a fluorescence microscope.

Wound-healing assay and quantification
For wound-healing assays, Nf2−/− MEFs and Nf2−/− Schwann cells (P18) were infected with retro- and adenovirus constructs, respectively, containing merlin WT, S10A or empty virus as previously described (Schulze *et al*., 2002; Muranen *et al*., 2007). Plates were wounded 24–48 h after infection, and the wound healing was monitored. After 72 h, cells were fixed and stained with merlin A-19 pAb to control infection efficiency. Quantification of wound width was carried out by ImageJ software, and mean values and standard deviations were calculated. The experiment was repeated four times with similar results.

Live cell imaging
Nf2−/− MEFs were co-transfected with GFP-α-actinin and merlin 24–48 h before imaging. Cells were imaged with an inverted Olympus IX81 microscope and CellR program at +37 °C, 5% CO_2. Images were taken every 30 s for 5 h. GFP expression images were taken before and after the experiment, and the cells were stained for merlin to verify expression. Imaging was done from seven cells of both constructs with similar results.

Acknowledgements

We thank Dr Giovannini for the Nf2−/− MEFs and Schwann cells and Dr Hanemann for the retroviral merlin construct. We also thank H Ahola and A Björg-Agustsdottir for their skillful technical assistance. This study was supported by the grants of Department of Defense W81XWH-05-1-0469, the Finnish Cancer Organizations, the Medical Research Fund of Turku University Central Hospital District, Helsinki Graduate School of Biotechnology and Molecular Biology, Biomedicum Helsinki Foundation, Medicinska Understödsföreningen Liv och Hälsa, Emil Aaltonen Foundation, Oskar Öflund Foundation and Svenska kulturfonden.

References

Alfthan K, Heiska L, Grönholm M, Renkema GH, Carpén O. (2004). Cyclic AMP-dependent protein kinase phosphorylates merlin at serine 518 independently of p21-activated kinase and promotes merlin–ezrin heterodimerization. *J Biol Chem* **279**: 18559–18566.

Bai Y, Liu YJ, Wang H, Xu Y, Stamenkovic I, Yu Q. (2007). Inhibition of the hyaluronan–CD44 interaction by merlin contributes to the tumor-suppressor activity of merlin. *Oncogene* **26**: 836–850.

Baser ME, R Evans DG, Gutmann DH. (2003). Neurofibromatosis 2. *Curr Opin Neurol* **16**: 27–33.

Brault E, Gautreau A, Lamarine M, Callebaut I, Thomas G, Goutebroze L. (2001). Normal membrane localization and actin association of the NF2 tumor suppressor protein are dependent on folding of its N-terminal domain. *J Cell Sci* **114**: 1901–1912.

Bretscher A, Edwards K, Fehon RG. (2002). ERM proteins and merlin: integrators at the cell cortex. *Nat Rev Mol Cell Biol* **3**: 586–599.

Böhling T, Turunen O, Jääskelainen J, Carpén O, Sainio M, Wahlström T *et al*. (1996). Ezrin expression in stromal cells of capillary hemangioblastoma. An immunohistochemical survey of brain tumors. *Am J Pathol* **148**: 367–373.

den Bakker MA, Tascilar M, Riegman PH, Hekman AC, Boersma W, Janssen PJ *et al*. (1995). Neurofibromatosis type 2 protein co-localizes with elements of the cytoskeleton. *Am J Pathol* **147**: 1339–1349.

Giovannini M, Robanus-Maandag E, van der Valk M, Niwa-Kawakita M, Abramowski V, Goutebroze L *et al*. (2000). Conditional biallelic Nf2 mutation in the mouse promotes manifestations of human neurofibromatosis type 2. *Genes Dev* **14**: 1617–1630.

Golovnina K, Blinov A, Akhmametyeva EM, Omelyanchuk LV, Chang LS. (2005). Evolution and origin of merlin, the product of the neurofibromatosis type 2 (NF2) tumor-suppressor gene. *BMC Evol Biol* **5**: 69.

Gonzalez-Agosti C, Wiederhold T, Herndon ME, Gusella J, Ramesh V. (1999). Interdomain interaction of merlin isoforms and its influence on intermolecular binding to NHE-RF. *J Biol Chem* **274**: 34438–34442.

Gonzalez-Agosti C, Xu L, Pinney D, Beauchamp R, Hobbs W, Gusella J *et al*. (1996). The merlin tumor suppressor localizes preferentially in membrane ruffles. *Oncogene* **13**: 1239–1247.

Grönholm M, Sainio M, Zhao F, Heiska L, Vaheri A, Carpén O. (1999). Homotypic and heterotypic interaction of the neurofibromatosis 2 tumor suppressor protein merlin and the ERM protein ezrin. *J Cell Sci* **112**: 895–904.

Grönholm M, Vossebein L, Carlson CR, Kuja-Panula J, Teesalu T, Alfthan K *et al*. (2003). Merlin links to the cAMP neuronal signaling pathway by anchoring the RIbeta subunit of protein kinase A. *J Biol Chem* **278**: 41167–41172.

Hotulainen P, Lappalainen P. (2006). Stress fibers are generated by two distinct actin assembly mechanisms in motile cells. *J Cell Biol* **173**: 383–394.

Howe AK. (2004). Regulation of actin-based cell migration by cAMP/PKA. *Biochim Biophys Acta* **1692**: 159–174.

James MF, Manchanda N, Gonzalez-Agosti C, Hartwig JH, Ramesh V. (2001). The neurofibromatosis 2 protein product merlin selectively binds F-actin but not G-actin, and stabilizes the filaments through a lateral association. *Biochem J* **356**: 377–386.

Jin H, Sperka T, Herrlich P, Morrison H. (2006). Tumorigenic transformation by CPI-17 through inhibition of a merlin phosphatase. *Nature* **442**: 576–579.

Kim HA, DeClue JE, Ratner N. (1997). cAMP-dependent protein kinase A is required for schwann cell growth: Interactions between the cAMP and neuregulin/tyrosine kinase pathways. *J Neurosci Res* **49**: 236–247.

Kissil JL, Johnson KC, Eckman MS, Jacks T. (2002). Merlin phosphorylation by p21-activated kinase 2 and effects of phosphorylation on merlin localization. *J Biol Chem* **277**: 10394–10399.

Manent J, Oguievetskaia K, Bayer J, Ratner N, Giovannini M. (2003). Magnetic cell sorting for enriching Schwann cells from adult mouse peripheral nerves. *J Neurosci Methods* **123**: 167–173.

Morrison H, Sherman LS, Legg J, Banine F, Isacke C, Haipek CA *et al*. (2001). The NF2 tumor suppressor gene product, merlin, mediates contact inhibition of growth through interactions with CD44. *Genes Dev* **15**: 968–980.

Muranen T, Grönholm M, Lampin A, Lallemand D, Zhao F, Giovannini M *et al*. (2007). The tumor suppressor merlin interacts with microtubules and modulates schwann cell microtubule cytoskeleton. *Hum Mol Genet* **16**: 1742–1751.

Pelton PD, Sherman LS, Rizvi TA, Marchionni MA, Wood P, Friedman RA *et al*. (1998). Ruffling membrane, stress fiber, cell spreading and proliferation abnormalities in human Schwannoma cells. *Oncogene* **17**: 2195–2209.

Rong R, Surace EI, Haipek CA, Gutmann DH, Ye K. (2004). Serine 518 phosphorylation modulates merlin intramolecular association and binding to critical effectors important for NF2 growth suppression. *Oncogene* **23**: 8447–8454.

Rouleau GA, Merel P, Lutchman M, Sanson M, Zucman J, Marineau C *et al*. (1993). Alteration in a new gene encoding a putative membrane-organizing protein causes neuro-fibromatosis type 2. *Nature* **363**: 515–521.

Sainio M, Zhao F, Heiska L, Turunen O, den Bakker M, Zwarthoff E *et al*. (1997). Neurofibromatosis 2 tumor suppressor protein colocalizes with ezrin and CD44 and associates with actin-containing cytoskeleton. *J Cell Sci* **110**: 2249–2260.

Schulze KM, Hanemann CO, Muller HW, Hanenberg H. (2002). Transduction of wild-type merlin into human schwannoma cells decreases schwannoma cell growth and induces apoptosis. *Hum Mol Genet* **11**: 69–76.

Shaw RJ, McClatchey AI, Jacks T. (1998). Regulation of the neurofibromatosis type 2 tumor suppressor protein, merlin, by adhesion and growth arrest stimuli. *J Biol Chem* **273**: 7757–7764.

Shaw RJ, Paez JG, Curto M, Yaktine A, Pruitt WM, Saotome I *et al*. (2001). The Nf2 tumor suppressor, merlin, functions in rac-dependent signaling. *Dev Cell* **1**: 63–72.

Sherman L, Xu HM, Geist RT, Saporito-Irwin S, Howells N, Ponta H *et al*. (1997). Interdomain binding mediates tumor growth suppression by the NF2 gene product. *Oncogene* **15**: 2505–2509.

Shimizu T, Seto A, Maita N, Hamada K, Tsukita S, Tsukita S *et al*. (2002). Structural basis for neurofibromatosis type 2. Crystal structure of the merlin FERM domain. *J Biol Chem* **277**: 10332–10336.

Small JV, Stradal T, Vignal E, Rottner K. (2002). The lamellipodium: where motility begins. *Trends Cell Biol* **12**: 112–120.

Surace EI, Haipek CA, Gutmann DH. (2004). Effect of merlin phosphorylation on neurofibromatosis 2 (NF2) gene function. *Oncogene* **23**: 580–587.

Tang X, Jang SW, Wang X, Liu Z, Bahr SM, Sun SY *et al*. (2007). Akt phosphorylation regulates the tumour-suppressor merlin through ubiquitination and degradation. *Nat Cell Biol* **9**: 1199–1207.

Thaxton C, Lopera J, Bott M, Baldwin ME, Kalidas P, Fernandez-Valle C. (2007). Phosphorylation of the NF2 tumor suppressor in schwann cells is mediated by Cdc42-pak and requires paxillin binding. *Mol Cell Neurosci* **34**: 231–242.

Trofatter JA, MacCollin MM, Rutter JL, Murrell JR, Duyao MP, Parry DM *et al*. (1993). A novel moesin-, ezrin-, radixin-like gene is a candidate for the neurofibromatosis 2 tumor suppressor. *Cell* **75**: 826.

Turunen O, Sainio M, Jääskelainen J, Carpén O, Vaheri A. (1998). Structure–function relationships in the ezrin family and the effect of tumor-associated point mutations in neurofibromatosis 2 protein. *Biochim Biophys Acta* **1387**: 1–16.

Xiao GH, Beeser A, Chernoff J, Testa JR. (2002). p21-activated kinase links Rac/Cdc42 signaling to merlin. *J Biol Chem* **277**: 883–886.

Xu HM, Gutmann DH. (1998). Merlin differentially associates with the microtubule and actin cytoskeleton. *J Neurosci Res* **51**: 403–415.

Zhou R, Cao X, Watson C, Miao Y, Guo Z, Forte JG *et al*. (2003). Characterization of protein kinase A-mediated phosphorylation of ezrin in gastric parietal cell activation. *J Biol Chem* **278**: 35651–35659.

Supplementary Information accompanies the paper on the Oncogene website (http://www.nature.com/onc).

Ezrin is key regulator of Src-induced malignant phenotype in three-dimensional environment

Heiska Leena‡, Zhao Fang‡, Saotome Itsiko#, McClatchley Andrea I#, and Carpén Olli‡¶§

‡Biomedicum Helsinki, Department of Pathology, Neuroscience Program, University of Helsinki and Helsinki University Hospital, FIN-00014 Helsinki, Finland; #MGH Cancer Center and Harvard Medical School of Pathology, Charlestown, MA; and ¶Department of Pathology, University of Turku and Turku University Hospital, FIN-20520 Turku, Finland

Running title:
Key words:

§ Corresponding author:
Olli Carpén
Department of Pathology
Kiinamyllynkatu 10
20520 Turku, Finland
Tel.: 358-2-3337217
Fax: 358-2-3337459
E-mail: ocarpen@utu.fi

SUMMARY

The oncogenic tyrosine kinase Src is activated in various cancers. Src activation promotes invasive and metastatic behaviour and may therefore play a role at later stages of cancer development. Src has numerous substrates and it activates a myriad of signaling pathways. It is not clear, however, which of these alterations promote malignant phenotype. One of Src substrates is ezrin, a multifunctional protein that organises actin cytoskeleton and regulates signal transduction. Ezrin is essential in experimental metastatic osteosarcoma and increased ezrin expression correlates with metastatic behaviour and poor outcome of diverse cancers. To study, whether Src and ezrin act in concert in tumorigenesis, we reconstituted genetically ezrin-deficient cell lines with wild-type or phosphorylation deficient ezrin together with constitutively active Src. In two-dimensional cultures, Src induced malignant features independent of whether the cells expressed wild-type or mutant ezrin or were ezrin deficient. However, only cells expressing wild type ezrin and active Src grew efficiently in soft agar. Furthermore, expression of ezrin significantly promoted Src-induced growth and invasion in Matrigel, a three-dimensional extracellular matrix from mouse tumor. Wild-type and mutant ezrin expressing cells had identical morphology on culture plates but showed marked differences in three dimensional matrix, where only wild-type ezrin was targeted to specific regions on the plasma membrane. We conclude that the pathways activated by Src depend on the type of environment and that ezrin is a crucial element of Src-induced malignant features of cells growing in three dimensional matrices.

INTRODUCTION

The nonreceptor tyrosine kinase Src is the first identified proto-oncogene (reviewed in {{1037 Martin,G.S. 2001;}}). Src-dependent oncogenic mechanisms affect a wide variety of cellular functions and signaling pathways, for example pathways leading to cell survival, migration and invasion. Increased expression or activation of Src has been shown in many types of human primary cancers and especially in metastastic tumors {{891 Irby,R.B. 2000;893 Frame,M.C. 2002;892 Summy,J.M. 2003;}} and hence, Src inhibitors are extensively investigated for cancer therapy {{1044 Summy,J.M. 2006;}}. Increased Src activity is thought not to be essential for early tumorigenic events. Rather, Src appears to provide a selective advantage to tumor cells during metastatic processes by facilitating invasion and spreading to distant organs {{1044 Yeatman,T.J. 2004;}}.

One of Src kinase substrates is ezrin, a linker protein that connects cell membrane and actin cytoskeleton (reviewed in {{425 Bretscher,A. 2002;615 Tsukita,S. 1999;}}). Ezrin belongs to the ERM (ezrin-radixin-moesin) proteins, which fold as inactive molecules through an N- to C-terminal association. Ezrin is activated via binding to PIP_2 and phosphorylation of a conserved threonine residue {{277 Fievet,B.T. 2004;}}. Ezrin is implicated in signal transduction networks both as a regulator and an effector; it interacts with various members of protein kinase A, Rho and phosphatidylinositol-3 kinase signaling pathways. Ezrin is the only ERM protein shown to be directly phosphorylated on tyrosine by the Src family kinases Lck and Src {{387 Autero,M. 2003;897 Heiska,L. 2005;901 Srivastava,J. 2005;}}. The Src-induced phosphorylation of ezrin tyrosine 477 leads to binding of a Kelch-repeat family protein KBTBD2 (Kelch-repeat and BTB/POZ domain binding 2) {{897

Heiska,L. 2005;}}. On the other hand, Src binds ezrin through its SH2 domain {{37 Bretscher,A. 2000;901 Srivastava,J. 2005;}}. Src and ezrin act cooperatively in deregulation of cell-cell contacts and scattering of carcinoma cells {{832 Elliott,B.E. 2004;}}. However, the cellular effects of ezrin's Src-dependent phosphorylation are largely unknown.

Ezrin has been indicated in human tumorigenesis and especially metastatic processes {{182 McClatchey,A.I. 2003;275 Curto,M. 2004;}}. Upregulation of ezrin correlates to invasive characteristics of malignant cell lines {{644 Akisawa,N. 1999;604 Ohtani,K. 1999;}} as well as to malignancy, metastasic behavior and poor clinical outcome of diverse cancers {{28 Geiger,K.D. 2000;95 Makitie,T. 2001; 458 Ohtani,K. 2002;1039 Ilmonen,S. 2005;1042 Weng,W.H. 2005;1040 Kobel,M. 2006;1041 Kobel,M. 2006;}}. Ezrin was discovered in a subtractive hybridization screen for metastasis-associated genes of rat pancreatic and mammary carcinomas {{132 Nestl,A. 2001;}}. By a microarray approach, Khanna et al. identified ezrin as an essential protein for experimental metastasic osteosarcoma and a marker of poor outcome in spontaneous canine osteosarcomas and in pediatric osteosarcomas {{123 Khanna,C. 2001;151 Khanna,C. 2004;}}. The ezrin-dependent osteosarcoma metastasis was later linked to mammalian target of rapamycin (mTOR) pathway downstream of Akt {{1043 Wan,X. 2005;}}. Furthermore, microarray-based profiling of highly and poorly metastatic rhabdomyosarcoma lines and a subsequent analysis of the corresponding human patient samples showed that ezrin expression is a key prometastatic regulator {{150 Yu,Y.L. 2004;1007 Yu,Y. 2006;}}. Ezrin was required for breast cancer metastasis in a mouse model, and Src kinase and PI3K were the effectors of ezrin in the metastatic process {{832 Elliott,B.E. 2004;}}.

Src is thought to induce malignant phenotype by altering various signaling pathways. However, until now, there is no single down-stream element that would unite the characteristic phenotypic changes, *i.e.* adhesion-independent survival, increased invasiveness and ability to grow, pre-eminently in three dimensional matrices. Since increased ezrin expression and Src activity correlate with malignant behavior *in vivo* and since ezrin is substrate for Src {{897 Heiska,L. 2005;}}, we investigated whether ezrin and Src act in concert in induction of metastatic characteristics. We utilized genetically engineered ezrin deficient mouse embryonic fibroblasts and reintroduced wild-type (WT) ezrin or an unphosphorytable mutant form to them in combination with constitutively active Src. Our results show that ezrin is a major regulator of Src-induced anchorage-independency, growth and cell invasion and that a form of ezrin that cannot be phosphorylated by Src does not promote these activities. Moreover, the interplay between ezrin and Src is only evident in cells grown in three-dimensional environment.

MATERIALS AND METHODS

Cell lines

Embryonic fibroblasts derived from ezrin -/- mouse {{887 Saotome,I. 2004;}} were spontaneously immortalized by serial dilution and maintained in D-MEM medium including 10% fetal calf serum (FCS) and antibiotics. Two independently immortalized MEF lines were established and all experiments performed with the two different sets of cells. For establishing the stable ezrin add-back

lines, the wild-type (WT) and the mutant versions of the full-length ezrin cDNA were introduced to pBABEpuro vector {{899 Morgenstern,J.P. 1990;}}. 293 Eco Phoenix retrovirus packaging cell line was transfected with the different constructs, the virus containing supernatant collected and used in the transduction of the MEFs according to a standard protocol {{898 Miller,A.D. 1993;}}.The expression vector containing cell populations were selected with 2.5 mg/ml of puromycin (Sigma) in the medium. To express constitutively active Src, the cells were further introduced with a retroviral construct pLXSH-SrcY527F {{776 Cary,L.A. 2002;}}, kindly provided by Dr. J. A. Cooper (Fred Hutchinson Cancer Research Center, Seattle, WA), and selected with 0.25 mg/ml of hygromycin B (Calbiochem). The amino acid numbering of ezrin is according to Krieg et al. {{777 Krieg,J. 1992;}}.

Antibodies

Phosphotyrosine was detected with the monoclonal anti-phosphotyrosine antibody (mAb) clone PT-66 (Sigma-Aldrich). The polyclonal rabbit antibody against human ezrin (Ez9) has been described {{4 Alfthan,K. 2004;}}. Mouse IgG1 (Dako Cytomation, Glostrup, Denmark) or rabbit preimmune serum were used as controls. Rabbit phosphospecific antibodies against active (pY418)Src and against phosphorylated (pT558)moesin were from BioSource International (Camarillo, CA) and Santa Cruz Biotechnology (Santa Cruz, CA), respectively. Rat monoclonal anti-moesin antibody M22 was a kind gift of Dr. Sa. Tsukita (Kyoto University, Kyoto, Japan), and mouse anti-cortactin mAb was from Upstate (Lake Placid, NY).

Immunoprecipitation of ezrin

The cells were lysed in cold RIPA buffer (50 mM TrisHCl, 150 mM NaCl, 1% NP-40, 0.5% deoxycholate, 0.1% SDS, 1 mM orthovanadate, proatease inhibitor mix, pH 7.4) and centrifuged at 16 000 x g for 10 min. Ezrin was immunoprecipitated from the supernatants with the Ez9 antibody followed by incubation with the protein G Sepharose beads (Amersham Pharmacia). The beads were washed four times in RIPA buffer and suspended to Laemmli buffer. The immunoprecipitate was resolved on SDS-PAGE, blotted on nitrocellulose and analyzed by immunoblotting with appropriate antibodies using ECL-detection (Amersham Pharmacia).

Cell proliferation assay

On day 0, 5 x 10^3 cells/well were plated on a 24 well cell culture plate in quadruple. On the day of analysis, the wells were washed with PBS and incubated with 200 µl of 40 mg/ml MTT ([3-(4,5-dimethylthiazol-2-yl)-2,5-diphenyltetrazolium-bromide], Sigma) in PBS for 3 hours, after which the liquid was discarded and the converted dye suspended into 200 µl of DMSO. 100 µl aliquots were analyzed with a microtiter plate reader at 550 nm.

Cell adhesion analysis

The cells were serum starved overnight, detached with trypsin, washed twice in excess PBS and plated 2 x 10^5 cells per well in medium without serum on 96 well cell culture plates coated with fibronectin (10 µg/ml). The cells were monitored by light microscopy during attachment. To quantify the attached

cells, the wells were washed with PBS after different time periods, the attached cells stained with crystal violet, and the bound dye measured after extraction with 0.1 % Triton X-100 with a microtiter plate reader at 595 nm.

Fluorescence microscopy, confocal microscopy and 3-D reconstruction

Cells were grown on glass coverslips, fixed in 3,5 % formaldyhyde, permeabilized in 0,1 % Triton X-100 in PBS, incubated with the primary antibody for 30 min at 37 C, washed and incubated with the secondary antibody similarly. The secondary antibody was rhodamine conjugated donkey anti-rabbit or anti-mouse $F(ab')_2$ (Jackson Immunoresearch). For labeling of F-actin, rhodamine conjugated phalloidin (Molecular Probes) was used. To stain the cells inside Matrigel (growth-factor reduced Matrigel, BD BioSciences, Bedford, MA), a modification of the method described by Debnath et al. {{1032 Debnath,J. 2003;}} was used. Briefly, eight-well glass chamber slide was coated with a layer of Matrigel (50 µl per well). A mixture of 5 x 10^3 cells, Matrigel (1/3 of the total volume) and culture medium was added on the solidified bottom layer in a volume of 100 µl per well. The solidified mixture was overlaid with cell culture medium and the slide incubated for 24 – 48 h. The wells were fixed in 3.5 % paraformaldehyde, permeabilized in 0.5 % Triton X-100 for 10 min, and rinsed three times with 130 mM NaCl, 7 mM Na_2HPO_4, 3.5 mM NaH_2PO_4, 100 mM glycine. The wells were blocked in 10 % normal swine serum diluted into IF buffer (130 mM NaCl, 7 mM Na_2HPO_4, 3.5 mM NaH_2PO_4, 0.1 % bovine serum albumine, 0.2 % Triton X-100, 0.05 % Tween-20) for 2 h. The primary antibody was incubated overnight in the blocking solution. The wells were washed three times 15 min with the IF buffer, incubated with the secondary antibody diluted in the blocking buffer, followed by washes with the IF buffer. The slide was mounted with Mowoil (Calbiochem) mixed 1:3 with 1,4-diazabicyclo[2.2.2. octane] (Sigma). All the steps were done at room temperature. The slides were visualized under epifluorescence microscope and Leica SP2 confocal microscope. Serial sections for 3D reconstruction were taken by confocal microscope using half thickness of the objective lens's z-resolution as step size. The 3D reconstruction was performed by Leica LCS 3D software package.

Spheroid formation and cell scattering experiments

The spheroids were formed by a method described by Bizik {{1067 Eleveld-Trancikova,D. 2002;}}. Briefly, 5 x 10^3 cells were made to form spheroids by plating them on U-bottomed microtiter wells, which were precast with a thin film of 1 % agar. The cells were incubated for 24 – 48 hours. The formed spheroids were carefully removed and transferred on a 24 well plate, which was precast with a solution containing 1 mg/ml type I collagen (BD Biosciences), 10 % fetal calf serum and 50 mM $NaHCO_3$. The spheroids were overlaid with culture medium and observed by light microscope.

Cell culture in Soft agar and insuspension

5 x 10^4 cells were plated in triplicate in 0.3 % agar containing DMEM and 10 % fetal calf serum on a layer of precast 0.6 % agar. The number and size of the resulting colonies was determined by microscopic visualization after 14 – 21 days. For growth in suspension, 5 x 10^5 cells were seeded on bacterial 35 mm plates in medium containing 0.5 % methyl cellulose (Sigma). The clusters of > 10

cells from two different plates of each subclone were counted under a light microscope after 7 - 10 days.

Invasion assay

Invasion was measured using growth factor reduced Matrigel invasion chamber (BD Biosciences, Bedford, MA) according to manufacturer's protocol. The inserts were rehydrated with 0.5 ml cell culture medium, 5 x 10^4 cells were seeded to the chamber in medium containing 1 % fetal calf serum, and the plate wells were filled with 0.75 ml medium containing 10 % fetal calf serum. After 36 hours, the non-invading cells were removed with a cotton swap, the membrane fixed in 3,5 % paraformaldehyde and the invaded cells stained with crystal violet. The cells were counted using 20 x magnification from 5 different fields.

Cell culture inside Matrigel

96 well microtiter cell culture plates were precast with 50 µl of Matrigel diluted 1:3 in culture medium. The layer was overlaid with 100 µl of a mixture containing 5 x 10^3 cells, Matrigel (1/3 of the volume) and medium. After the gel had solidified, the wells were overlaid with medium and incubated for 14 days. The Matrigel plug was fixed in 100 µl of 3.5 % paraformaldehyde, indubated on ice until liquified, and the cells counted using hemocytometer.

RESULTS

Characterization of MEF cell lines

To study the role of ezrin in Src-induced cellular functions in a model without intervening endogenous ezrin, we utilized MEF cells from the ezrin knock-out mouse {{887 Saotome,I. 2004;}}. In two previous publications, the target residues of Src kinase on ezrin have been mapped as Y145 and Y477 {{901 Srivastava,J. 2005;897 Heiska,L. 2005;}}. Therefore, the ezrin -/- MEF cells were stably introduced with the WT, the Y145F mutant, or the Y477F mutant full-length ezrin expression constructs or with the plasmid vector alone. Ezrin expression in addback cells was verified by immunoblotting (Fig. 1A). The ezrin -/- MEFs introduced with the plasmid vector as a control did not show any ezrin expression. The endogenous levels of a related ERM protein, moesin were equal in the parent MEFs or in the subclones (Fig. 1B). This indicates that the presence or absence of ezrin is not compensated by upregulation of other ERM proteins. Similarly, the level of phosphorylated threonine 558 of moesin was unchanged as detected with an anti-p(558T)moesin antibody (Fig. 1C). In longer exposures, the anti-(pT558)moesin antibody faintly cross-reacted with a band corresponding to the molecular size of ezrin in the ezrin-containing subclones (data not shown); this reactivity was equal between the clones harboring the WT or the mutant forms of ezrin. The result indicates that the presence or absence of the WT or the mutated forms of ezrin does not affect threonine phosphorylation and conformational activation of the ERM proteins.

To express active Src kinase, the cells were further introduced with a constitutively active Src (Y527F) expression construct. The expression of active Src was verified by immunoblotting of the cell lysates

with an anti-(pY418)Src antibody, which recognizes Src only when its autoactivating Y418 residue is phosphorylated (Fig. 1D). The cells expressing Y527FSrc showed prominent overall tyrosine phosphorylation compared to the cells which were not expressing active Src, as detected with an anti-(pY)antibody (data not shown). Introduction of active Src construct lead to upregulation of ezrin in the MEF addback clones (compare lane 2 in fig. 1A with lanes 4-6), in line with previous fingerprint analysis of Src-regulated changes in gene expression (Malek et al. 2002).

To study, whether ezrin serves as a Src substrate in this model and to identify the substrate tyrosine, we immunoprecipitated ezrin from the various sublines. The anti-(pY)antibody did not react with the WT ezrin in the absence of active Src (Fig. 1E). On the contrary, in the presence of Src kinase activity both the WT and the Y145F mutant ezrin were phosphorylated on tyrosine, whereas mutation of Y477 abolished the reactivity. The results verify that ezrin is a substrate for Src-induced tyrosine phosphorylation and Y477 is the main target in the MEF subclones. Therefore, in the following experiments the cells expressing empty vector, WT ezrin or the Y477F mutant ezrin were included.

Ezrin is not required for Src-induced alterations in cells grown on two-dimensional surfaces

Next we examined the localization of ezrin in the different sublones grown on coverslips. In the ezrin -/- MEF addback cells, both the WT (Fig. 2A) and the Y477F form of ezrin (not shown) localized to short microvilli-like extensions at the cell membrane. The staining was specific, as the vector control cells were not stained by the anti-ezrin antibody (Fig. 2D). Introduction of active Src changed the cellular morphology from the normal fibroblast-like to more a polygonal and refracted appearance; *i.e.* the shape characteristic for transformed cells. No differences were seen between the localization of WT and the mutant form of ezrin. Both forms were partly concentrated to the plasma membrane and partly located diffusely in the cytoplasm (Fig. 2B, C). Brightly stained spots of ezrin were seen at cellular protrusions or in filopodial structures. Occasionally the staining in the cytoplasm showed a fine reticular pattern. The actin cytoskeleton was prominently altered after introduction of active Src. The pronounced stress fibers (Fig. 2E) disappeared, and actin was concentrated heavily on podosomal or rosette-like structures regardless of the ezrin protein status in the cells (Fig. 2F; not all subclones are shown). The active form of Src also located on the podosome-like structures described originally in Rous sarcoma virus-transformed fibroblasts {{1033 Tarone,G. 1985;}} (Fig. 2G). The localization of active Src was similar in the subclones containing WT or the Y477F mutant ezrin (Fig. 2H). The typical podosomal structures further contained cortactin, a well-known Src substrate (not shown). In ezrin-containing subclones these structures occasionally contained ezrin, whether the mutant or the WT form (data not shown). The results confirm earlier studies of the effects of Src kinase activity to the cell cytoskeleton and show that ezrin is not required for podosome formation in fibroblasts. Furthermore, the results indicate that the role of ezrin tyrosine phosphorylation by Src is not in targeting of either ezrin or Src in two-dimensional cell cultures.

To further address the role of ezrin tyrosine phosphorylation, we set up standard assays for functions implicated in Src activation. First, we measured the proliferation capacity of the different subclones

grown on cell culture plates (Fig. 3A). The absence or presence of the WT or mutated ezrin did not affect the adhesion dependent growth of the clones. On the contrary, the presence of active Src clearly enhanced the proliferation of all clones compared to the parental clones which were not introduced with the Src expression construct (the clone harboring WT ezrin is shown in the figure).

Next we studied the effects on cell adhesion or migration. The cellular adhesion was judged both visually and quantitatively by plating serum-starved cells on fibronectin coated dishes for different time periods. No ezrin-dependent differences in attachment or in the kinetics of adherence were seen, when the morphology and appearance of the attaching cells was monitored by microscopical examination (not shown). Adhesion was further studied by quantitative measurements. The presence of active Src increased the rate of adherence in all subclones (Fig. 3B). In the classical wound healing experiments the subclones containing different ezrin constructs or the plasmid control did not show any differences in migration (data not shown). The cells containing constitutively active Src were highly motile and easily detached from the substrate in this assay.

A tyrosine phosphorylable form of ezrin is required for Src-induced malignant behavior of cells in three-dimensional matrix

In earlier studies ezrin has been implicated in migration of cancer cells in three-dimensional matrices or in tubulogenesis of kidney cells in collagen matrix {{202 Sahai,E. 2003;733 Crepaldi,T. 1997;638 Gautreau,A. 1999;}}. We set up assays involving 3D matrices in order to evaluate possible differences of the subclones and the significance of the Src-induced phosphorylation. First we studied the localization of ezrin in cells expressing different forms of ezrin in combination with active Src and growing inside a 3D matrix. In cells WT ezrin cells seeded in Matrigel (Fig. 4A), ezrin was concentrated in large submembraneous patches or polarized on one side of the cell. Instead, the Y477F mutant ezrin was located diffusely inside the cell and did not concentrate to the surface or localize to cell extensions. Active Src was concentrated the same way, as visualized with anti-(pY418)Src antibody (Fig. 4B) in cells harboring either the WT or the Y477 mutant ezrin. This indicates that targeting of Src is not dependent on ezrin phosphorylation, but in three-dimensional matrix ezrin targeting is dependent on Src kinase. In contrast, the focal adhesion scaffold protein paxillin, also a substrate of tyrosine phosphorylation via Src and the focal adhesion kinase FAK, was localised in a significantly more diffuse manner also in cells containing WT ezrin. To analyze other components in the WT ezrin containing patches, we double stained cells with fluorescent phalloidin or anti-cortactin antibody (Fig. 4C). The results showed that ezrin concentrates contained also aggregates of filamentous actin. Cortactin, a well characterized actin-binding Src substrate, was partially colocalized to the concentrated ezrin areas, but not exclusively. In Y477F cells the staining patterns of cortactin and ezrin differed more notably.

To study the migration and scattering of cells, cell spheroids were formed and seeded on a collagen gel. The morphology of the scattering cells was distinct; the cells harboring WT ezrin showed a rounded morphology (Fig. 4D, left). As earlier publications have implicated Rho kinase in the ezrin-dependent

amoeboid mode of cancer cell motility {{202 Sahai,E. 2003;}}, we treated the WT cells with the Rho kinase inhibitor Y-27632. The treated cells stayed longer as a compact spheroid, and the scattered cells showed an extended morphology (Fig 4D, middle). If the spheroids were treated with the Src kinase family selective inhibitor PP2, the sheroids on collagen were disrupted, and the individual cells were not viable (Fig 4D, right) indicating that Src kinase activity was required for the maintenance of the spheroids and for the viability of the cells in these conditions. The cells harboring the Y477F mutant ezrin showed an extended morphology resembling the Rho inhibitor treated WT cells (Fig. 4D, lower left). These results imply that the Src induced phosphorylation of ezrin is specifically involved in the growth and migration patterns of cells in three-dimensional environments.

We also studied the ability of the subclones to grow in soft agar (Fig. 5). The cells expressing WT ezrin but lacking active Src did not were not able to form colonies in soft agar. The cells containing active Src and the plasmid control induced few cell colonies, whereas the cells harboring both active Src and WT ezrin induced large, multicellular colonies visible already after some days. In 2-3 weeks, the number of colonies formed by WT ezrin expressing cells was four fold as compared to cells expressing active Src alone (Fig. 5B). If the cells expressed Y477F, growth in soft agar was greatly diminished. Moreover, if the medium in soft agar contained PP2, a Src family kinase selective inhibitor, the growth of the clone containing both WT ezrin and active Src was abolished. The results show that efficient growth of MEF cells in soft agar requires both Src kinase activity and ezrin with an intact Y477 residue.

As Src activation is required for resistance to anoikis (REF esim Windham 2002, Frisch 1994, Hisano 2003, Wei 2004), we studied the subclones when grown in suspension with methyl cellulose (Fig. 6A). Again, coexpression of WT ezrin and active Src promoted cell growth several fold better than Src alone. Furthermore, Y477F ezrin did not provide any growth-promoting effect. The result indicates that the presence of WT ezrin is beneficial in situations of impaired anchorage or anoikis. As ezrin has been shown to be involved in the migration of cancer cells {{202 Sahai,E. 2003;}}, the ability of the subclones to invade three-dimensional matrices was analyzed by counting the cells capable to transverse a layer of Matrigel cast on one side of a porous membrane (Fig. 6B). The results show that the presence of the WT but not Y477F ezrin facilitated the migration of the cells through the matrix in a Src kinase dependent manner. To analyze the ability of the cells to grow inside a 3D matrix, we quantified the cells growing inside Matrigel after 7 days (Fig. 6C). The cells harboring WT ezrin showed increased cell numbers compared to the other subclones. In summary, the results of these experiments indicate that the presence of WT but not Y477F form of ezrin promotes Src-dependent functions that are related to the cell's ability to migrate, invade and proliferate in a three-dimensional environment such as mammalian tissue.

DISCUSSION

Oncogenic processes and formation of metastases require complex alterations in cell behavior. Cells must proliferate, survive apoptosis, lose contact inhibition and polarity, become independent of

adhesion and gain ability to invade. Src kinase is the first characterized oncogene and linked especially with metastatic processes. We have used a study model of MEFs expressing active form of Src to delineate ezrin's role in malignant behavior. While our results do not show any ezrin dependent effects on morphology, proliferation or adhesion of the cells in the usual two-dimensional cell culture conditions, the picture becomes different when the cells are subjected to growth in a three-dimensional environment. Specifically therein, the presence of WT ezrin promotes functions related to malignancy, whereas introduction of the Y477F mutated ezrin does not give cells any advantage in comparison to the parental cells lacking ezrin protein.

Src is implied in many important pathways in tumor biology. Elevated or activated Src is particularly associated with later events in oncogenesis and with advanced metastatic cancers (reviewed in {{1044 Yeatman,T.J. 2004;}}. Src activity is an independent indicator of poor clinical prognosis in all stages of human colon carcinoma {{1052 Aligayer,H. 2002;}}, but increased Src levels and activating mutations are detected as colon tumors progress {{1048 Talamonti,M.S. 1993;1047 Cartwright,C.A. 1994;1045 Mao,W. 1997;1046 Irby,R.B. 1999;}}. Src activity is not required for proliferation or growth of tumors, whereas altered adhesion, invasion and the presence of micrometastases are strictly Src-dependent {{1049 Jones,R.J. 2002;1051 Boyd,D.D. 2004;1038 Boyer,B. 2002;}}. Inhibition of Src leads to decreased incidence of metastases in breast cancer and pancreatic adenocarcinoma {{1056 Rucci,N. 2006;1057 Trevino,J.G. 2006;}} as well as decreased invasion of prostate carcinoma and glioma cells {{1054 Slack,J.K. 2001;1055 Angers-Loustau,A. 2004;}}.

Several studies provide compelling evidence for ezrin's role as a prometastatic factor. Two distinct mouse tumor models show that ezrin is necessary for the metastatic capacity of osteosarcoma and rhabdomyosarcoma {{123 Khanna,C. 2001;151 Khanna,C. 2004;150 Yu,Y.L. 2004;}}. Ezrin inhibition significantly reduces osteosarcoma lung metastases in mice, and high ezrin expression in primary tumors is associated with significantly shortened DFI in dogs and human pediatric patients. In addition to mesenchymally derived cancers, ezrin has been identified in a screen which was searching for metastasis-associated genes in colorectal and mammary cancer {{132 Nestl,A. 2001;}}. Significant correlations between ezrin overexpression and increased malignancy or infiltrative growth are seen in uveal and cutaneous melanoma, astrocytoma, endometrioid and ovarian carcinoma and soft tissue sarcoma {{95 Makitie,T. 2001;1039 Ilmonen,S. 2005;28 Geiger,K.D. 2000;1041 Kobel,M. 2006;1040 Kobel,M. 2006;928 Weng,W.H. 2005;}}. Invading tumor cells of lung adenocarcinoma are strongly positive for ezrin, but not for moesin or radixin {{31 Tokunou,M. 2000;}}. In a mouse model of breast carcinoma inhibition of ezrin significantly reduces metastases to lung {{900 Elliott,B.E. 2005;}}.

Src affects various signal pathways and has several substrates. Ezrin is a known Src family kinase target {{387 Autero,M. 2003;897 Heiska,L. 2005;901 Srivastava,J. 2005;}}. Although the litterature on Src substrates is extensive, none of the target proteins has previously been shown to confer specific advantage in a three dimensional environment only. For many years it has been appreciated that two-dimensional culturing of cells is a highly unnatural model with cells attached only at their ventral

surface on an abnormally rigid structure. Three-dimensional culture systems can serve as a design which corresponds more closely to *in vivo* environments and provides a system to mimic *eg.* dissemination of cancer cells. The differences between two-dimensional and three-dimensional culture affect many cellular functions. For instance, adhesion structures are different both in composition and in structure (ref. Cukierman 2001; roskelley Bissell 1995); similarly, the migration of cells rely on different mechanisms (ref. Friedl). Moreover, gene expression profiles and signal transduction of cells grown in two- vs. three-dimensional culture differ (Birgesdotter, Cukierman). The differences are relevant to our understanding of cells in their physiological environment and especially in complex phenomena like oncogenesis and tumor dissemination.

Our findings have substantial implications for future studies, as they point out to a specific regulation of cells which is confined to growth in three-dimensional conditions mimicking the circumstances in tissues. Not surprisingly, the cell lysates of the MEF subclones growing in normal cell culture conditions did not show differences when probed with antibodies recognizing active forms of the ezrin-linked signalling molecules (Akt, MAPK, mTOR/p70S6/4EBP1; data not shown). However, as the Src-dependent phosphorylation of ezrin plays a role only in 3D conditions, the biochemical dissection of the pathways involved has to be done from extractions *in situ*. Sensitive methods using microarray or proteomic approach will be of interest for the evaluation of Src-induced pathways linking ezrin to tumorigenesis.

The pathways downstream ezrin in a three-dimensional environment are currently under investigation. Several signal transduction networks are connected to ezrin, e.g. the cell survival pathway PI3K, which can lead to oncogenesis by disruption of the apoptotic control of cell proliferation. In osteosarcoma metastasis the Akt, MAPK and mTOR/S6K1/4EBP1-pathway pathways are important in ezrin-mediated early metastatic survival {{151 Khanna,C. 2004; 1043 Wan,X. 2005;}}. Interestingly, ezrin also interacts with hamartin, the gene product of the TSC1 tumour suppressor gene, which is a negative regulator of the mTOR pathway {{63 Lamb,R.F. 2000;}}. Src is one of the regulators of PI3K/Akt and mTOR signaling networks, providing one possible link to ezrin-mediated malignant behavior.

Contrary to MEF cells, ezrin Y145 has been reported as a Src target in porcine epithelial kidney cells. The Y145F mutation delays epithelial cell spreading on fibronectin by inhibiting events leading to FAK activation {{901 Srivastava,J. 2005;}}. Overexpression of ezrin and active Src leads to increased scattering and disrupted cell-cell contacts in mammary carcinoma cells {{832 Elliott,B.E. 2004;}}. Our experiments suggest that the presence of ezrin and active Src promotes malignant behavior more widely than only in epithelial cells, although the exact molecular mechanisms may vary in different tissues and cell types.

Ezrin is also participating to Rho family signaling pathways by interacting with Rho GTPase regulating factors and as a target for Rho-dependent threonine phosphorylation (reviewed in {{425 Bretscher,A. 2002;}}). Intriguingly, ezrin is required for the amoeboid mode of cancer cell invasion in a 3D

Matrigel matrix; inhibition of ezrin or Rho/ROCK signaling blocks the amoeboid motility, whereas proteolytic activity or matrix metalloproteinases are not needed {{202 Sahai,E. 2003;}}. The location of ezrin in the cells which use the amoeboid-type of invasion is highly concentrated to the direction of the movement, analogous to our results with the MEF cells growing inside Matrigel matrix. Moreover, the scattering ezrin WT MEF cells from spheroids on collagen have similar rounded morphology as in amoeboid motility; inhibition of Rho kinase activity or expression of Y477F mutated ezrin alter cell morphology from rounded to extended, analogous to a switch from amoeboid to mesenchymal invasion. However, many compensating pathways are exploited when one mechanism of invasion is blocked and adaptive mechanisms occur {{1066 Wolf,K. 2003;}}. A link between ezrin and matrix metalloproteinase expression and activity has been reported {{118 Wick,W. 2001;}}. Obviously more experiments are needed to clarify the role of ezrin for the invasion of cancer cells.

We show that ezrin promotes Src-dependent functions which are related to cell's ability to survive anoikis, invade and proliferate, indicating one possible mechanism giving selective advantage in tumorigenesis and metastatic processes. As the vast majority of the human deaths in cancer is specifically due to metastases, most clinical benefit would be obtained by overcoming dissemination and initial steps of metastatic progression. Currently, several Src-kinase inhibitors are in clinical trials {{1064 Summy,J.M. 2006;}}. However, more research is still needed to identify specific and relevant targets for cancer treatment and prevention of metastases.

FIGURE LEGENDS

Fig. 1. Characterization of the ezrin -/- MEF cells and their addback subclones. A. Cell lysates were separated by SDS-PAGE and immunoblotted with a polyclonal anti-ezrin antibody. WT = ezrin wild-type; ctr = vector control (pBABEpuro); Y145F = ezrin Y145F mutant; Y477F = ezrin Y477F mutant; Src CA = constitutively active Src. B. The same cell lysates were probed with an anti-moesin antibody. C. The lysates were probed with an antibody recognizing phosphorylated T588moesin. D. The lysates were probed with an antibody recognizing active Src (phosphorylated on Y418). E. Ezrin was immunoprecipitated from cell lysates and tyrosine phosphorylation was detected with an anti-phosphotyrosine antibody (left panel). The same filter was stripped and subsequently probed with the anti-ezrin antibody (right panel). WCL = whole cell lysate; pre-imm = preimmune control immunoprecipitation. The arrows indicate the positions for the specific bands in each subfigure.

Fig. 2. Immunofluorescence analysis of the ezrin -/- MEF addback cells grown on coverslips. Upper panel: Immunofluorescence staining of ezrin; (A) cells harboring WT ezrin but lacking active Src; (B) cells harboring WT ezrin and active Src; (C) cells harboring the Y477F mutant ezrin and active Src; (D) cells harboring the vector control and active Src. Lower panel: The localisation of F-actin detected by phalloidin in cells containing ezrin but lacking active Src (E); and in cells introduced with ezrin and active Src (F). The localization of active Src in the cells harboring WT ezrin (G) or Y477F mutant ezrin (H).

Fig. 3. Proliferation or adhesion of the ezrin -/- MEF addback cells is not dependent on the Src-induced ezrin phosphorylation. A. Cell growth was analyzed at different time points using the MTT-assay as described in Materials and Methods. Circle: cells harboring WT ezrin but lacking active Src; square: cells harboring the vector control and active Src; triangle: cells harboring WT ezrin and active Src; diamond: cells harboring the ezrin Y477F mutant and active Src. B. Cells were serum-starved overnight and plated on fibronectin coated dishes for 40 min. The attached cells were stained with crystal violet and the amount of bound dye measured by absorbance at 595 nm.

Fig. 4. MEF addback cells expressing WT ezrin and Y477F mutant demonstrate phenotypic differences in three-dimensional matrices. A. Cells grown in Matrigel were stained for ezrin and analyzed by confocal microscopy. The cells containing WT ezrin and growing inside three-dimensional matrix display locally concentrated ezrin, whereas the Y477F mutant ezrin is diffusely distributed. B. Cells grown in Matrigel were stained with an antibody against the active form of Src (anti-pY418Src) or an antibody against paxillin. Active Src is concentrated locally in the cells containing either WT ezrin or the Y477F mutant ezrin (left and middle). On the contrary, paxillin is localized diffusely (right). C. Cells grown in Matrigel were double stained with an antibody against ezrin and fluorescent phalloidin or an antibody against cortactin. The ezrin containing patches contain also filamentous actin (left). Cortactin was partially colocalized with the WT ezrin concentrated regions (middle), but did not colocalize with the Y477F ezrin mutant (right). D. Scattering WT and Y477F ezrin expressing cells display different morphology on collagen matrix. The cells were seeded on a collagen matrix as spheroids of 5000 cells. The scattering of the cells inside collagen was detected after 24 h. The scattering WT cells have rounded, amoeboid morphology (left). If 10 µmol of the Rho kinase inhibitor Y-27632 is present, the scattering cells display extended morphology (middle); if 5 µmol of the Src kinase family selective inhibitor PP2 is present (right), the spheroid is disrupted and the cells are not viable. The scattering Y477F ezrin expressing cells have elongated cell morphology (lower left).

Fig. 5. WT but not Y477F ezrin promotes Src-induced growth in soft agar. A. Photographs of the MEF -/- addback cells growing in soft agar. B. Quantification of the colonies growing in soft agar in the absence or presence of 5 µmol PP2, a Src-family selective inhibitor.

Fig. 6A. WT but not Y477F ezrin promotes Src-induced growth in suspension and invasion and growth in three-dimensional matrix. A. Cells were grown in 0.5 % methyl cellulose on bacterial plates. After 7 days, the number of colonies larger than 10 cells were counted by microscopic examination. B. Cells were seeded on a layer of Matrigel on a porous filter. The cells invading through the layer and migrating to the other side of the membrane were visualized by crystal violet staining and counted after 36 hours. C. Cells were seeded inside a layer of Matrigel. After 14 days, the matrices were fixed, the gel liquidified on ice and the cells were counted. The graphs in each subfigure are representatives of at least three different experiments with similar results.

ACKNOWLEDGMENTS

We thank J.A. Cooper for the pLXSH-SrcY527F plasmid; Sa. Tsukita for the anti-moesin antibody; and H. Ahola for technical assistance. Finnish Cancer Organizations, US Department of Defense grant W81XWH-05-1-0469.

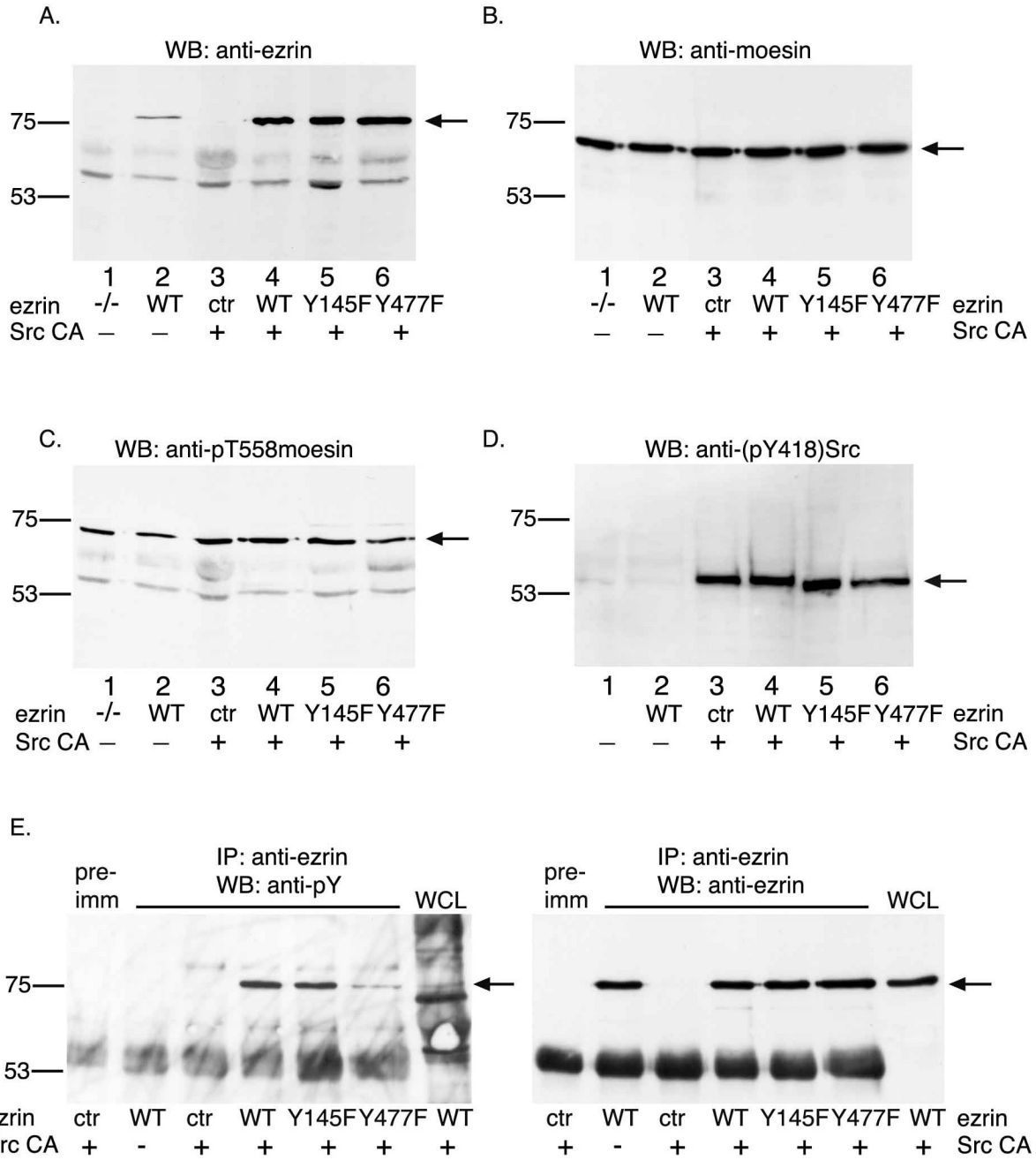
A.
WB: anti-ezrin
75
53
1 2 3 4 5 6
ezrin -/- WT ctr WT Y145F Y477F
Src CA – – + + + +
B.
WB: anti-moesin
75
53
1 2 3 4 5 6
-/- WT ctr WT Y145F Y477F ezrin
– – + + + + Src CA
C.
WB: anti-pT558moesin
75
53
1 2 3 4 5 6
ezrin -/- WT ctr WT Y145F Y477F
Src CA – – + + + +
D.
WB: anti-(pY418)Src
75
53
1 2 3 4 5 6
WT ctr WT Y145F Y477F ezrin
– – + + + + Src CA
E.
pre-imm
IP: anti-ezrin
WB: anti-pY
WCL
75
53
ezrin ctr WT ctr WT Y145F Y477F WT
Src CA + - + + + + +
pre-imm
IP: anti-ezrin
WB: anti-ezrin
WCL
ctr WT ctr WT Y145F Y477F WT ezrin
+ - + + + + + Src CA

Figure 1

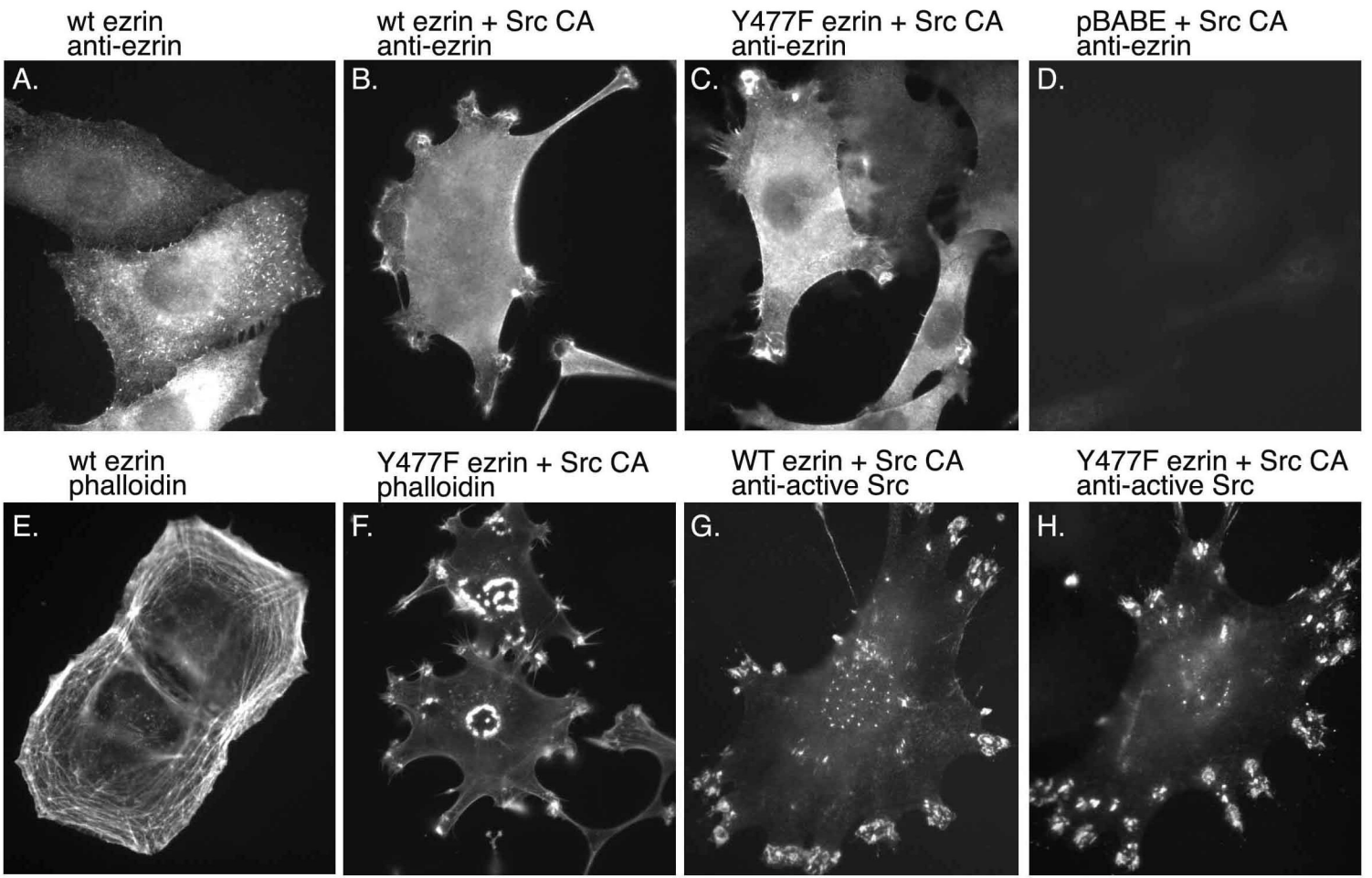
wt ezrin
anti-ezrin
A.
wt ezrin + Src CA
anti-ezrin
B.
Y477F ezrin + Src CA
anti-ezrin
C.
pBABE + Src CA
anti-ezrin
D.
wt ezrin
phalloidin
E.
Y477F ezrin + Src CA
phalloidin
F.
WT ezrin + Src CA
anti-active Src
G.
Y477F ezrin + Src CA
anti-active Src
H.

Figure 2

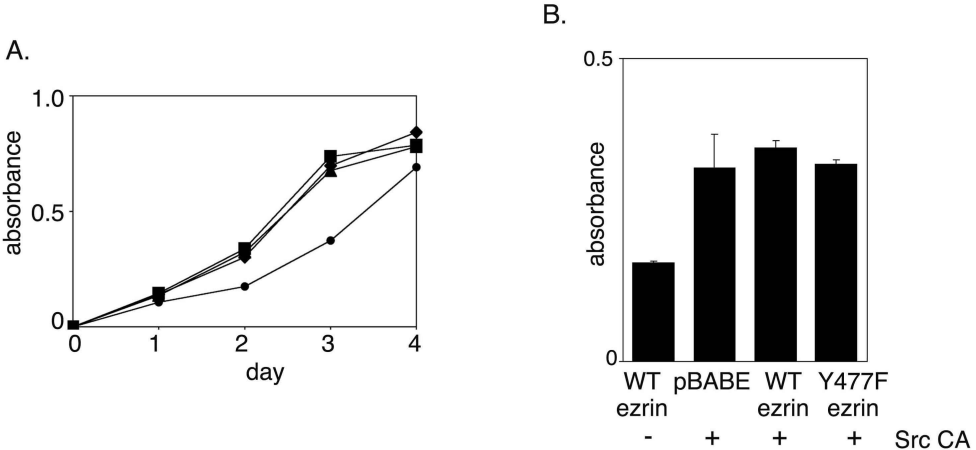
A.
1.0
0.5
0
absorbance
0
1
2
3
4
day
B.
0.5
0
absorbance
WT ezrin
pBABE
WT ezrin
Y477F ezrin
-
+
+
+
Src CA

Figure 3

A

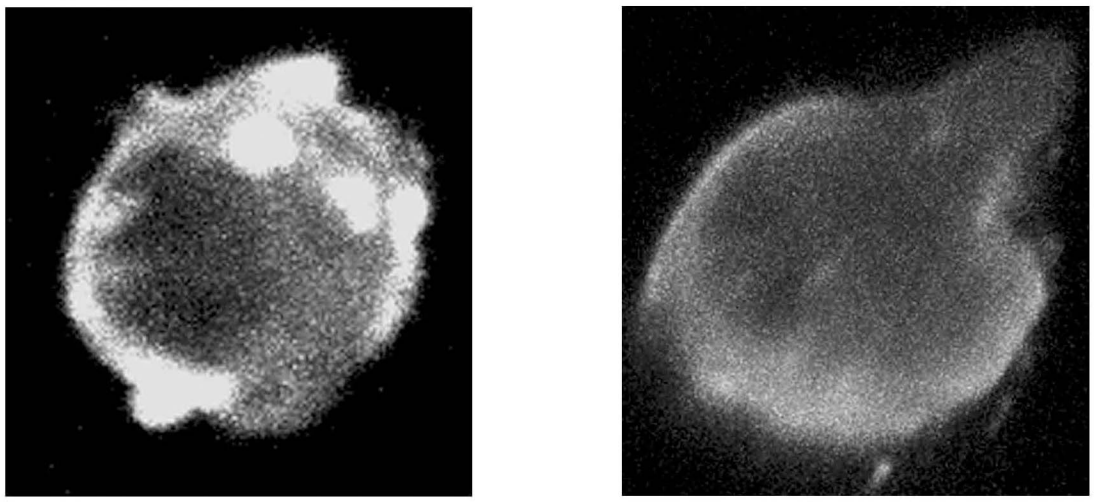

B

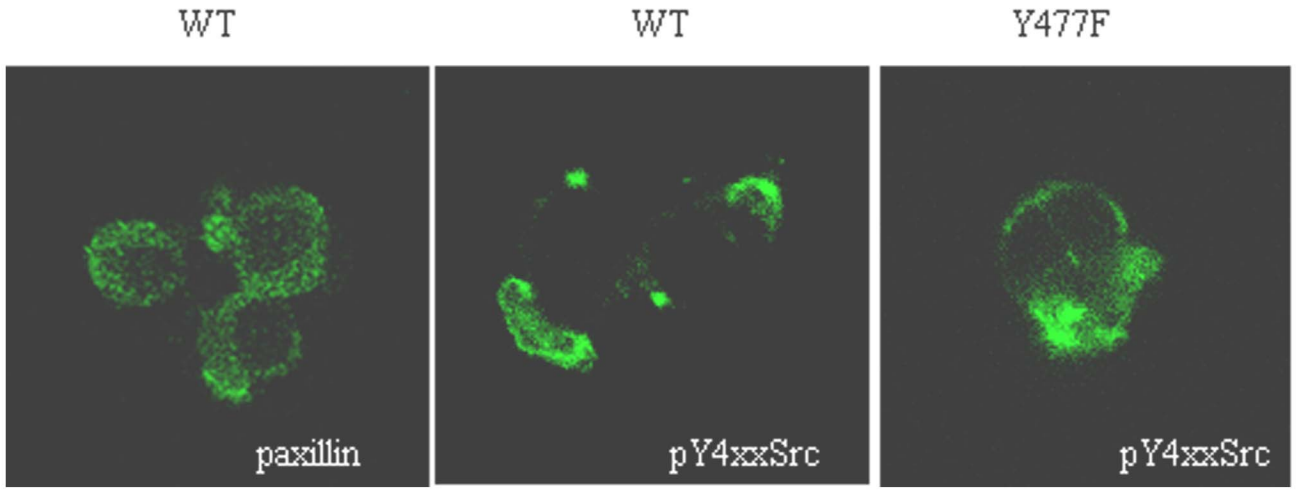

C

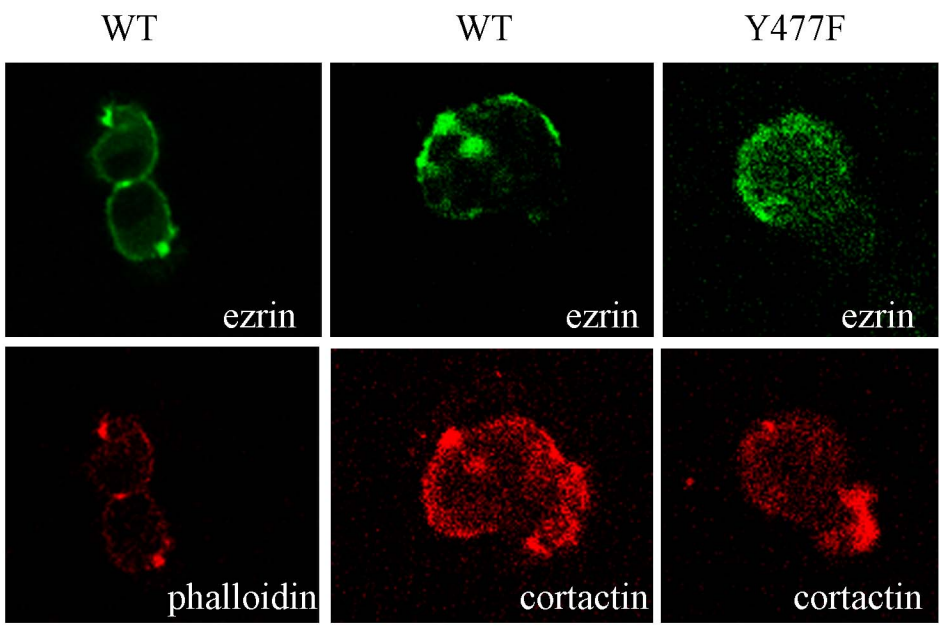

D

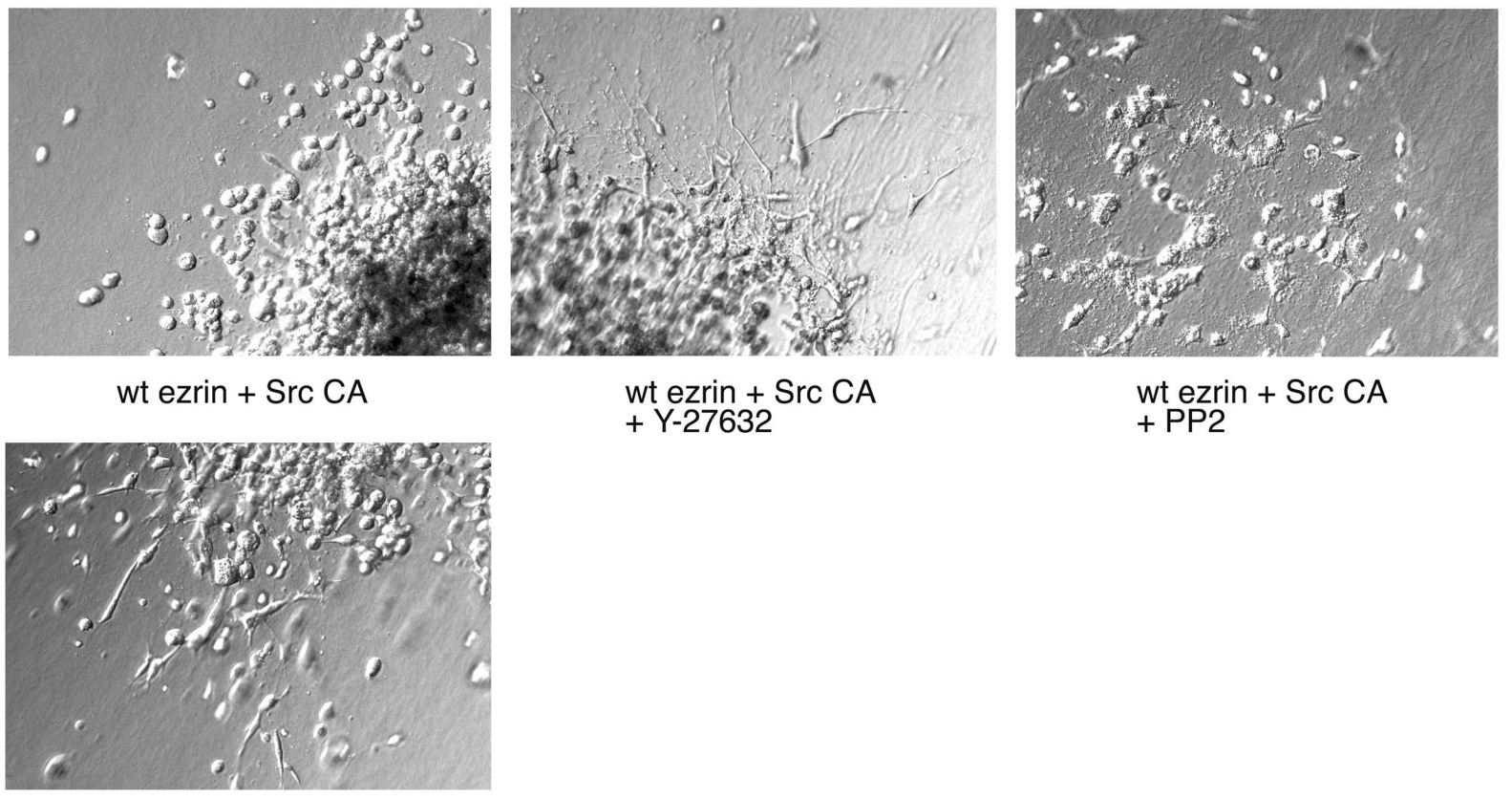

Figure 4

A.

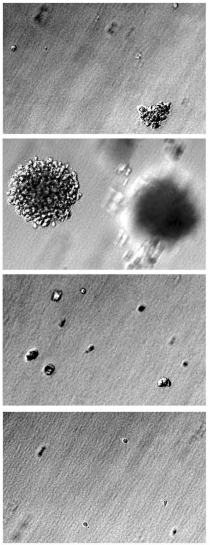
pBABE +
Src CA
WT ezrin +
Src CA
Y477F ezrin +
Src CA
WT ezrin
(no Src)

B.

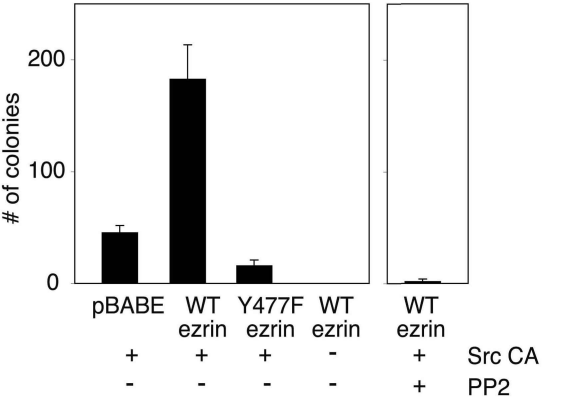
# of colonies
200
100
0
pBABE
WT ezrin
Y477F ezrin
WT ezrin
WT ezrin
+ + + - +
Src CA
- - - - +
PP2

Figure 5

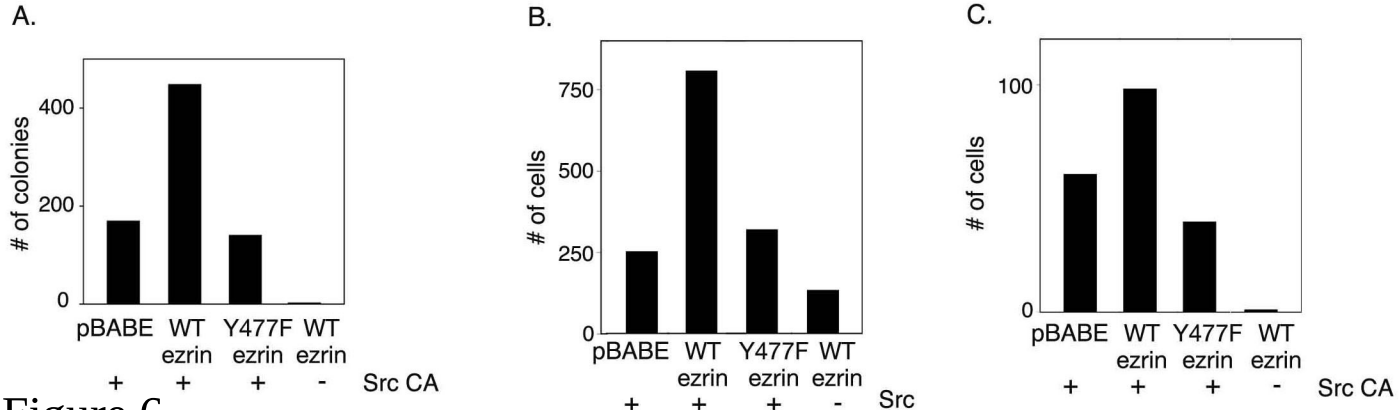
A.
# of colonies
400
200
0
pBABE
WT ezrin
Y477F ezrin
WT ezrin
+
+
+
-
Src CA
B.
# of cells
750
500
250
0
pBABE
WT ezrin
Y477F ezrin
WT ezrin
+
+
+
-
Src
C.
# of cells
100
0
pBABE
WT ezrin
Y477F ezrin
WT ezrin
+
+
+
-
Src CA

Figure 6